DEVELOPMENT OF MULTI-NOZZLE EMITTERS FOR NANO-ESI MASS SPECTROMETRY AND FABRICATION OF 1D POLYMER STRUCTURES USING MICROSTRUCTURED FIBERS AS TEMPLATES

By

YUEQIAO FU

A thesis submitted to the Department of Chemistry

in conformity with the requirements

for the degree of Doctor of Philosophy

Queen's University

Kingston, Ontario, Canada

March, 2015

Abstract

Nano-electrospray ionization mass spectrometry (nano-ESI-MS) has become an important analytical tool due to its high sensitivity through improved desolvation from smaller droplet production as well as high sample utilization due to reduced solvent and sample consumption. The reliability and sensitivity of nano-ESI-MS is largely dependent on the properties of the emitter. However, the standard single-aperture, tapered nano-ESI emitters have some serious limitations including high clogging tendency, poor robustness, and narrow flow rate range.

To address these problems, emitters generating multiple electrosprays (MESs) have been explored, offering significantly improved sensitivity by splitting the flow into smaller streams and higher clogging resistance from multiple paths. The objective of this thesis is to develop MES emitters based on microstructured fibers (MSFs) to conquer the limitations associated with the standard emitters meanwhile to maintain higher flow rates more compatible with front-end separation techniques.

MSF, a fiber having many hollow channels running along its length was chosen to develop nano-ESI emitters because of its dimensional compatibility, structural consistency, design diversity, and feasibility for surface modification, providing a convenient and customizable template material. First, a multi-nozzle emitter was developed using a commercial MSF with an array of polymer nozzles fabricated by optimized procedures involving *in-situ* polymerization of microtubes in the channels and wet chemical etching of the silica at the tip to form the nozzles. However, no MES behaviour was observed due to the densely packed channel pattern. Custom MSFs were subsequently designed and

fabricated with nine or six channels arranged in a radial pattern to promote MES. While the MSFs themselves did not support MES, the formation of nozzles made by either polymer or silica at the tip face enables independent electrospray from each nozzle, showing MES behaviour with significant signal enhancement relative to a standard emitter at the same total flow rate. Furthermore, a variety of MSFs were used as templates to fabricate one-dimensional polymer microstructures including tubes, wires and porous monoliths. Because of the properties of the MSFs, the structures formed from these template channels share their low polydispersity, ultrahigh aspect ratio and axial alignment, showing great applicability in diverse fields.

Co-Authorship

The work discussed in this thesis was mainly designed, conducted and analyzed by the author in the Department of Chemistry of Queen's University under the supervision of Dr. Oleschuk. Part of the work presented in the thesis was co-authored by Dr. Gibson, who assisted the author in preparing experiments and editing manuscripts. Part of the work described in Chapter 3 was co-authored by Dr. Proulx and Dr. Croteau from INO, who fabricated the microstructured fibers designed in our laboratory. Dr. Covey and Dr. Schneider from AB Sciex collaborated with the group and tested the polymer multi-nozzle emitters at their facility. Part of the work described in Chapter 2 and 6 were conducted by undergrad students Christine McGregor and Timothy Hutama under the supervision of the author in their summer projects. Portions of the thesis have been published or will be published in the following journals:

1. **Y. Fu**, G. T. T. Gibson, R. D. Oleschuk, *Journal of Materials Chemistry* **2012**, *22*, 8208-8214 (cover article).

2. **Y. Fu**, G. T. T. Gibson, A. Proulx, A. Croteau, B. B. Schneider, T. R. Covey, R. D. Oleschuk, *Analytical Chemistry* **2015**, *87*, 747-753.

3. K. J. Bachus, K. J. Langille, **Y. Fu**, G. T. T. Gibson, R. D. Oleschuk, *Polymer* **2015**, *58*, 113-120.

4. **Y. Fu**, G. T. T. Gibson, C. McGregor, R. D. Oleschuk, *Canadian Journal of Chemistry* **2015**, *93*, 477-484.

5. R. D. Oleschuk, **Y. Fu**, G. T. T. Gibson, T. Hutama, US provisional patent application, 62/ 108,295.

Acknowledgements

First and foremost I would like to thank my supervisor Dr. Richard Oleschuk for his inspiration, guidance and encouragement and all the support he gave me during my entire study as well as in preparing this thesis and manuscripts. I would also like to acknowledge my committee members Dr. Diane Beauchemin and Dr. Guojun Liu for offering valuable suggestions.

I would also like to thank all the past and present group members in the O-group: especially Dr. Shuqin Su, Dr. Graham Gibson, Dr. Adam Daley, Dr. Zhenpo Xu, Ningsi Mei, Kyle Bachus, Xilong Yuan, David Simon, Katherine Langille, Christine McGregor and Timothy Hutama for their generous help and friendship. I am very lucky to work with such an intelligent and diligent group of people.

In addition, I want to especially thank Dr. Jiaxi Wang who trained and helped me to operate the LTQ-Orbitrap in the departmental mass spectrometer facility. I also enjoyed the discussions with Dr. Wang and Dr. Dean Xiong in Dr. Guojun Liu's group.

I would like to thank NSERC (Natural Sciences and Engineering Research Council of Canada), Canadian Foundation for Innovation, FedDev Ontario, AB SCIEX, CMC Microsystems, and Queen's University for providing the funding, equipment and technical assistance to support my research. Dr. Younes Messaddeq and Steeve Morency from Centre d'optique, photonique et laser (COPL) at Université Laval are greatly appreciated for fabricating a microstructured fiber with doped regions designed in our laboratory.

Finally, I would also like to thank my husband Qingxiang Song, as well as my daughter Marina for their endless love and support. My parents Fengru Liu and Jianzeng Fu, and my parents-in-law Baoxiang Hu and Zhanyou Song are also greatly appreciated. Without their generous support, I wouldn’t be where I am today.

Statement of Originality

All the work presented in this thesis is the origin work performed by the author in the Department of Chemistry, Queen's University, unless otherwise noted. Liquid chromatography-mass spectrometry data in Chapter 3 were collected by Dr. Schneider at AB Sciex. Any published (or unpublished) ideas, methods, techniques and data from the work of others are fully acknowledged in accordance with standard referencing.

Table of contents

LIST OF TABLES

LIST OF FIGURES

List of Abbreviations

1D	one-dimensional
amu	atomic mass units
a.u.	arbitrary unit
ACN	acetonitrile
AF	ammonium bifluoride
AIBN	2,2'-azobisisobutyronitrile
API	atmospheric pressure ionization
aq.	aqueous
BA	butyl acrylate
BDDA	1, 3-butanediol diacrylate
BDE	bond dissociation energy
BME	benzoin methyl ether
BSA	bovine serum albumin
CCD	charged-coupled devices
CE	capillary electrophoresis
CEM	chain ejection model
CERC	Canada’s excellence research chair
cps	counts per second
CRM	charged residue model
CTMS	chlorotrimethylsilane
Da	dalton
DRIE	deep reactive ion etching

DVB	divinylbenzene
ESI	electrospray ionization
FWHM	full-width at half-maximum
GFP B	Glu-fibrinopeptide B
HF	hydrofluoric acid
HFDCS	heptadecafluoro-1, 1, 2, 2-tetrahydrodecyl dimethylchlorosilane
HPLC	high performance liquid chromatography
i.d.	inner diameter
IEM	ion evaporation model
LC	liquid chromatography
LE	leucine enkephalin
m/z	mass to charge ratio
M^3	microfabricated monolithic multinozzle
MALDI	matrix assisted laser desorption ionization
MES	multiple electrospray
MS	mass spectrometry
MS/MS	tandem mass spectrometry
MSF	microstructured silica fiber
MW	molecular weight
o.d.	outer diameter
PEEK	poly ether ether ketone
PLOT	porous layer open tubular
PPM	porous polymer monolith

PS-DVB	polystyrene-divinylbenzene
RSD	relative standard deviation
S/N	signal to noise ratio
SAPs	stress-applying parts
SEM	scanning electron microscope
TFDCS	tridecafluoro-1, 1, 2, 2-tetrahydrodecyl)dimethylchlorosilane
TIC	total ion current
XIC	extracted ion current
γ-MPS	3-(trimethoxysilyl)propyl methacrylate
μ-TAS	micro total analysis system

Chapter 1 Introduction

1.1 Overview

Electrospray is a well-known process involving the application of a high voltage to a solution flowing through the small orifice of an emitter. Under the influence of the intense electric field, the liquid meniscus at the orifice is shaped into a cone with a jet emitting from the cone tip, this jet being dispersed into a spray of fine, charged droplets.[1, 2] Because of the morphology of the liquid meniscus, the regime is labeled cone-jet mode.[3] Electrospray can also be operated in several other modes.[4] The electrospray in cone-jet mode can easily produce monodisperse particles and it is also stable, as opposed to most other electrostatic alternatives that are unstable and usually chaotic.[1, 5] This technique has been widely utilized in various fields such as microcombustion, thin film deposition, fabrication of micro- and nanoparticles, as well as "out of this world applications" such as colloidal and ion propulsion for the positional control of microsatellites. Of the numerous applications of electrospray, its use as an ionization methodology is currently the most well-studied and recognized.[6-8]

Electrospray ionization (ESI) is a soft ionization method that was initially described by Dole *et al*.[9] and later spearheaded by the pioneering work of Fenn. Fenn fine-tuned the technique in the 1980s, leading to his 2002 Noble Prize in Chemistry shared with Tanaka who developed Matrix-Assisted Laser Desorption Ionization (MALDI), another soft ionization method.[10, 11] ESI and its lower-flow analog nanoelectrospray ionization (nano-ESI), generate singly or multiply charged gas-phase ions that can be analyzed by a mass spectrometer for the qualitative and quantitative study of dissolved analytes. Multi-

charging makes it possible to detect molecular masses of hundreds, to hundreds of thousands of Daltons with mass spectrometers that have much lower mass ranges. ESI can handle a vast variety of analytes such as inorganic ions as well as ionized polymers, nucleic acids, peptides and proteins, which are complex species of biological interest, and could not previously be vaporized without significant fragmentation or decomposition.[10, 12] ESI-MS has become an indispensable analytical tool that finds unprecedented utility in various disciplines including proteomics, metabolomics, glycomics, pharmacokinetics, forensics, quality control, and as a compound identification tool for synthetic chemists.[12-20] The appeal for its use is largely due to its extraordinary ability to analyze large molecules without inducing significant fragmentation, its characteristic high sensitivity, selectivity and wide applicability. Furthermore, because ESI works at atmospheric pressure with a quite simple setup and operates with continuous flow, at rates compatible with separations methods, this technique can be utilized as an effective interface and directly coupled to liquid chromatography (LC) and capillary electrophoresis (CE) with MS, allowing automated analysis of complex mixtures. This instrumentation is used in almost every biological chemistry laboratory around the world.[21, 22]

Among the application areas of LC-ESI-MS or MS/MS, proteomics, the large-scale study of proteins, particularly their structures and functions, is attracting more and more research attention after the completion of the human genome project in 2003. Proteomics has become a driving force for the development of advanced MS technologies.[23-25] Envisioned as one of the most promising approaches for the discovery of disease biomarkers and novel therapeutic targets, proteomics seeks to create protein expression profiles for hundreds or even thousands of proteins simultaneously in a single

experiment.[26, 27] One of the challenges encountered by current proteomic technologies is that expressed proteins, which are important to proteomic studies, often occur at trace amounts of particular species necessitating extremely sensitive detection technologies.

Nano-ESI, which operates at flow rates less than 1000 nL/min, is one of the most remarkable advances in ESI technology development.[12, 28] The shift to the lower flow rates associated with nano-ESI-MS has afforded increased sensitivity through improved desolvation from smaller droplet production without the need for nebulizing gas and greatly minimized matrix effects due to a reduction in charge competition. In addition, sample utilization efficiency is higher at low flow rates due to the lower sample consumption and consequently elongated acquisition time.[29, 30]

As a small component in the overall ESI process, the ESI emitter, through which the fluidic sample is delivered and sprayed into a mass spectrometer across a potential difference, plays a crucial role in the performance of nano-ESI due to its geometry and the flow rate it allows. Wilm and Mann developed the first nano-ESI emitter that was a pulled-glass capillary with a tapered tip of 1-3 μm inner diameter. These tapered emitters, however, have some serious limitations including a susceptibility to clogging due to the small tip aperture (<20 μm), poor reproducibility in manufacture, and a limited range of possible flow rates, impeding reproducibility for quantitation, fast online sample preparation, and wide acceptance of nano-ESI-MS in more diverse application areas.

To address these limitations but still achieve competitive sensitivity to that of single aperture tapered emitters, emitters with multiple channels or arrays have been explored accordingly.[14, 31-34] The emitters generating multiple electrosprays (MESs) have been

found to significantly improve sensitivity as well as to elongate the emitter lifetime by reducing clogging tendencies. The increase in sensitivity associated with the MES emitters was achieved due to the increased desolvation efficiency as a result of splitting the flow into smaller streams.[34] Various microfabrication techniques have been employed by several groups to produce MES emitters.[31, 34-36] However, to replace the standard single tapered emitters, MES emitters will need to be more easily fabricated, compatible with conventional analytical separation methodologies, as well as being more cost effective and robust.

To this end, a series of robust and multichannel emitters[37] have been developed in our group based on commercially available silica microstructured fibers (MSFs), which represent a relatively new class of fiber optic material that confines light by using a holey microstructured cladding.[38] Rather than guiding light, however, the micrometer-sized channels of the commercial MSFs have been utilized as fluidic conduits and demonstrated their applications for CE[39], open-tubular LC[40], microreactor array[41] and ESI-MS with a dual role as a frit and a nano-ESI emitter.[42] When tested for MES generation, however, the commercial MSFs were found to be unable to support independent electrospray from individual channels.[37] A raised nozzle at each channel exit would provide a greater separation of individual electrosprays to prevent spray coalescing. Due to their customizable nature, MSFs can be fabricated with a wide variety of channel numbers, patterns, and spacing, offering a solution to practical MES emitter fabrication. Meanwhile, MSFs fashioned from silica can also be used as templates, which are easily removed by wet chemical etching for the fabrication of tubes and wires composed of various materials with remarkable functions.[43-45]

The objective of this thesis is to develop multi-nozzle nanoelectrospray emitters based on MSFs to show higher robustness and to provide better ESI sensitivity and stability compared to the standard tapered emitters, in addition to utilize MSFs as templates to fabricate polymer microstructures with high aspect ratio and low polydispersity. This introduction consists of some fundamental aspects of nanoelectrospray, including a literature review of the history and theory of ESI-MS, the design and fabrication techniques of various nano-ESI emitters including single tapered emitters and MES emitters, as well as a brief introduction of MSFs and their novel applications such as templates.

1.2 The fundamental aspects of ESI-MS

1.2.1 History of ESI-MS

The history of MS begins with Thomson who invented the first mass spectrometer in the early twentieth century. Since then, the mass spectrometer has become an indispensable tool in molecular studies.[46] In a typical MS procedure, a sample undergoes vaporization, and the components of the sample are ionized by one of a number of ionization methods that results in the formation of gas-phase ions. The ions are separated in an analyzer according to their mass-to-charge ratio (*m/z*), typically by accelerating them and subjecting them to an electric or magnetic field, and are detected in proportion to their abundance. The ion signal is then plotted versus *m/z* to produce a mass spectrum.[47]

Small molecules are easily vaporized and ionized by bombarding them with energetic particles like electrons, photons, or ions of other atoms or molecules. However, it was not easy to vaporize and ionize large polyatomic molecules, especially bio-molecules such as proteins/peptides, without extensive fragmentation and decomposition since many

bio-molecules are non-volatile and thermally unstable.[48] Thus, relatively “soft” ionization techniques were in great demand, through which fragmentation and decomposition of large molecules can be minimized. The major historical developments regarding ionization methods for MS are listed in Table 1.1. Two dominant “soft” ionization techniques were developed, ESI and MALDI, allowing MS to expand into the realm of biochemistry.[49] The major contributors of the two ionization techniques, John Fenn and Koichi Tanaka shared the 2002 Nobel Prize in Chemistry "for their development of soft desorption ionisation methods for mass spectrometric analyses of biological macromolecules".[50] Unlike ESI, MALDI is based on the so-called “energy-sudden” approach in that sufficiently rapid heating can vaporize complex molecules before they have time to decompose.[51] In particular, analytes are embedded in a solid matrix, and gaseous ions are formed by exposure to a laser pulse.[52] Electrospray, on the other hand, is a phenomenon that generates a mist of fine droplets from the conical tip of a liquid emitted from a capillary under a high electric field. The pioneering work on electrospray was carried out by Zeleny in 1914, who first photographed the instability of electrified liquid surfaces with various modes, including dripping, spindle, oscillating-jet, cone-jet and multi-jet modes.[1, 4, 53] The conical shape is called a “Taylor cone” named after Taylor who described a theoretical explanation of this phenomenon in 1964.[2]

Table 1.1 Historical development of ionization methods since the invention of MS [49]

Investigator(s)	Year	Contribution
Dempster	1918	Electron ionization
Munson and Field	1966	Chemical ionization
Dole	1968	ESI
Beckey	1969	Field desorption
MacFarlane and Torgerson	1974	Plasma desorption
Barber	1981	Fast atom bombardment
Tanaka, Karas, and Hillenkamp	1983	MALDI
Fenn	1984	ESI on biomolecules
Mann and Wilm	1991	nano-ESI

The applicability of electrospray as a "soft" ionization technique for macromolecules was initially reported by Dole *et al.* in 1968.[9] In Dole's remarkable work, he demonstrated that highly charged droplets from solutions of non-volatile solute species generate intact gaseous ions of those species through the tip of an electrically charged capillary with defined parameters. He successfully ionized polystyrene of high average molecular weight (411,000 Da) by dispersing the highly charged droplets in an evaporation chamber filled with an inert gas (nitrogen) at a relatively high (atmospheric) pressure. The presence of such gas facilitated vaporizing solvent from those highly charged droplets and reduced the kinetic energies of the gaseous ions that would otherwise require mass analyzers capable of analyzing high-energy ions.[51]

Fenn and his colleagues fine-tuned Dole's electrospray experiment and made some important modifications on Dole's design in the 1980s.[54] In their setup, they introduced a drying gas flowing opposite to the flux of charged droplets and ions from the electrified capillary. Such a gas could remove the solvent vapor from the evaporating droplets,

assisting desolvation in order to avoid solvent and any other “junk” that was not ionized from entering the vacuum system of the mass spectrometer.[51] In their extraordinary paper published in 1989, proteins with high molecular weight (76,000 Da for conalbumin) were detected with a quadrupole mass analyzer. The tendency for multiple charging is profoundly beneficial because the effective mass range of any analyzer increases by a factor equal to the number of charges per ion. Therefore, a large molecule can be measured by an analyzer with a limited mass range.[10] Each peak in the mass spectrum for any one species differs from an adjacent peak only by one adduct charge and each peak in one of these multiple peak spectra is an independent measure of the parent ion mass. Thus, a more reliable and accurate measurement of the parent molecule mass could be obtained by averaging those independent values than any single-peak spectrum could provide.[51]

1.2.2 Mechanism of ESI

The electrospray process generally comprises three steps: droplet formation, droplet shrinkage, and gaseous ion formation.[55] The steps occur in the atmospheric pressure region of the apparatus as shown in Figure 1.1. Ions present in solution migrate toward the counter electrode (the mass spectrometer orifice plate) under a high electric potential of several kilovolts, causing the formation of the Taylor cone as the ions bring solvent with them. When the electrostatic forces overcome the surface tension, the cone becomes unstable. As a result, a narrow liquid jet is emitted at the tip of the cone where the electric field is very high. This regime is referred to as cone-jet mode due to the morphology of the liquid meniscus. After a short distance the jet becomes unstable and becomes a set of charged mutually repelling droplets.[14] In positive ion mode, the droplets have an excess of positive ions at the surface. As the droplets get smaller due to solvent evaporation, they

reach the Rayleigh limit where they undergo “Coulombic explosions” to break up into a plurality of smaller charged offspring droplets that are subjected to further desolvation and fission events until they are small enough to produce gas-phase ions.[51] Some of the ions resulting from the preceding steps enter the vacuum region of the interface that is either a very small orifice, or a capillary leading to the mass spectrometer. While some of the other modes have been and are being used for ESI-MS, like multi-jet mode, it appears that the cone-jet mode is the most efficient, stable and often used mode.[56]

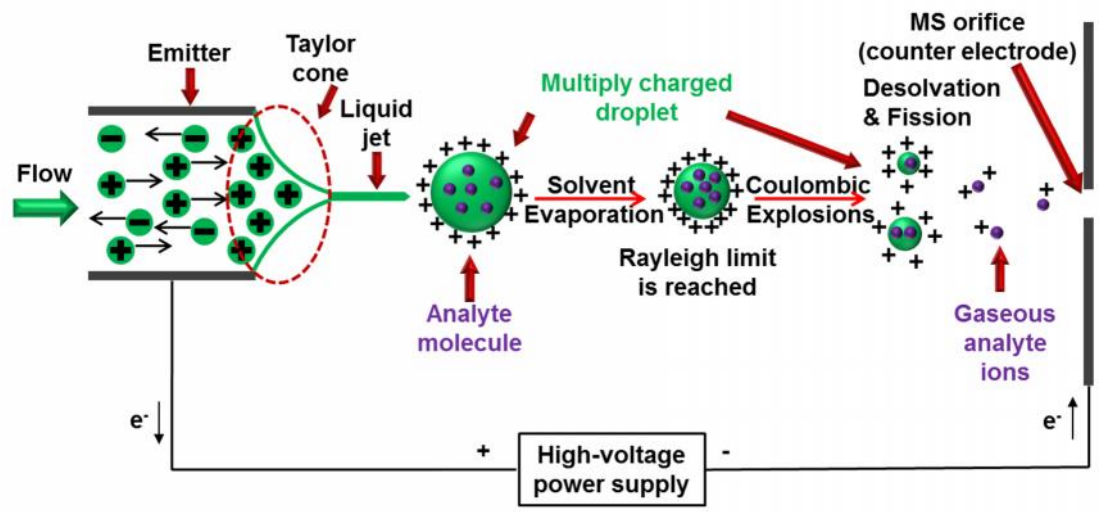

Figure 1.1 Schematic of electrospray processes in positive ion mode.

The mechanism for the production of gaseous analyte ions from highly charged nanodroplets in the final ESI step remains controversial.[56-58] There are two possible scenarios/theories that have considered. The first one proposed is based upon the early studies by Dole *et al.*[9] They assumed that the offspring droplets generated from a first Rayleigh instability would undergo continued desolvation and fission events until the ultimate droplets were so small that each would only contain one solute molecule. The solute molecule would retain some of the droplet’s charge and thus become a free gas-phase ion when the last of the solvent evaporated from the droplet. This assumption is

known as the charged residue model (CRM). The second possibility, which is referred to as the ion evaporation model (IEM) proposed by Thomson and Iribarne,[59] is that before forming the ultimate droplets that only contain one solute molecule, the electric field at a droplet's surface becomes intense enough to eject a solute ion from the droplet surface into the ambient gas by field emission.[51] In summary, the IEM is experimentally well-supported for low molecular weight analytes like small (in)organic ions, whereas the CRM is much more plausible to apply to large globular species such as dendrimers and natively folded proteins.[56] Recently, Konermann *et al.* have proposed another ESI process for unfolded/hydrophobic polymers (proteins), which proceeds via a chain ejection model (CEM) that is an IEM-like mechanism based on both modeling and experimental results. The schematic summary of the ESI mechanisms is illustrated in Figure 1.2.[60, 61]

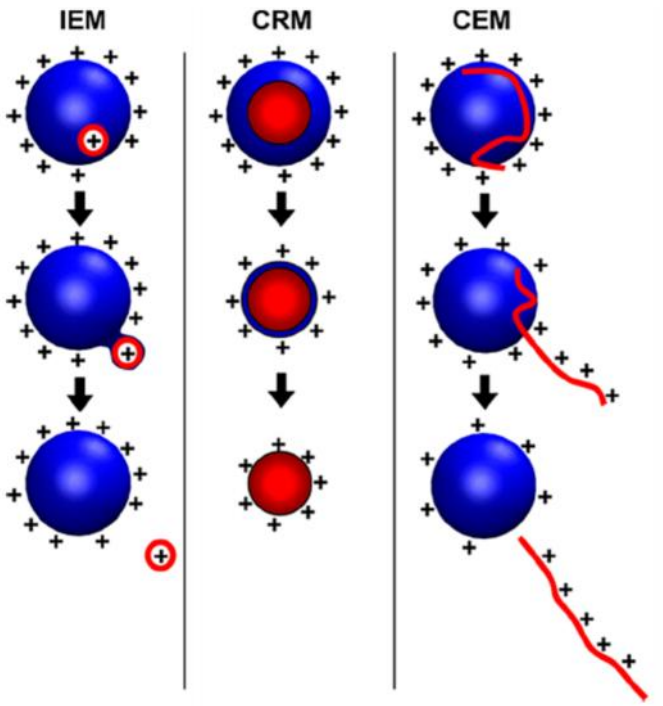

Figure 1.2 Summary of ESI mechanisms. IEM: Small ion ejection from a charged nanodroplet. CRM: Release of a globular protein into the gas phase. CEM: Ejection of an unfolded protein.[61]

1.2.3 Nanoelectrospray ionization (Nano-ESI)

Wilm and Mann quantitatively described electrospray processes based on the original Taylor cone theory.[62] A relationship was first established to predict the size of an emission zone at the tip of a stable Taylor cone (assuming a cone angle of 49.3° at static equilibrium). A schematic of a Taylor cone (zoom-in) and an illustration of the radius of the emission region are shown in Figure 1.3. The emission radius on the tip of a Taylor cone, at which droplets are emerging, is proportional to the 2/3 power of the flow rate. This correlation indicates that the emission radius, and thus the size of the emanated droplets, is reduced when the flow rate is decreased. When the emitted droplets become smaller, desolvation is more efficient since fewer droplet fission events and less solvent evaporation is required prior to ion release into the gas phase. At flow rates of a few nanoliters per minute, droplets become small enough to contain on average one analyte molecule, resulting in almost immediate ion emission. This was confirmed by experiments and led to the birth of nano-ESI with flow rate typically less than 1000 nL/min.[12, 28]

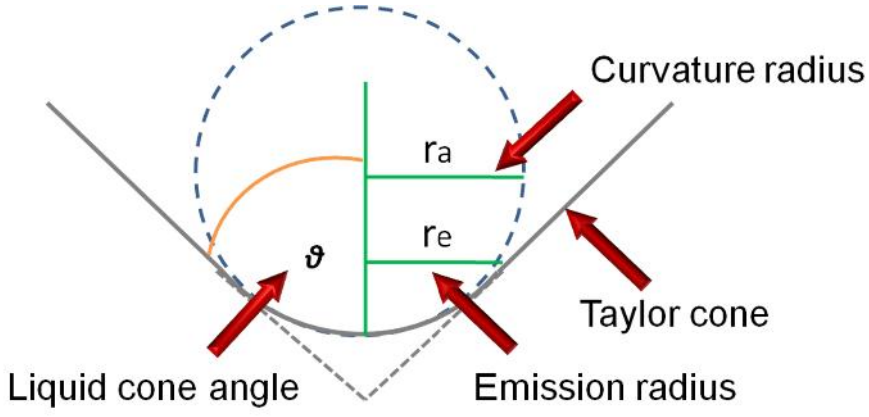

Figure 1.3 Schematic of a Taylor cone and an illustration of the radius of the emission region.[62]

The main benefits of nanoelectrospray include improved ionization and desolvation efficiency because the smaller droplets emitted from the capillary afford increased surface charge per analyte, which results in increased sensitivity. Additionally, the enhanced desolvation allows the capillary to be positioned closer to the mass spectrometer inlet, further decreasing ion transmission losses.[27] The overall efficiency of nano-ESI is determined by the flux of ions reaching the detector of a mass spectrometer divided by the flux of analyte ions emitted from the emitter.[29] Moreover, at lower flow rates, sample utilization efficiency is higher due to the elongated acquisition time, which is beneficial when only a small amount of biochemical samples are available. Nano-ESI is also advantageous for the detectability of analytes with non-surface activity such as sugars, for spraying of solvents with high surface tensions such as water, as well as for the tolerance towards the presence of high amounts of salt contaminations or buffers in the sample solution.[30, 63] With these remarkable merits, nanoelectrospray sounds like it should be the technique of choice for proteomics, metabolomics and glycomics.[64]

In the electrospray process described above, the cone-jet mode is a crucial condition for stable electrospray and the size, shape, reproducibility and stability of the Taylor cone are highly dependent on the emitter tip architecture.[65, 66] The ESI emitter thus plays an important role in the success of electrospray that is ultimately determined by the emitter's geometry and composition. Emitters for nanoelectrospray with a single aperture tapered tip can be fabricated by laser-heated pulling of fused-silica tubing, followed by chemical etching or grinding, and surface metallization for electrical contact. The inner diameter of the emitter is 1-3 μm, allowing a very low flow rate (~20 nL/min).[28, 67] However, these emitters have some severe limitations, including a propensity to clog due to their small

apertures, limited range of possible flow rates, loss of conductivity and poor reproducibility in manufacture.[14] Clogging is mainly due to foreign particles, buffer contamination and improperly cleaved fused silica tubing.[68, 69] Since the emergence of nano-ESI, nanoelectrospray research has pursued the development of robust and reliable nano-ESI emitters,[70] the coupling of nano-ESI-MS to miniaturized sample manipulation devices,[71] and the development of high throughput systems involving nano-ESI.[13, 72] Due to robustness concerns, however, the nano-ESI technique has unfortunately not been widely utilized as a routine bio-analytical tool.

1.2.4 Multiple electrospray ionization

To alleviate the drawbacks associated with single aperture tapered emitters as well as increase sample throughout, a new paradigm has appeared taking advantage of multiple spray. Emitters functioned to generate multiple electrosprays have been found to significantly enhance ESI-MS sensitivity with reduced clogging tendencies. Based on the theoretical prediction and experimental results, total spray current is proportional to the square root of the number of individual spray emitters under the same overall flow rate and solvent conditions when each emitter operates in the stable cone-jet mode (Equation 1.1),[34]

$$I_{total} = \sqrt{n}\, I_s \qquad \textbf{Equation 1.1}$$

where I_{total} is the total spray current, n is the number of emitters, and I_s is the spray current of an individual emitter. Spray current is also proportional to the square root of the flow rate of solvent that is sprayed in stable cone-jet mode.[34, 73] Therefore, a number of electrospray emitters increase the spray current compared to a single emitter under the same conditions. From these statements, we can see that in order to maximize the benefits of ESI,

we should have many emitters forming separate Taylor cones. It follows that using a high total flow rate where each individual emitter is spraying with a flow rate low enough to produce small droplets from the emitters will offer enhanced desolvation and ionization efficiency. It should be emphasized that an increase in spray current does not necessarily mean a proportional increase in a given ion signal, largely because it involves ion transmission efficiency from the electrospray into the mass analyzer and ultimately to the detector.[14]

1.2.5 Characterization of ESI emitter's performance

In general, factors such as electrospray voltage, solvent composition, flow rate, and the distance from an emitter tip to the mass spectrometer orifice, as well as emitter geometry and interface design (*e.g.* with or without sheath flow and heat), have been found to affect the achievement of a stable nanoelectrospray with a Taylor cone.[21, 62, 65, 66, 74-76] The formation of a Taylor cone is a dynamic phenomenon involving interactions between liquid and the emitter exit, liquid and liquid, liquid and air, due to surface tension.[62] During electrospray, the size of a Taylor cone base is defined by the external, not the internal diameter of an emitter. Malformation of a Taylor cone due to incomplete wetting of an emitter tip was found to have significant effects on spray current.[77] Therefore, not only the emitter geometry but also wetting properties of an emitter exit could be important factors to produce stable electrospray.

Various approaches have been used to measure and compare the sensitivity of detection from nano-ESI-MS. Intensity of ion current (total or extracted), which is generated by the constant infusion of an analyte is a typical signal to monitor to

quantitatively demonstrate the sensitivity (ionization and transmission efficiency) and stability of an emitter design. Sensitivity could be described as a detection limit at a specific signal/noise ratio and stability defined as the relative standard deviation (RSD) of either the total ion current (TIC) or extracted ion current (XIC). In order to probe a change in sensitivity at various flow rates, signal change per unit of analyte reflects the sensitivity more accurately under different conditions. A signal response factor is calculated using the average TIC or XIC intensity divided by the amount of analyte consumed over a certain amount of acquisition period using the following Equation 1.2,[78]

$$RF = \frac{I}{[c \times (\frac{dV}{dT}) \times t]}$$ **Equation 1.2**

where: *RF* is the response factor; *I* is the average intensity of TIC/XIC; *c* is the concentration of analyte; d*V*/d*t* is the flow rate; and *t* is the acquisition time.

Electrospray voltage not only affects the electrospray performance but also determines if an electrospray is able to be initiated. Higher voltage is required when the surface tension of the solvent is high, such as water (72.75 versus 22.95 mN/m of methanol at 20ºC)[79] or the distance between the emitter and the mass spectrometer orifice is long (several centimeters). If the voltage is too low, the solution at the emitter tip builds up in favour of forming a Taylor cone, and no ion current is detected.[62] Moreover, ionization efficiency is greatly dependent on the nature of the chosen analyte.[80] A variety of flow rates in the nanoelectrospray regime should be tested for the emitter evaluation. An emitter needs to be able to spray a solvent composition that runs from highly aqueous to highly organic (typical LC reverse phase solvent gradient). Ultimately, the emitter should be tested

and monitored for a significant period of time (*e.g.* hours or days) to demonstrate its longevity and robustness.[14]

1.3 Development of nanoelectrospray emitters

1.3.1 Single nanoelectrospray emitters

Wilm and Mann first introduced a practical design for a needle-like emitter capable of producing a stable Taylor cone at true nano-flow rates down to 20 nL/min in the mid-1990s.[28, 62] This emitter is a gold-coated glass capillary that is heated and pulled until separated, thus both the outer diameter (o.d.) and inner diameter (i.d.) dimensions are tapered to a fine point. Using proper equipment and technique, such a capillary can be drawn to a very fine filament with fairly reproducible dimensions. In the initial experiments, the emitter opening is further enlarged by touching the tip against the interface plate to allow the i.d. of the emitter to become 1-2 μm. It is difficult to control the reproducibility of the emitter aperture using this method, which would subsequently impact the electrospray process. To provide better control on the dimensions at the opening, the emitter tip is usually etched by a hydrofluoric acid (HF) solution.[67] This type of emitter as shown in Figure 1.4 is commercially available and is most widely used in nano-ESI applications.[14]

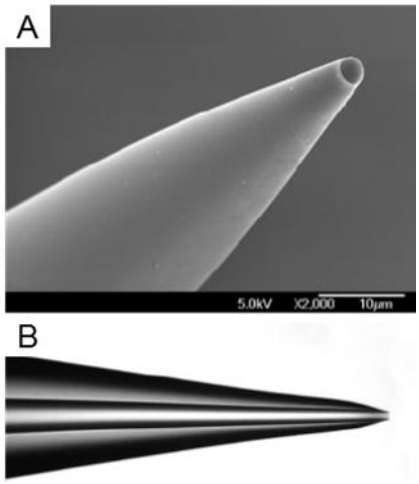

Figure 1.4 SEM image A) and optical image B) of a typical drawn emitter where both inner and outer diameters are tapered[14, 81]

Fabricating emitters with smaller diameters is a trend in nano-ESI applications, because the early studies of the nanoelectrospray process suggested that the smaller the emitter openings, the lower the flow rates they allowed, and the reduced droplet size corresponding to the lower flow rate was essential for improving the desorption and ionization efficiency of the analyte. Although the optimal flow rate is also determined by other factors, the i.d. of the emitter is the most effective and easiest factor to vary.[30, 63] However, without coupled to HPLC, emitters with an i.d. less than 20 μm have an inherent tendency to become clogged as shown in Figure 1.5. Sometimes, emitters with smaller i.d. are clogged too quickly to use practically. Even when the sample solution is scrupulously filtered prior to testing, the life span of the emitters with i.d. of 5 μm or less is only 8-12 hours on average before clogging.[68, 69] This drawback ultimately hinders sample throughput, especially for proteomics where many samples are run on a mass spectrometer every day.

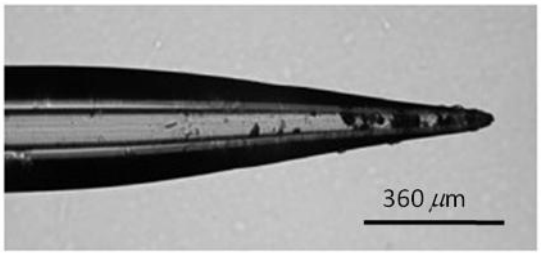

Figure 1.5 Optical image of a tapered emitter that has clogged under normal use.[14]

In order to reduce clogging tendency and improve fabrication methods, several research groups immersed the end of fused silica capillaries in an etchant such as HF to make an emitter without a tapered opening.[35, 82, 83] The o.d. of the capillary is effectively reduced by the isotropic etching process, and the wall at the opening can be very thin depending on the etching time. To maintain constant i.d. of the emitter, water is passed through the capillary during the etching process to prevent the inside of the capillary from being etched, alleviating the clogging challenge of the pulled tips. Moreover, the thin wall of the exit would facilitate the stabilization of the Taylor cone since the solvent wetting of the outside of the tip is largely prevented.[82] Reproducibility of the inter-emitter fabrication is greatly improved by allowing the etching to continue until the silica tip touching the HF reservoir is completely removed, automatically ceasing the etching process and all capillaries are thus etched to the same extent (Figure 1.6).[35]

Another way to prevent wetting of the tip surface other than tapering the tip is to chemically modify it to make its surface hydrophobic since aqueous based solvents are used in most applications. By this approach, the Taylor cone should be mainly supported by the i.d. of the tip, whose surface has hydrophobic coatings such as polymers or a trimethylsilyl monolayer.[37, 84] Such modified emitters show a stable Taylor cone with restricted size, which makes controllable cone-jet nanoelectrospray possible and gives

better mass spectra. This method is also beneficial for the tapered emitters which are claimed to provide stable electrospray for highly aqueous samples and better sensitivities.[85, 86]

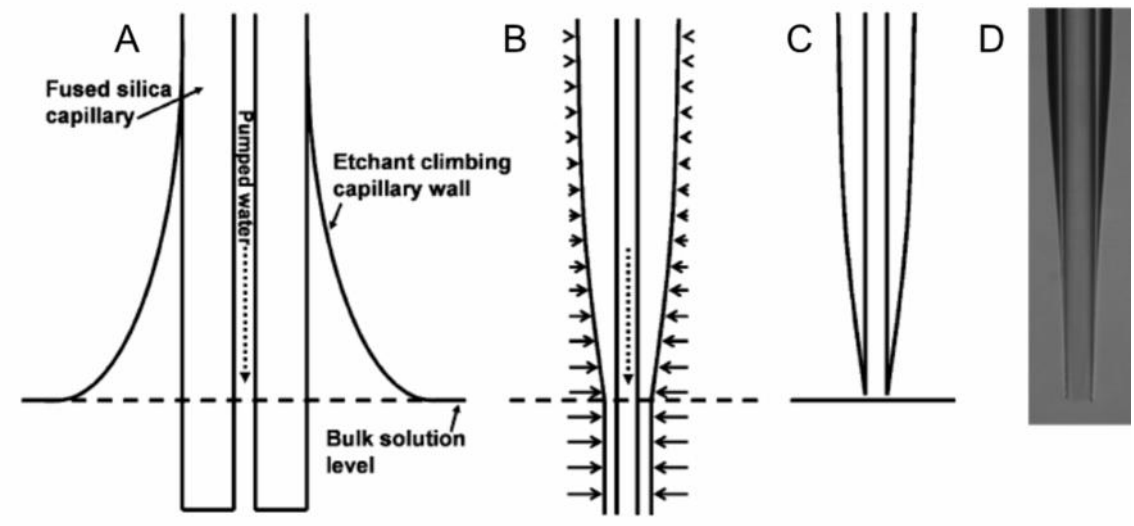

Figure 1.6 Schematic depiction of the emitter etching procedure. A) Surface tension causes the etchant to climb the capillary exterior. B) The etch rate in the resulting meniscus decreases as a function of distance from the bulk solution. Horizontal arrows are vectors indicating etch rate. C) Completed emitter after the capillary has etched through and physically separated from the etchant solution. D) Optical image of an emitter with only the o.d. tapered by etching from a 20-µm-i.d. and 200-µm-o.d. capillary.[35]

In the electrospray process, an electrical potential needs to be applied to the emitter and the mass spectrometer orifice which acts as the counter electrode. However, some emitters are fabricated with non-conductive silicate materials, thus making electrical contact to the emitter a challenge. Several electrical contact modes have been developed successfully, including making a liquid junction by incorporating an electrode into the solution upstream of the emitter, inserting a metal wire into the emitter and coating the outside of the emitter with a conductive material (Figure 1.7).[14, 28, 67, 70, 82, 87, 88] Among these methods, the liquid junction in a form of a union or tee is the simplest and most convenient way to apply voltage for any emitter type or design. However, the liquid

junction should not be too remote from the emitter exit, otherwise the electrical resistance provided by the solution will be significant and will increase the voltage required to produce the same current.[89] Although voltage can be directly applied on conductive emitters such as stainless steel emitters,[90] the difficulty of fabricating such emitters with small i.d. and their short lifetime suffered from deterioration due to discharge make them less widely available for nanoelectrospray applications.

Coating the outside of a silicate emitter with a conductive material like gold is the simplest way to fabricate a conductive emitter, which was the method of choice in the beginning of nanoelectrospray.[22, 62, 67] However, such emitters are susceptible to deterioration due to electrical discharges and electrochemical stress, which in turn decreases the life time.[91] Several nanoelectrospray emitters have been developed based on conductive particles such as gold or graphite powder embedded with polymer coating like polyimide, which have shown good long-term stability and flexibility.[92, 93] Aside from the metallic coating, conductive organic polymers such as polyaniline have also been utilized to coat silicate-based emitters in a number of publications.[70, 86, 88] The polymer coating is much more resistant to electrical discharge compared to the metallic coating, rendering the emitters more robust than the conventional ones.

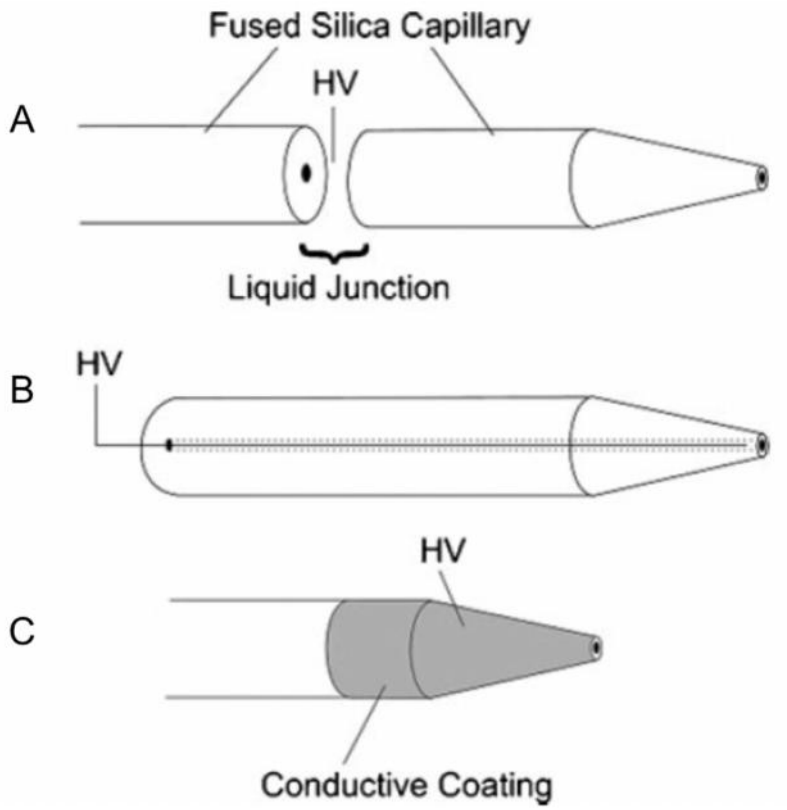

Figure 1.7 Schematic of various electrical contact modes: A) liquid junction; B) wire placed at the emitter exit; C) conductive coating on the outside of the emitter.[14]

1.3.2 Multi-ESI emitters

1.3.2.1 Multiplexed emitters for sequential measurement

Electrospray emitters have been integrated into microfluidic devices, which involve on-line MS analysis coupled to sample separation techniques like CE and LC. Such devices, usually chip-like platforms, are called microchips or micro-total analysis systems (μ-TAS), which handle small quantities of samples and increase analysis speeds.[94] Some devices have been fabricated to incorporate multiple nanoelectrospray emitters into a single microchip for parallel and high-throughput analysis and for avoiding sample carryover and cross-contamination. Furthermore, the chip interface allowed efficient coupling between various components to reduce the dead volume/time. Microfabrication techniques

including photolithography, etching, laser ablation and hot embossing have been utilized to make these microchips with multiple emitters based on glass, silicon and polymer materials in various fashions.[14, 36, 95-98]

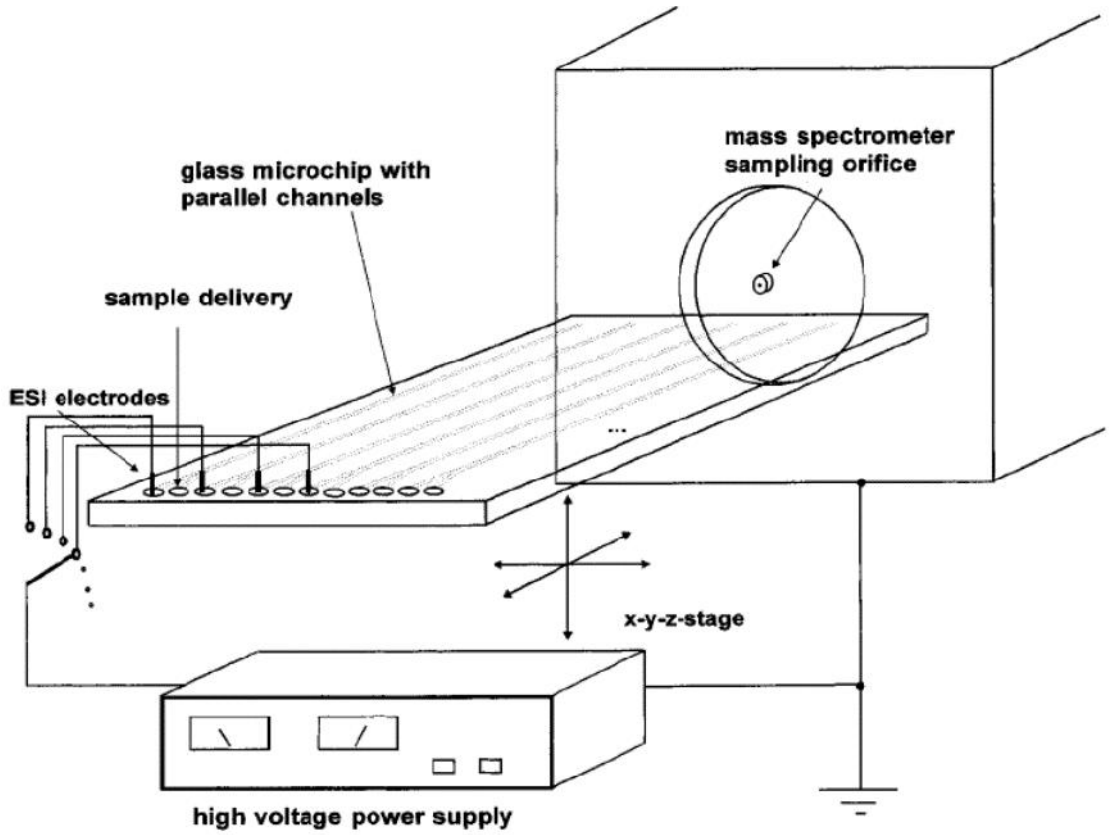

Figure 1.8 Schematic of a multichannel microchip with emitters sequentially aligned in front of a mass spectrometer orifice.[95]

In general, parallel microchannels with reservoirs or ESI emitter arrays were positioned on a controllable stage for sequential analysis of samples. The emitters were successively aligned in front of the mass spectrometer orifice and the samples infused by the individual emitters are detected one at a time (Figure 1.8).[95] Conversely, multitrack electrospray chips with multiple emitters having fixed positions to the inlet of mass spectrometer were made, where the electrosprayed samples are all directed towards the mass spectrometer orifice successively (Figure 1.9).[97] The polymer chip, has six channels

and nozzles which are formed by cutting the distal end of the chip in a “V” shape. It can be noticed that the individual emitters on these multiplexed devices electrospray sequentially and not simultaneously, which means MESs are not being generated. As a result, there is no improvement of the ESI-MS sensitivity, although the microfabrication techniques for these devices are highly relevant to the development of simultaneous MES emitters.[14]

Figure 1.9 Schematic of a multitrack electrospray chip of six emitters with fixed position to a mass spectrometer orifice.[97]

1.3.2.2 MES emitters for simultaneous measurement

The rapid growth in the applications of ESI-MS has been accompanied by continuous efforts to increase its sensitivity, especially for biological studies. In general, ESI-MS sensitivity increases as the liquid flow rate through the ESI emitter decreases with reducing size of the emitter aperture.[62] In theory, spray current from the multielectrosprays is proportional to the square root of the number of individual electrosprays compared to the current from a single electrospray under the same flow rate (Equation 1.1).[73] Smith and co-workers[34] first fabricated an emitter array generating MES, inducing an increase in the spray current. The nine-emitter array microfabricated on a polycarbonate chip using

a laser etching method was arranged in a three by three configuration (Figure 1.10A). The inter-emitter spacing is 1.1 mm and the i.d. of the emitter orifice is 30 μm (Figure 1.10B). After the array was fabricated, the surface of the polycarbonate chip was treated with CF_4 plasma to increase the hydrophobicity of the surface preventing the emitter exit from wetting. The total flow rate is evenly divided, thus the flow rate to each individual emitter is reduced, resulting in an enhancement in sensitivity.

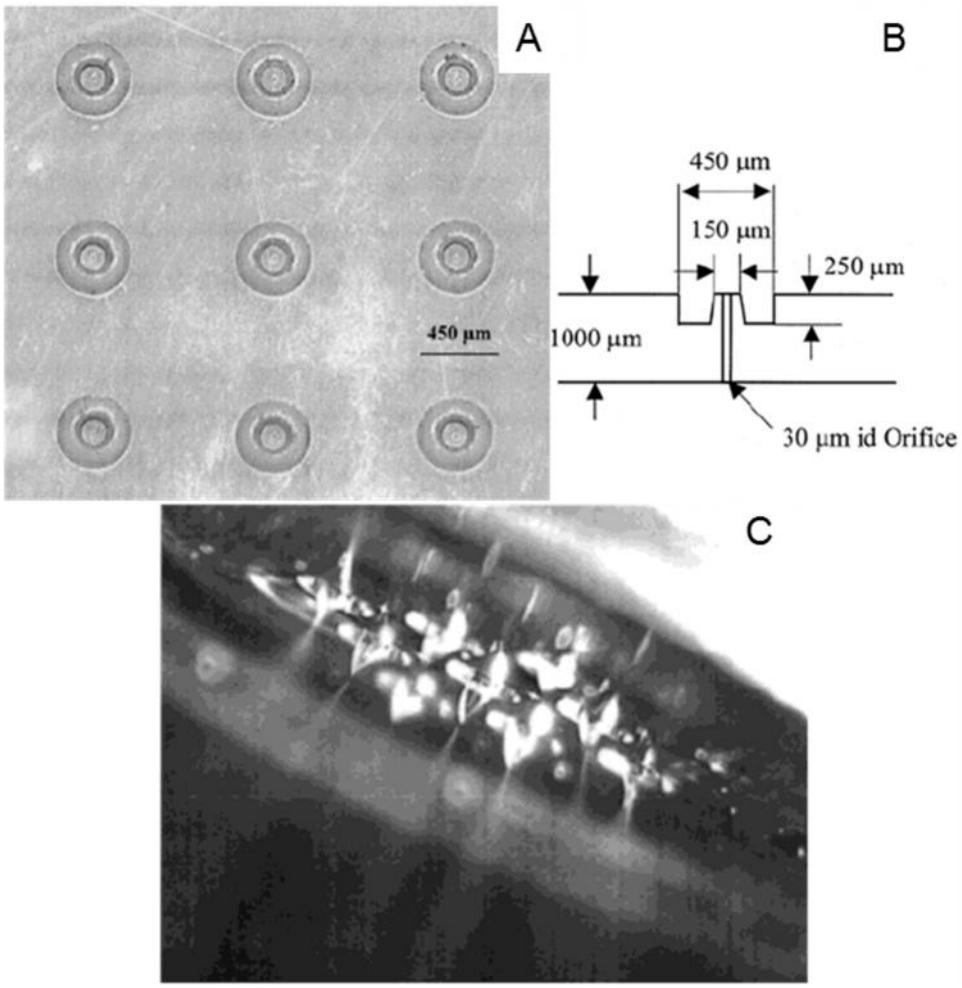

Figure 1.10 Microfabricated MES emitter array: A) top view of an array of nine electrospray emitters, B) dimensions of each spray emitter in the array, C) image of nine MESs in the stable cone-jet mode.[34]

The evaluation of the emitter array was conducted by a modified triple quadrupole mass spectrometer with a heated multicapillary inlet instead of a curtain gas-skimmer interface and an electrodynamic ion funnel to improve ion desolvation and transmission efficiency, or by an electrometer connected to a counter-electrode to measure total spray current. The ion funnel consists of a series of closely spaced ring electrodes whose inner diameters gradually decrease, serving to capture and focus ions as they pass through, significantly reducing the ion transmission losses occurring at the mass spectrometer inlet.[99] Sensitivity was enhanced by a factor of 2-3 by this MES device with the spray nozzle numbers ranging from two to nine at relatively high flow rates (1-8 μL/min) compared to a single electrospray emitter under the same operating conditions. The experimental results showed a good agreement with the theoretical prediction, indicating that each emitter sprayed independently in a steady cone-jet mode (Figure 1.10C). However, a high voltage at ~7 kV is required to establish the stable electrosprays, and a specific design of the mass spectrometer orifice and ion optics is necessary for effectively collecting the gas-phase ions from the emitter arrays.[34] When the number of emitters in the array increases, a higher voltage is required for the steady cone-jet mode due to the electric shielding effect.[100]

Another type of microchip-based MES emitter was developed by Wang and co-workers,[31] which is called ‘‘microfabricated monolithic multinozzle’’ (M^3) emitter via a deep reactive ion etching (DRIE) process and a selective silicon etching step on silicon wafers. A linear array of ten protruding emitters (2 μm wide and 8 μm high) are produced (150-250 μm long) from the end of the silicon stem by this method, with an inter-emitter distance of ~10 μm and a linear density of 100 nozzles/mm (Figure 1.11). The sensitivity

and stability of the M^3 emitter with a single nozzle (10 μm × 8 μm) is comparable to a standard pulled fused-silica nanoelectrospray emitter (~10 μm i.d.) by infusing Glu-fibrinopeptide B (GFP B) at 600 nL/min. Due to their silicon composition, the emitters need a higher applied voltage (4.5 kV-4.8 kV) to generate ESI than that of the standard emitter. Furthermore, they compared the performance of M^3 emitters with single nozzle, two-nozzle and five-nozzle under the same flow rate at 600 nL/min, which means the flow rate at each emitter was 120 nL/min on average for the five-nozzle emitter. However, the M^3 emitters showed only slightly higher sensitivity than that of the single-nozzle emitter, which is probably due to the poor transmission efficiency of their unmodified mass spectrometer source and ion optics.

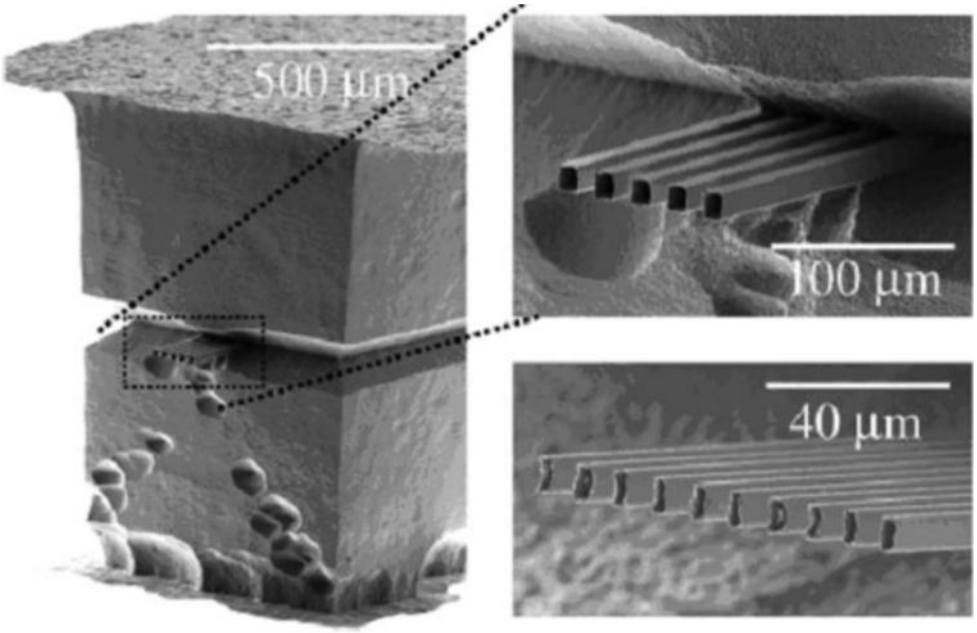

Figure 1.11 SEM image of the M^3 emitters fashioned from silicon.[31]

To develop MES emitters with better performance, the Smith's group[32] fabricated a capillary-based multiplexed ESI (multi-ESI) device specifically designed to be coupled to capillary LC with a low dead volume. This device consisted of a linear array of 19 fused-

silica capillaries (150 μm o.d., 19 μm i.d.) arranged in parallel and spaced uniformly (500 μm center-to-center interspatial distance) by an aluminum holder (Figure 1.12). The distal ends of the capillaries were bundled together and fed through a 1.5 cm-long tubing sleeve. The array of silica capillaries were etched simultaneously to form only externally tapered, evenly aligned emitters with water pumping through them during the etching step (Figure 1.6).[35] Under this fabrication strategy, the relatively large orifices of the emitters can mitigate clogging problems for the internally tapered emitters, providing extended emitter lifetime.

The performance of the multi-ESI emitters showed that the spray current increased as the theory predicted (Equation 1.1). A modified mass spectrometer multi-inlet was utilized to make sure that the increased number of ions was efficiently transmitted to the mass spectrometer, because the standard single inlet would limit the ion transmission efficiency. The multi-inlet comprised a linear array of 19 (400 μm i.d.) stainless steel capillaries lined up to the multi-ESI emitter array. Using this configuration, the transmitted current was observed to improve about 5-fold compared to the single emitter/single inlet platform in a chamber simulating the rough vacuum stage of a mass spectrometer. To ensure that the increased transmitted ion current translates to enhanced sensitivity in the mass spectrometer, reserpine solutions with various concentrations from 0.1 μM to 10 μM were analyzed by both the standard and multi-ESI emitter/multi-inlet configurations with an in-house built ESI/ion funnel source. Finally, a sensitivity increase of ~9-fold was achieved with a total flow rate of 1 μL/min. Interestingly, the sensitivity gain was greater than the transmitted current gain, which is ascribed to improved desolvation resulting from the smaller charged droplets generated by the nanoelectrospray from the multi-ESI emitter

array. They further tested the multi-ESI emitter/multi-inlet performance using a complex peptide mixture resulting from a bovine serum albumin tryptic digest. Significant sensitivity gains ranging from 2.4 to 12.3-fold were achieved compared to the standard configuration for different peptide species which probably have different ionization efficiencies.[32]

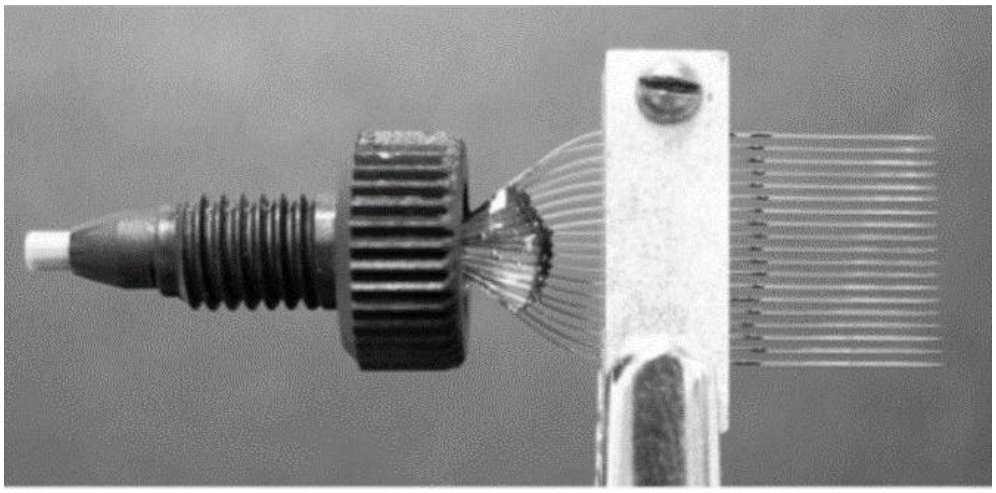

Figure 1.12 Photograph of a linear array of 19 chemically etched fused-silica capillary emitters.[32]

To further enhance ion transmission efficiency, the mass spectrometer multi-inlet was redesigned with larger but fewer multiple inlets (9 × 490 μm i.d.) aligned with 19 fused-silica capillaries (150 μm o.d., 20 μm i.d.) as multi-ESI emitters.[80] The intensity of tryptic fragments from proteins spiked into a human plasma sample was increased 11-fold on average for the multi-ESI emitters/multi-inlet relative to a single emitter/single inlet configuration at a total flow rate of 2 μL/min. The increased sensitivity compared to their previous report was attributed to the improved ion transmission efficiency due to the improved inlet architecture.[101]

Another key challenge with planar, closely spaced multi-ESI emitters is inhomogeneous electric fields experienced by individual emitters due to the electrical interference among the neighbouring electrosprays. This electrical shielding effect makes the outermost emitters experience higher electric fields than the interior emitters at the same applied potential.[102] Thus, it is difficult to operate all the emitters in the nanoelectrospray regime optimally. Developing multi-ESI emitters with a large number of emitters or high emitter densities would ultimately be impeded by this shielding effect that becomes more severe as the emitter density increases.[100]

Several solutions have been proposed to overcome the shielding effect.[7, 33, 36, 103-106] Deng *et al*.[33] utilized an extractor electrode plate with multiple holes which are positioned with corresponding multiplexed electrospray emitters microfabricated using DRIE of silicon wafers at a distance on the same order as the inter-emitter spacing (~0.5 mm) to limit cross-talk between neighboring electrosprays and to minimize the shielding effect by localizing the electric field (Figure 1.13A). Uniform nozzles protruding from 150 to 450 µm were patterned with an i.d. of 120 µm and o.d. ranging from 180 to 240 µm. Under this configuration, MESs in the cone-jet mode were achieved by a device with 91 nozzles arranged in a hexagonal pattern (Figure 1.13B, 1.13C), although the individual emitters were not operated in the nanoelectrospray regime (the minimum average flow rate is ~4.6 µL/min/nozzle) and not used in ESI-MS but for applications in other aerosol areas.[105]

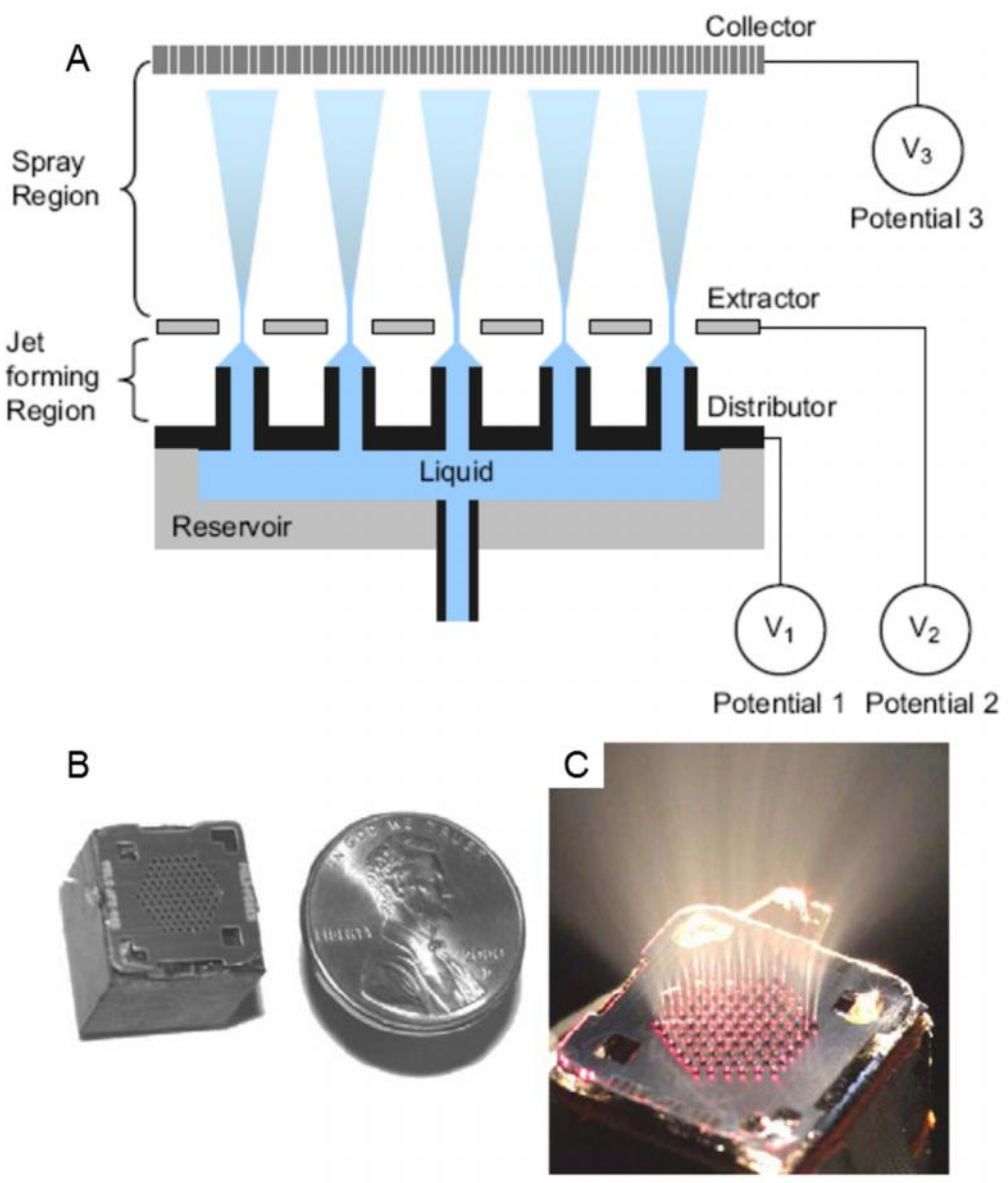

Figure 1.13 A) Schematic of the distributor-extractor-collector electrode configuration of a multiplexed electrospray device; B) microfabricated device has 91 individual emitters, with an American penny as size standard; C) a number of electrosprays issuing from the device.[33]

Recently, the Wang's group further developed a silicon-based microfluidic device that they called multinozzle emitter array chip (MEA chip) as a novel platform, enabling both high-throughput and high-sensitivity applications, such as small volume proteomics using LC-nanoESI-MS.[107] The chip was fabricated on a two-layer 4-inch silicon-substrate

using the similar method to that of the M^3 emitters, consisting of 24 identical units distributed uniformly in a circular array format (Figure 1.14A). Each unit contains an input hole for sample injection, a LC channel for separation, and a multinozzle emitter for nano-ESI-MS for identification and quantification of proteins and peptides. The through-holes are designed for filling screws during assembly. Beads coated with desired chemistry are packed in the LC channel (length × width × depth: 5 cm × 200 μm × 200 μm). Frits are used to retain beads inside the channel (Figure 1.14B). Each emitter has protruding nozzles with a length of 150 μm, a cross-sectional area of 10 μm × 10 μm and a wall thickness of 0.5 μm. To enhance the electric fields at the nozzle tips, the end of the emitter stem was sharpened with an angle of ~20°.[108] MS sensitivity of MEA emitters using GFP B illustrates a power-law relation to spraying nozzle numbers (1-6) with a power constant of 0.39 closed to the theoretical constant of 0.5 (square root of the number of emitters based on the Equation 1.1), excluding the 10-nozzle ones from the curve fitting. Electrosprays from the 10-nozzle emitters were greatly spread out and producing a larger plume resulting in much less ion collection and transmission efficiency (Figure 1.14C). Importantly, the sensitivity of MEA emitters was remarkably higher than that of the commercial PicoTip silica emitters with similar aperture dimensions (10 μm i.d.) as shown in Figure 1.14D. When the LC channels were packed with C18 5-μm beads, on-chip LC-MS analysis of hemoglobin and its tryptic digests from microliters of blood was achieved with a detection limit less than five red blood cells. These silicon devices, however, have several drawbacks including that the fabrications of the silicon nozzles require clean room and expensive equipment while the DRIE process makes the silicon chip very fragile, with a high risk of failure during handling and operating.[36]

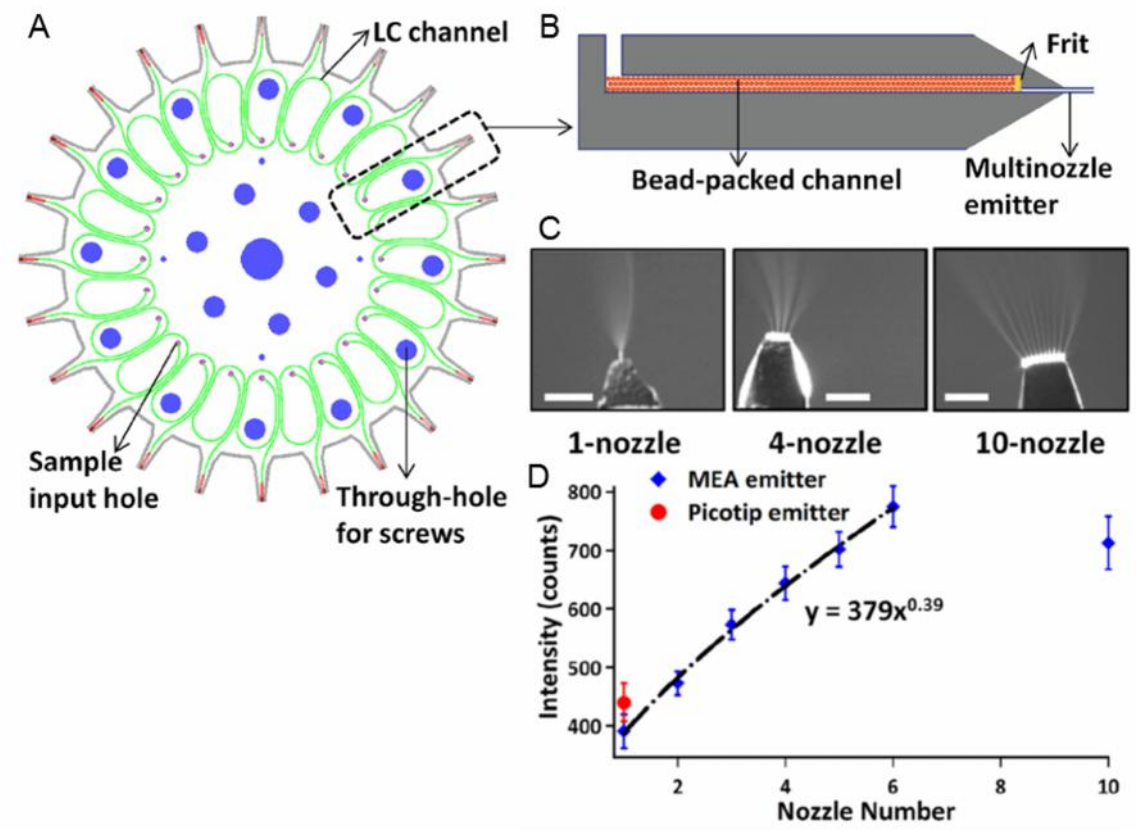

Figure 1.14 24-plex MEA chip. A) Schematic of the design. B) Schematic of the cross-sectional view of a single unit (not to scale). C) Representative images for electrospray of 1-, 4-, and 10-nozzle emitters. Scale bars are 500 μm. D) Sensitivity dependence on the nozzle numbers of MEA emitters (diamond). A Picotip emitter was used as a comparison (circle).[107]

To mitigate the shielding problem, the Smith's group further modified the multi-ESI emitter arrays with capillaries placed in a circular arrangement,[109] so that all the emitters operated in a similar electric field environment, and all the electrosprays operated in the same regime (Figure 1.15). Note that the individual emitters are shielded uniformly in the circular array rather than the shielding effect being minimized. The mass spectrometer multi-inlet was also modified accordingly to match the circular emitter array to make sure that the ion transmission efficiency is as high as possible. However, the sensitivity enhancement for the circular array of 12 emitters was only 2.2-fold compared to a single emitter for a mixture of peptides, even with the help of heated multi-inlet and

ion funnel. The decrease in ion transmission efficiency of the multi-ESI emitter array is due to an increase in space-charge effect from the greater ESI current, resulting in larger diffusional losses when the ions are transported through the multi-inlet.

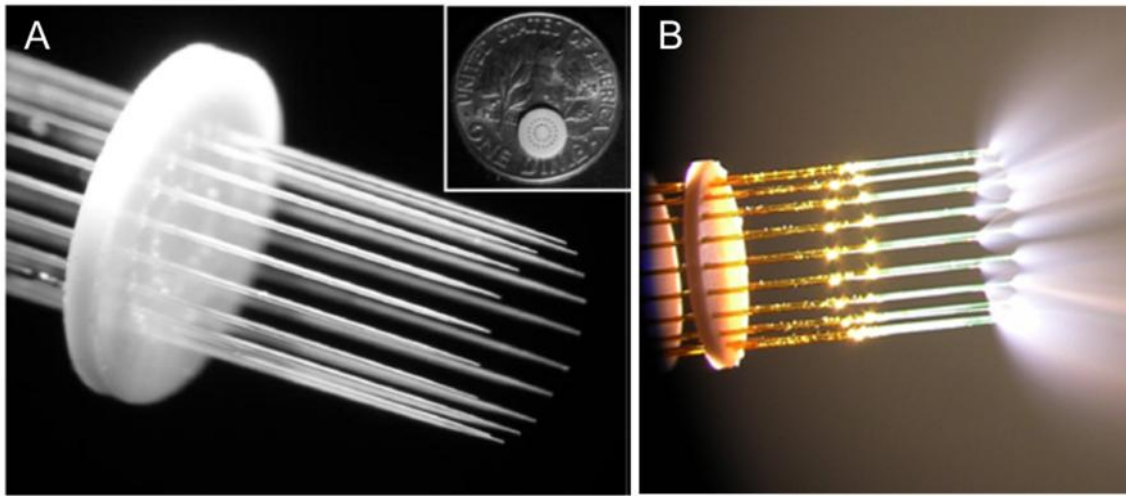

Figure 1.15 Photographs of A) a circular array of 19 chemically etched emitters to improve electric field homogeneity with an American dime as size standard (inset) and B) 19 electrosprays emitting from this array in the cone-jet mode.[109]

In an attempt to resolve the major ion losses at the ESI-MS interface, the Smith's group have developed a subambient pressure ionization with nanoelectrospray (SPIN)-MS interface, in which the ESI emitter is positioned in the first vacuum chamber adjacent to the entrance of an electrodynamic ion funnel allowing the entire electrospray plume to be focused and transmitted by the ion funnel into the analyzer with high efficiency without the transmission losses through the capillary interface.[110, 111] The circular emitter array was also operated in the SPIN source; however, no MS sensitivity improvement was achieved due to wetting of the outer surface of the emitters in the subambient chamber leading to unstable and nonuniform electrosprays.

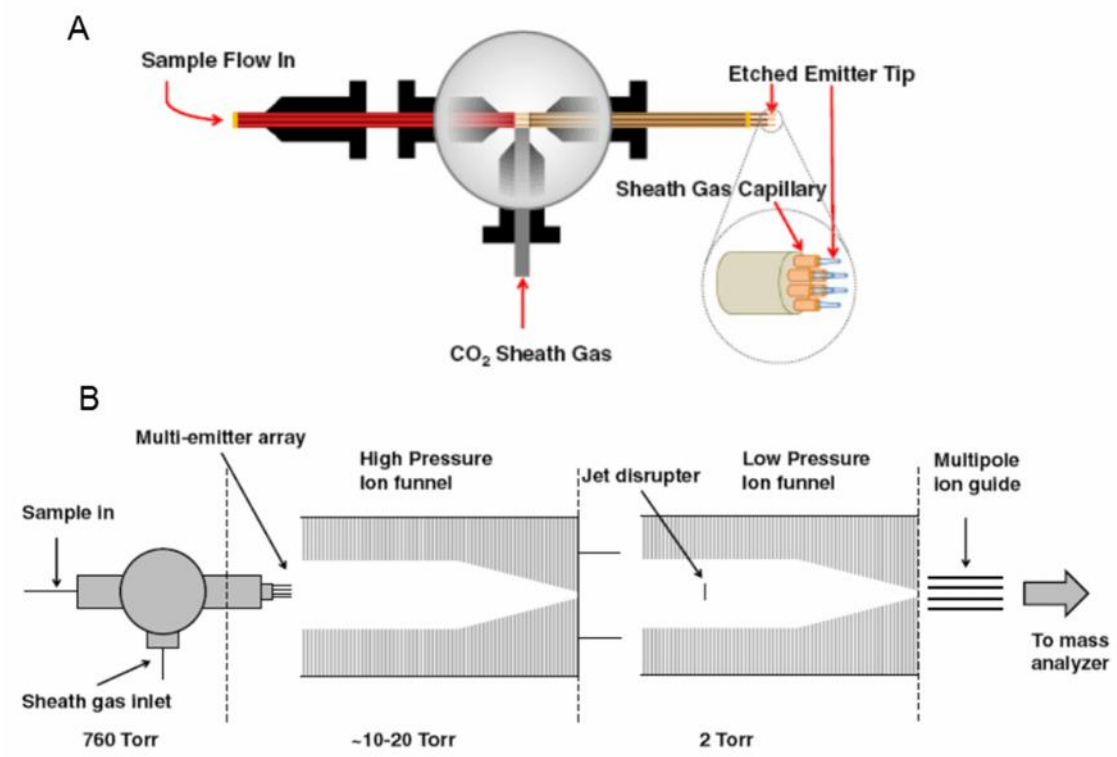

Figure 1.16 A) Fabrication of emitter arrays with individual sheath gas capillaries around each emitter; B) instrumentation configuration of the SPIN source interface coupled with a multi-emitter array positioned at the entrance of the ion funnel.[112]

Recently, this group has developed a new emitter array that incorporates individualized sheath gas capillaries for each chemically etched emitter to effectively solve the emitter wetting problem and generate stable MESs at subambient pressures.[112] A heated CO_2 sheath gas (~160 °C) was provided around the ESI emitter (150 µm o.d., 10 µm i.d.) via a fused silica capillary (360 µm o.d., 200 µm i.d.) to ensure sufficient droplet desolvation and electrospray stability (Figure 1.16A). The gain in MS sensitivity becomes remarkable when the emitter array in the SPIN source (Figure 1.16B) is compared with a single emitter in the conventional ESI source. For instance, the 10-emitter array in SPIN source exhibited an average enhancement factor (peak intensity ratio of the most abundant charge state) of 15.1 for a mixture of peptides infused at a total flow rate of 200 nL/min, and as high as a 30-fold increase was observed specifically for neurotensin and melittin

ions. Incorporation of electrospray emitter array with the SPIN source creates a powerful tool for maximizing both ionization and ion transmission efficiency for ultrasensitive ESI-MS analysis.[113]

1.4 Microstructured fibers (MSFs) as nanoelectrospray emitters and as templates

MES emitters are undoubtedly attractive to the ESI-MS community, especially the proteomic researchers for enhanced sensitivity, increased sample throughput and longer lifetime from reduced clogging tendencies. However, some current emitter designs are cumbersome and expensive requiring specific fabrication equipment, while some designs require a corresponding multi-MS inlet and special ion optics (ion funnel), which would further increase instrument costs. Therefore, single-aperture tapered emitters remain the standard nanoelectrospray emitters due to their commercial availability and ease of fabrication.

In an attempt to supplant the standard emitters, we have developed novel multichannel electrospray emitters based on the commercially available silica MSFs.[37] MSFs, or so-called photonic crystal fibers, are designed to confine light to the core that could be solid or hollow, using a periodic refractive index change induced by an array of microscopic hollow channels that arrange around the core and traverse the entire length of the fiber. To fabricate the MSFs, a bundle of glass capillaries is first stacked to a desired macroscopic preform and then the capillaries are fused together and drawn down to a fiber (a technique commonly referred to as ‘‘stack and draw’’) as shown in Figure 1.17. The dimensions and cross-section pattern of the MSFs can be precisely controlled by this manufacturing process which could provide high versatility and could incorporate solid,

empty or doped glass regions in the MSFs.[38] Due to their unusual and excellent optical properties, a number of types of MSFs have been employed in many applications in diverse areas, such as biomedicine, imaging, sensing, spectroscopy and telecommunications.[114]

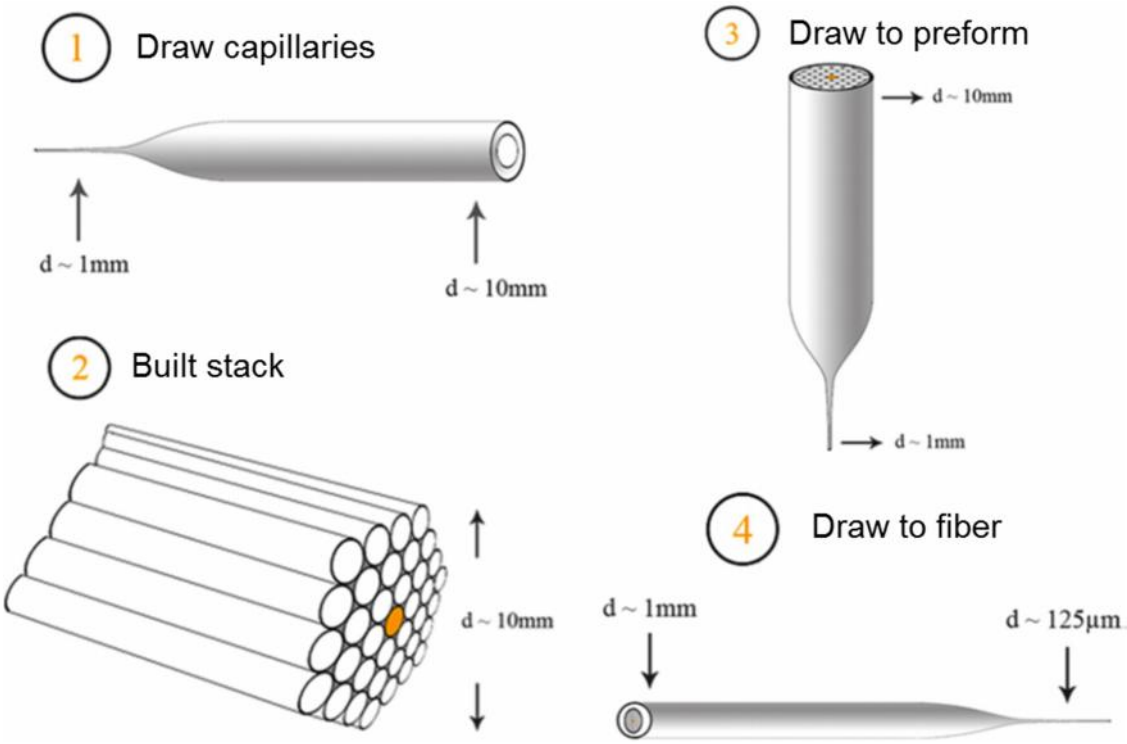

Figure 1.17 Stack-and-draw MSF fabrication technique.[114]

Aside from these applications, MSFs, whose microscopic channels serve as fluidic conduits, have already been utilized for microfluidic applications including CE[39], open-tubular LC[40], microreactor array[41] and nano-ESI-MS in our group.[37] A MSF with 30 independent channels (4-5 µm i.d.) as shown in Figure 1.18 was used as a nanoelectrospray emitter to provide stable electrospray at flow rates from 10 to 500 nL/min with more considerable sensitivity gains at low nano flow rates (*e.g.* 20 nL/min). On the other hand, the o.d. of this type of MSF (~330 µm with protective coating) is similar to that of the standard tapered emitters, thus the MSFs can be directly used as robust emitters on a routine analytical device without extra instrumental cost.

The silica-based MSF emitters can also be modified using a silylation reagent, chlorotrimethylsilane, to improve their nanoelectrospray characteristics by minimizing the wetting effect, allowing the effective electrospray of 99.9% aqueous samples (v/v) with excellent stability. A major advantage of the emitters is their high resistance to clogging, since they have enough non-tapered channels to maintain effective electrosprays. However, the electrosprays from the individual channels of the MSFs tend to coalesce and form a single Taylor cone even with the hydrophobic treatment of the tip. The small spacing (~7 μm) of the channels probably leads to the single electrospray.

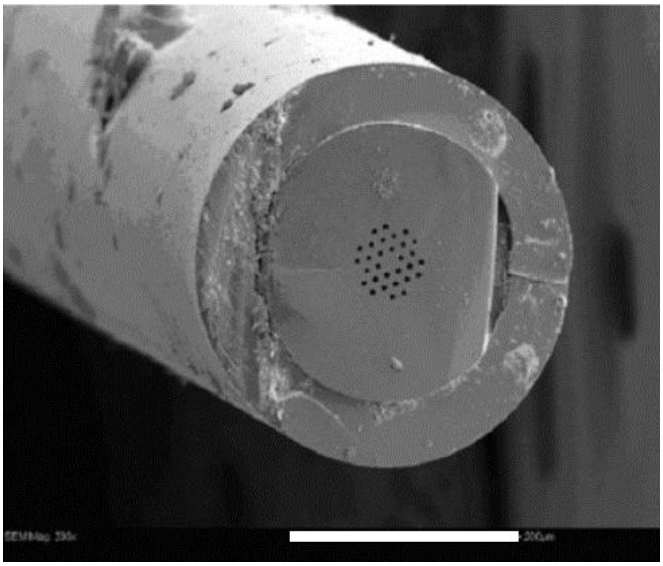

Figure 1.18 SEM image of a MSF emitter having thirty 4-5 μm holes (magnification 200x, scale bar is 200 μm).

On the other hand, the channels of MSFs made from silica can also be used as templates, which are easily removed by wet chemical etching for the production of an array of 1D structures composed of various materials with high aspect ratio compared to those formed in the conventional hard templates such as anodic aluminum oxide[115], track-etched polymer[116] or nanochannel array glass.[117] Metals and various semiconducting materials (*e.g.* Si, Ge) have previously been fabricated within the MSFs by a microfluidic high

pressure chemical vapor deposition technique for optoelectronic devices with extraordinary functions (Figure 1.19).[43, 44]

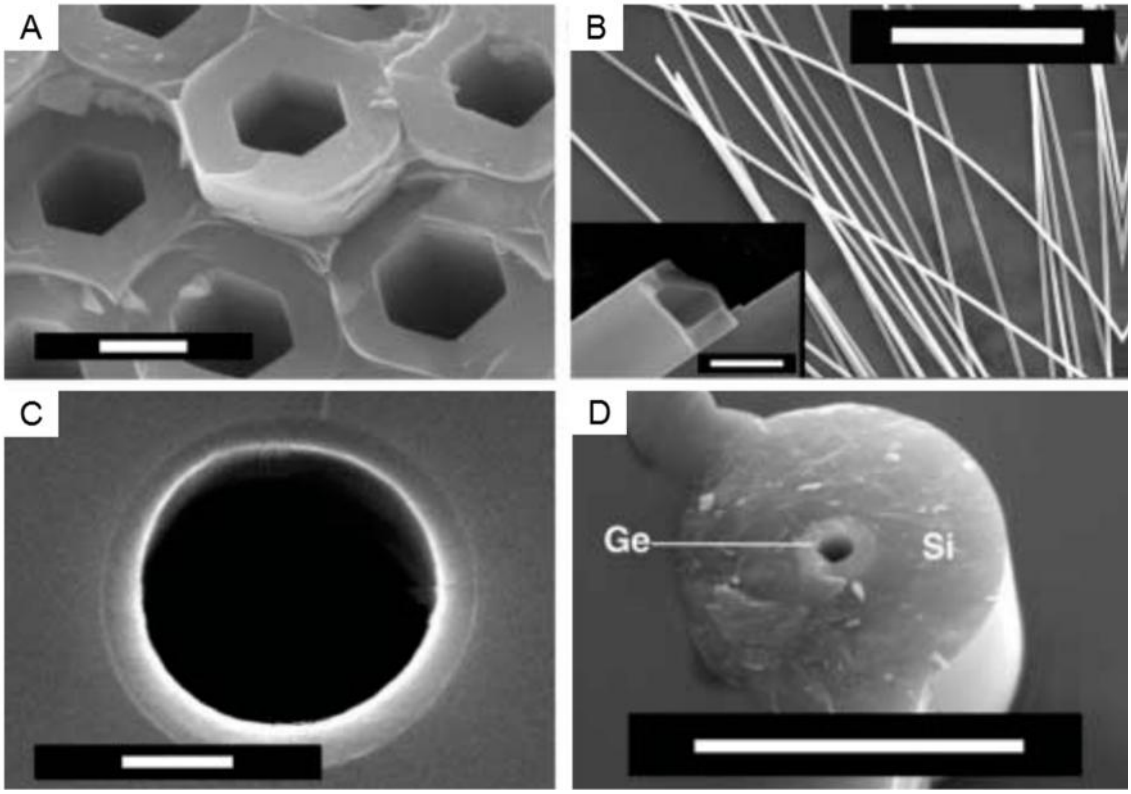

Figure 1.19 SEM images of A) hexagonal silicon tubes in a honeycomb MSF template (scale bar, 1 µm); B) long silicon tubes etched out of the template (scale bar, 100 µm), (inset) one of these tubes at higher magnification, showing the flat sides of the hexagon (scale bar, 2 µm); C) compound semiconductor GeS_2 tube (scale bar, 500 nm); D) silicon cladding on germanium core (scale bar, 6 µm).[43]

1.5 Project objectives

The thesis study aims at improving the MS sensitivity and stability using MES emitters made from MSFs compared with traditional tapered nanoelectrospray emitters as well as expanding MSFs' applications to broader areas. To be specific, the main body of the thesis will address the following objectives, in individual chapters.

To prevent electrospray cross-talk and coalescing from the emitters based on MSF, a raised polymer nozzle array which would provide a greater separation of individual

electrosprays was fabricated at each channel exit of MSF. The development of nanoelectrospray emitters based on a commercial MSF with an optimized polymer nozzle array is discussed in Chapter 2. Optimization process is extensively investigated. Part of the chapter has been published in the Canadian Journal of Chemistry and the Polymer.

To develop multi-nozzle emitters showing true MES behaviour, custom-designed MSFs were designed. Because commercial MSFs are designed and marketed for optics applications, custom-designed silica MSFs would be a better choice to be fabricated and investigated as MES emitters, preventing the structural limitations of the commercial ones. The study of custom-designed silica MSFs as MES emitters with nozzle arrays either made by polymer or silica are thoroughly discussed in Chapter 3 and Chapter 4. Main part of the Chapter 3 has been published in the Analytical Chemistry and the rest part of this chapter will be published in the Canadian Journal of Chemistry. Chapter 4 has been fully filed for a US provisional patent application.

To utilize MSFs as templates to fabricate 1D polymer microstructures, a series of MSFs were demonstrated that they could generate polymer tubes, wires and porous monoliths with high aspect ratio and low polydispersity. Detailed discussions are in Chapter 5 which has been fully published in the Journal of Materials Chemistry.

1.6 References

[1] J. Zeleny, *Physical Review* **1917**, *10*, 1-6.

[2] G. Taylor, *Proceedings of the Royal Society of London. Series A, Mathematical and Physical Sciences* **1964**, 383-397.

[3] M. Cloupeau, B. Prunet-Foch, *Journal of Electrostatics* **1989**, *22*, 135-159.

[4] A. Jaworek, A. Krupa, *Journal of Aerosol Science* **1999**, *30*, 873-893.

[5] M. Cloupeau, B. Prunet-Foch, *Journal of Aerosol Science* **1994**, *25*, 1021-1036.

[6] O. Salata, *Current nanoscience* **2005**, *1*, 25-33.

[7] B. Q. T. Si, D. Byun, S. Lee, *Journal of Aerosol Science* **2007**, *38*, 924-934.

[8] A. Gomez, W. Deng, Eds., *Fundamentals of cone-jet electrospray*, John Wiley & Sons, Inc., 2011.

[9] M. Dole, L. L. Mack, R. L. Hines, R. C. Mobley, L. D. Ferguson, M. B. Alice, *Journal of Chemical Physics* **1968**, *49*, 2240-2249.

[10] J. B. Fenn, M. Mann, C. K. Meng, S. F. Wong, C. M. Whitehouse, *Science* **1989**, *246*, 64-71.

[11] K. Tanaka, *Angewandte Chemie International Edition* **2003**, *42*, 3861-3870.

[12] M. Wilm, A. Shevchenko, T. Houthaeve, S. Breit, L. Schweigerer, T. Fotsis, M. Mann, *Nature* **1996**, *379*, 466-469.

[13] B. N. Pramanik, A. K. Ganguly, M. L. Gross, *Applied Electrospray Mass Spectrometry: Practical Spectroscopy Series*, Vol. 32, CRC Press, 2002.

[14] G. T. T. Gibson, S. M. Mugo, R. D. Oleschuk, *Mass Spectrometry Reviews* **2009**, *28*, 918-936.

[15] W. F. Smyth, P. Brooks, *Electrophoresis* **2004**, *25*, 1413-1446.

[16] S. Zuehlke, U. Duennbier, T. Heberer, *Chemosphere* **2007**, *69*, 1673-1680.

[17] W. F. Smyth, V. Rodriguez, *Journal of Chromatography A* **2007**, *1159*, 159-174.

[18] I. Eide, K. Zahlsen, *Energy & Fuels* **2007**, *21*, 3702-3708.

[19] S. D. Richardson, *Analytical Chemistry* **2008**, *80*, 4373-4402.

[20] K. Guo, C. Ji, L. Li, *Analytical Chemistry* **2007**, *79*, 8631-8638.

[21] N. B. Cech, C. G. Enke, *Mass Spectrometry Reviews* **2001**, *20*, 362-387.

[22] G. A. Valaskovic, N. L. Kelleher, F. W. McLafferty, *Science* **1996**, *273*, 1199-1202.

[23] N. Lion, T. C. Rohner, L. Dayon, I. L. Arnaud, E. Damoc, N. Youhnovski, Z.-Y. Wu, C. Roussel, J. Josserand, H. Jensen, J. S. Rossier, M. Przybylski, H. H. Girault, *Electrophoresis* **2003**, *24*, 3533-3562.

[24] R. D. Smith, K. Tang, Y. Shen, *Molecular BioSystems* **2006**, *2*, 221-230.

[25] K. O. Nagornov, M. V. Gorshkov, A. N. Kozhinov, Y. O. Tsybin, *Analytical Chemistry* **2014**, *86*, 9020-9028.

[26] M. Kubicek, S. M. Sanz-González, F. Verdeguer, V. Andrés, *Letters in Drug Design & Discovery* **2004**, *1*, 237-246.

[27] R. D. Smith, Y. Shen, K. Tang, *Accounts of chemical research* **2004**, *37*, 269-278.

[28] M. Wilm, M. Mann, *Analytical Chemistry* **1996**, *68*, 1-8.

[29] A. El-Faramawy, K. W. M. Siu, B. A. Thomson, *Journal of the American Society for Mass Spectrometry* **2005**, *16*, 1702-1707.

[30] A. Schmidt, M. Karas, T. Dulcks, *Journal of the American Society for Mass Spectrometry* **2003**, *14*, 492-500.

[31] W. Kim, M. Guo, P. Yang, D. Wang, *Analytical Chemistry* **2007**, *79*, 3703-3707.

[32] R. T. Kelly, J. S. Page, K. Tang, R. D. Smith, *Analytical Chemistry* **2007**, *79*, 4192-4198.

[33] W. Deng, J. F. Klemic, X. Li, M. A. Reed, A. Gomez, *Journal of Aerosol Science* **2006**, *37*, 696-714.

[34] K. Tang, Y. Lin, D. W. Matson, T. Kim, R. D. Smith, *Analytical Chemistry* **2001**, *73*, 1658-1663.

[35] R. T. Kelly, J. S. Page, Q. Luo, R. J. Moore, D. J. Orton, K. Tang, R. D. Smith, *Analytical Chemistry* **2006**, *78*, 7796-7801.

[36] B. Lojewski, W. Yang, H. Duan, C. Xu, W. Deng, *Aerosol Science and Technology* **2012**, *47*, 146-152.

[37] S. Su, G. T. T. Gibson, S. M. Mugo, D. M. Marecak, R. D. Oleschuk, *Analytical Chemistry* **2009**, *81*, 7281-7287.

[38] P. Russell, *Science* **2003**, *299*, 358-362.

[39] B. Rogers, G. T. T. Gibson, R. D. Oleschuk, *Electrophoresis* **2011**, *32*, 223-229.

[40] A. B. Daley, R. D. Wright, R. D. Oleschuk, *Analytica Chimica Acta* **2011**, *690*, 253-262.

[41] R. D. Oleschuk, M. Douma, *CA2714910A1*, 2011.

[42] L. Mats, G. T. T. Gibson, R. D. Oleschuk, *Microfluidics and Nanofluidics* **2014**, *16*, 73-81.

[43] P. J. A. Sazio, A. Amezcua-Correa, C. E. Finlayson, J. R. Hayes, T. J. Scheidemantel, N. F. Baril, B. R. Jackson, D.-J. Won, F. Zhang, E. R. Margine, V. Gopalan, V. H. Crespi, J. V. Badding, *Science* **2006**, *311*, 1583-1586.

[44] J. R. Sparks, P. J. A. Sazio, V. Gopalan, J. V. Badding, *Annual Review of Materials Research* **2013**, *43*, 527-557.

[45] Y. Fu, G. T. T. Gibson, R. D. Oleschuk, *Journal of Materials Chemistry* **2012**, *22*, 8208-8214.

[46] J. J. Thomson, *Philosophical Magazine (1798-1977)* **1911**, *20*, 752-767.

[47] E. De Hoffmann, V. Stroobant, *Mass spectrometry: principles and applications*, Wiley-Interscience, 2007.

[48] J. Fenn, *Journal of Biomolecular Techniques: JBT* **2002**, *13*, 101.

[49] S. Borman, Russell H., Siuzdak G., *Today's Chemist at Work* **2003**, 47-49.

[50] http://nobelprize.org/nobel_prizes/chemistry/laureates/2002/.

[51] J. B. Fenn, *Angewandte Chemie, International Edition* **2003**, *42*, 3871-3894.

[52] R. Knochenmuss, *Analyst* **2006**, *131*, 966-986.

[53] J. Zeleny, *Physical Review* **1914**, *3*, 69-91.

[54] M. Yamashita, J. B. Fenn, *Journal of Physical Chemistry* **1984**, *88*, 4451-4459.

[55] P. Kebarle, L. Tang, *Analytical Chemistry* **1993**, *65*, 972A-986A.

[56] P. Kebarle, U. H. Verkerk, *Mass Spectrometry Reviews* **2009**, *28*, 898-917.

[57] M. Wilm, *Molecular & Cellular Proteomics* **2011**, *10*, M111. 009407.

[58] P. Liuni, D. J. Wilson, *Expert Review of Proteomics* **2011**, *8*, 197-209.

[59] B. A. Thomson, J. V. Iribarne, *Journal of Chemical Physics* **1979**, *71*, 4451-4463.

[60] E. Ahadi, L. Konermann, *Journal of Physical Chemistry B* **2012**, *116*, 104-112.

[61] L. Konermann, E. Ahadi, A. D. Rodriguez, S. Vahidi, *Analytical Chemistry* **2013**, *85*, 2-9.

[62] M. S. Wilm, M. Mann, *International Journal of Mass Spectrometry and Ion Processes* **1994**, *136*, 167-180.

[63] M. Karas, U. Bahr, T. Dulcks, *Fresenius' Journal of Analytical Chemistry* **2000**, *366*, 669-676.

[64] E. J. Want, A. Nordström, H. Morita, G. Siuzdak, *Journal of proteome research* **2007**, *6*, 459-468.

[65] K. L. Smith, M. S. Alexander, J. P. W. Stark, *Physics of Fluids* **2006**, *18*, 092101-092107.

[66] C. N. Ryan, K. L. Smith, M. S. Alexander, J. P. W. Stark, *Journal of Physics D Applied Physics* **2009**, *42*, 155501-155508.

[67] G. A. Valaskovic, N. L. Kelleher, D. P. Little, D. J. Aaserud, F. W. McLafferty, *Analytical Chemistry* **1995**, *67*, 3802-3805.

[68] M. T. Davis, D. C. Stahl, S. A. Hefta, T. D. Lee, *Analytical Chemistry* **1995**, *67*, 4549-4556.

[69] W. Xiong, J. Glick, Y. Lin, P. Vouros, *Analytical Chemistry* **2007**, *79*, 5312-5321.

[70] E. P. Maziarz, S. A. Lorenz, T. P. White, T. D. Wood, *Journal of the American Society for Mass Spectrometry* **2000**, *11*, 659-663.

[71] T. D. Wood, M. A. Moy, A. R. Dolan, P. M. Bigwarfe, Jr., T. P. White, D. R. Smith, D. J. Higbee, *Applied Spectroscopy Reviews* **2003**, *38*, 187-244.

[72] T. R. Covey, D. Pinto, *Practical Spectroscopy Series* **2002**, *32*, 105-148.

[73] J. Fernandez de la Mora, I. G. Loscertales, *Journal of Fluid Mechanics* **1994**, *260*, 155-184.

[74] K. L. Smith, M. S. Alexander, J. P. W. Stark, *Journal of Applied Physics* **2006**, *100*, 014901-014906.

[75] K. L. Smith, M. S. Alexander, J. P. W. Stark, *Journal of Applied Physics* **2006**, *99*, 064901-064908.

[76] I. Marginean, R. T. Kelly, D. C. Prior, B. L. LaMarche, K. Tang, R. D. Smith, *Analytical Chemistry* **2008**, *80*, 6573-6579.

[77] L. Parvin, M. C. Galicia, J. M. Gauntt, L. M. Carney, A. B. Nguyen, E. Park, L. Heffernan, A. Vertes,

Analytical Chemistry **2005**, *77*, 3908-3915.

[78] S. Su, in *Chemistry*, Vol. Ph.D.Thesis, Queen's University, Kingston 2008.

[79] G. Vazquez, E. Alvarez, J. M. Navaza, *Journal of chemical and engineering data* **1995**, *40*, 611-614.

[80] R. T. Kelly, J. S. Page, R. Zhao, W.-J. Qian, H. M. Mottaz, K. Tang, R. D. Smith, *Analytical Chemistry* **2008**, *80*, 143-149.

[81] T. C. Poon, P. J. Johnson, *Clinica chimica acta* **2001**, *313*, 231-239.

[82] M. Emmett, R. Caprioli, *Journal of the American Society for Mass Spectrometry* **1994**, *5*, 605-613.

[83] J. H. Wahl, D. R. Goodlett, H. R. Udseth, R. D. Smith, *Analytical Chemistry* **1992**, *64*, 3194-3196.

[84] J. Liu, K. W. Ro, M. Busman, D. R. Knapp, *Analytical Chemistry* **2004**, *76*, 3599-3606.

[85] H. Tojo, *Journal of Chromatography, A* **2004**, *1056*, 223-228.

[86] Y. S. Choi, T. D. Wood, *Rapid Communications in Mass Spectrometry* **2007**, *21*, 2101-2108.

[87] C. G. Zampronio, A. E. Giannakopulos, M. Zeller, E. Bitziou, J. V. Macpherson, P. J. Derrick, *Analytical Chemistry* **2004**, *76*, 5172-5179.

[88] D. R. Smith, M. A. Moy, A. R. Dolan, T. D. Wood, *Analyst* **2006**, *131*, 547-555.

[89] G. S. Jackson, C. G. Enke, *Analytical Chemistry* **1999**, *71*, 3777-3784.

[90] M. Chen, K. D. Cook, *Analytical Chemistry* **2007**, *79*, 2031-2036.

[91] M. Wetterhall, O. Klett, K. E. Markides, L. Nyholm, J. Bergquist, *Analyst* **2003**, *128*, 728-733.

[92] S. Nilsson, M. Wetterhall, J. Bergquist, L. Nyholm, K. E. Markides, *Rapid Communications in Mass Spectrometry* **2001**, *15*, 1997-2000.

[93] M. Wetterhall, S. Nilsson, K. E. Markides, J. Bergquist, *Analytical Chemistry* **2002**, *74*, 239-245.

[94] R. D. Oleschuk, D. J. Harrison, *Trends in Analytical Chemistry* **2000**, *19*, 379-388.

[95] Q. Xue, F. Foret, Y. M. Dunayevskiy, P. M. Zavracky, N. E. McGruer, B. L. Karger, *Analytical Chemistry* **1997**, *69*, 426-430.

[96] H. Liu, C. Felten, Q. Xue, B. Zhang, P. Jedrzejewski, B. L. Karger, F. Foret, *Analytical Chemistry* **2000**, *72*, 3303-3310.

[97] L. Dayon, M. Abonnenc, M. Prudent, N. Lion, H. H. Girault, *Journal of Mass Spectrometry* **2006**, *41*, 1484-1490.

[98] S. Koster, E. Verpoorte, *Lab on a Chip* **2007**, *7*, 1394-1412.

[99] R. T. Kelly, A. V. Tolmachev, J. S. Page, K. Tang, R. D. Smith, *Mass Spectrometry Reviews* **2010**, *29*, 294-312.

[100] Y. Tatemoto, R. Ishikawa, M. Takeuchi, T. Takeshita, K. Noda, T. Okazaki, *Chemical Engineering & Technology* **2007**, *30*, 1274-1279.

[101] J. S. Page, R. T. Kelly, K. Tang, R. D. Smith, *Journal of the American Society for Mass Spectrometry* **2007**, *18*, 1582-1590.

[102] J. D. Regele, M. J. Papac, M. J. A. Rickard, D. Dunn-Rankin, *Journal of Aerosol Science* **2002**, *33*, 1471-1479.

[103] R. Bocanegra, D. Galan, M. Marquez, I. G. Loscertales, A. Barrero, *Journal of Aerosol Science* **2005**, *36*, 1387-1399.

[104] S. B. Q. Tran, D. Byun, V. D. Nguyen, H. T. Yudistira, M. J. Yu, K. H. Lee, J. U. Kim, *Journal of Electrostatics* **2010**, *68*, 138-144.

[105] W. Deng, C. M. Waits, B. Morgan, A. Gomez, *Journal of Aerosol Science* **2009**, *40*, 907-918.

[106] W. Deng, A. Gomez, *Journal of Aerosol Science* **2007**, *38*, 1062-1078.

[107] P. Mao, R. Gomez-Sjoberg, D. Wang, *Analytical Chemistry* **2013**, *85*, 816-819.

[108] P. Mao, H.-T. Wang, P. Yang, D. Wang, *Analytical Chemistry* **2011**, *83*, 6082-6089.

[109] R. T. Kelly, J. S. Page, I. Marginean, K. Tang, R. D. Smith, *Analytical Chemistry* **2008**, *80*, 5660-5665.

[110] J. S. Page, K. Tang, R. T. Kelly, R. D. Smith, *Analytical Chemistry* **2008**, *80*, 1800-1805.

[111] I. Marginean, J. S. Page, A. V. Tolmachev, K. Tang, R. D. Smith, *Analytical Chemistry* **2010**, *82*, 9344-9349.

[112] J. T. Cox, I. Marginean, R. T. Kelly, R. D. Smith, K. Tang, *Journal of the American Society for Mass Spectrometry* **2014**, *25*, 2028-2037.

[113] J. T. Cox, I. Marginean, R. D. Smith, K. Tang, *Journal of the American Society for Mass Spectrometry* **2015**, *26*, 55-62.

[114] A. S. Cerqueira, Jr., *Reports on Progress in Physics* **2010**, *73*, 024401-024421.

[115] X. Feng, Z. Jin, *Macromolecules* **2009**, *42*, 569-572.

[116] C. R. Martin, *Science* **1994**, *266*, 1961-1966.

[117] R. J. Tonucci, B. L. Justus, A. J. Campillo, C. E. Ford, *Science* **1992**, *258*, 783-785.

Chapter 2 Fabrication of a Polymer Nozzle Array on Commercial Microstructured Fibers as Nanoelectrospray Emitters

2.1 Overview

Electrospray ionization (ESI), and its lower flow analog nanoelectrospray ionization (nano-ESI) are soft ionization methods (*i.e.* they introduce minimal molecular fragmentation upon ionization) and are indispensable to mass spectrometry (MS) for the analysis of macromolecules.[1] The shift to the lower flow rates associated with nano-ESI-MS has afforded greater sensitivity through improved ionization efficiency due to smaller initial droplets formation, and has the additional benefit of reduced solvent and sample consumption.[2] A trade-off however, is reduced sample throughput since the sample is slowly delivered to the nanoelectrospray emitter and decreased method robustness. Additionally, widely used, single-tip tapered nanoelectrospray emitters with less than 20 μm diameter apertures often encounter problems such as frequent clogging and larger flow resistance due to the nature of the small aperture.[3]

In the interest of further enhancing sensitivity and signal, while allowing for faster analysis with more robust emitter, the flow can be split into multiple individual electrosprays from multiple emitters. In particular, if fluid at a given flow rate is split into "*n*" channels, each leading to independent electrosprays, the current arising from the overall electrospray is enhanced by a factor of $\sqrt{n}$ relative to a single electrospray at that flow rate.[4] Enhanced spray current results from converting a large flow into a number of small streams, which produce smaller droplets increasing ionization efficiency without changing the total volumetric flow rate. So-called multiple electrospray (MES) emitters

have been fabricated for this purpose in several ways by machining and microfabrication[5, 6] or by assembling a number of individual stainless steel or fused silica capillaries.[7, 8] MES emitters produced using these methods have been cumbersome or non-compact, and have presented disadvantages when used with conventional analytical separation methodologies.

For mass spectrometric applications particularly, the MES emitters need to be as compact as possible since the circular orifice of a mass spectrometer is small (typically <1 mm), otherwise any gains in spray current from the emitter are wasted as most the electrospray plume cannot get through or be collected by the orifice to increase analyte signal. Microstructured fibers (MSFs) embody this emitter requirement, which have all channels built into the same fiber with an outer diameter compatible with standard capillary connections. MSFs are a relatively new class of fiber optic materials that confine light through a periodic array of microscopic air-filled cladding channels which surround either a solid or hollow core waveguide, and traverse the entire fiber length.[9] MSFs are typically fabricated by constructing a preform at the macro scale, either by drilling holes in a cylinder or by stacking a series of tubes and rods in a desired pattern, and then drawing the preform at high temperature down to a thin fiber having the same feature proportions as the preform. In this way, the dimensions of the macroscopic preform are eventually reduced by 10^4 or more, and the resulting micron-sized channels and patterns of the MSFs are consistent and precisely controlled.[10, 11] Since their invention, MSFs have been used in a number of applications ranging from telecommunications to optical sensing and imaging.[12]

When used as electrospray emitters, unmodified MSFs were found to operate with a similar signal as commercial tapered emitters, but with superior clogging resistance, flow

rate range, and long-term spray stability because of the large number of channels.[13] Despite the distinct channels, however, the fluid passing through the MSF always wet the tip surface and generated a single Taylor cone, even when the silica at the tip face was modified with a trimethylsilyl moiety to render it hydrophobic, thus no significant enhancement of the spray current was observed. In order to isolate the channels, then, forming nozzles at their exit, raised above the tip face, would be necessary to prevent tip surface wetting and promote individual electrosprays. Such an emitter would have the advantage of enhanced signal intensity at a given flow rate, along with fiber dimensions fully compatible with conventional LC and MS instrumentation.

To fabricate the nozzles, polymer tubes are first formed by *in-situ* polymerization within the channels of a MSF, and then the polymer tubes protrude from the tip of the MSF emitter after the surrounding silica channels are partially etched away.[14] Known as porous layer open tubular (PLOT) chromatography, polymer layers such as this have been formed in single-tube capillaries for many years.[15] In this chapter, polymerization and etching conditions are optimized and investigated for the production of a uniform polymer nozzle array on a typical commercial MSF as nanoelectrospray emitters which show good ESI performance and comparable stability to that of the standard tapered electrospray emitter.

2.2 Experimental

2.2.1 Reagents and Materials

All reagents and materials used in this chapter are listed as follows: Glacial acetic acid, methanol, acetonitrile (HPLC grade) and deionized water (Protocol®) were purchased from Fisher Scientific (Ottawa, ON, Canada) and used without further purification. Formic

acid (analytical reagent, 98%) was purchased from BDH Chemicals (Toronto, ON, Canada). Leucine enkephalin (LE, **1**) (synthetic acetate salt), 3-(trimethoxysilyl)propyl methacrylate (γ-MPS, **2**) (98%), styrene (ReagentPlus®) (≥99%), divinylbenzene (technical grade, 80%, mixture of isomers), hydrofluoric acid (48 wt% in water, ≥99.99%), and 2,2'-azobisisobutyronitrile (AIBN, **3**) (≥98%) were purchased from Aldrich (Oakville, ON, Canada). Anhydrous ethyl alcohol was purchased from Commercial Alcohols (Toronto, ON, Canada). Crystalbond™ was purchased from Aremco Products Inc (Valley Cottage, NY, USA). Saturated ammonium bifluoride (AF) (20 wt% in water) was prepared from the solid ammonium hydrogen difluoride (reagent grade, 95%), which was purchased from Aldrich (Oakville, ON, Canada). Electrospray solvents were degassed in an ultrasonic bath for 20 minutes and filtered prior to use. A commercial microstructured fiber (MSF) was purchased from NKT Photonics (Birkerød, Denmark), with 126 channels (product numbers LMA-20) in a hexagonal pattern.

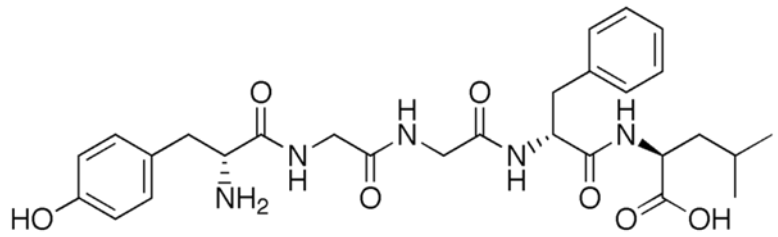

1

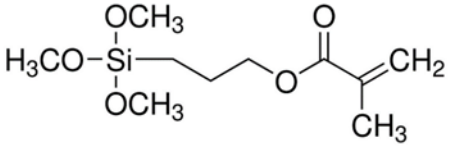

2

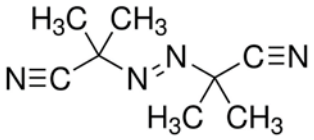

3

2.2.2 Synthesis of polymer nozzles in a MSF

For a general idea of the procedures for fabrication polymer nozzles in the channels

of a MSF, see Figure 2.1. The nozzles are fabricated using four fabrication steps and the representative scanning electron microscopy (SEM) images of a single channel at each step are also inset in this figure. Step A: MSFs were flushed with 0.1 M NaOH (aq.) for 1 hour with a syringe pump (Harvard Apparatus 11plus, Holliston, MA, USA) at a flow rate of 2-3 μL/min to expose surface silanol groups for a more homogeneous surface and for subsequent reaction with silanizing reagents.[16] As shown in Figure 2.2A, a syringe (3 mL, Monoject) with was filled with a solution and attached to a MSF via a Luer lock fitting (Upchurch Scientific) to introduce the solution into the channels of the MSF. The residual alkaline solution in the MSFs was neutralized by flushing with 0.1 M HCl (aq.) for 1 hour and deionized water for 1 hour. The pH of the eluted solution was monitored with litmus paper to ensure neutralization/acidification.

Step B: The inner walls of the MSFs were then functionalized with vinyl groups using a pre-treatment procedure described previously.[17] Briefly, the MSFs were filled with a solution of γ-MPS (20% v/v), deionized water (50% v/v), and glacial acetic acid (30% v/v) using a syringe pump, and then each end was immersed in the solution and left filled overnight (~16 hours) to optimize surface coverage. Afterward, the MSFs were flushed with acetonitrile (ACN) (95% in water) using an HPLC pump (Series 1500, Supercritical Fluid Technologies Inc.) to remove any unreacted γ-MPS and could then be used directly or stored (filled with the flushing solution) until needed.

Step C: The procedure for the formation of a polymer tube in MSFs was adapted from studies on coated capillaries for open-tubular capillary LC based on free-radical polymerization.[15] Briefly, an ultrasonically degassed solution composed of 20% monomer (styrene), 20% crosslinker (divinylbenzene (DVB)), 60% porogen (anhydrous ethanol),

and 5 mg initiator (AIBN, 0.5% w/v) was pumped into the pretreated MSF using a syringe pump for sufficient time to ensure that every channel was filled. Both ends of the MSF were sealed with gas chromatography injection septa (Supelco Thermogreen 9.5 mm, Bellefonte, PA, USA), and the MSF was heated in an oven (Isotemp Vacuum Oven Model 281A, Fisher Scientific) at 80 ^{o}C overnight. The MSF, now containing poly(styrene-divinylbenzene) layer in each channel, was then flushed with ACN (95% in water) by the HPLC pump to remove any residual polymerization reagents.

Step D: The long MSFs with polymer tubes were cut into ~4 cm-long pieces as emitters using a ceramic cleaving stone or a precision fiber cleaver (LDC-400) (Vytran LLC, Morganville, NJ, USA). The pieces were immersed in ACN for 2 minutes, which softens the acrylate polymer that typically coats commercial MSFs and allows it to be easily removed. One end of the fiber was then immersed in the etchant, either saturated aqueous AF or 48 wt% hydrofluoric acid (HF), to etch the silica channels and expose the polymer nozzles. This was accomplished using a PEEK capillary fitting with a fluoropolymer sleeve to hold the MSF in place as it is held in a microcentrifuge tube containing <300 μL of etchant, as shown in Figure 2.2B. Finally, the etched end of the fiber was immersed in deionized water to remove the etchant and any debris from the fiber end.

2.2.3 Imaging

During each fabrication step, the morphology of the MSFs could be visualized from a top view and/or side view at 400x-1000x magnification on an optical microscope (Nikon Eclipse ME600) and photographs were taken with a Nikon Coolpix 990 digital camera.

To further inspect and measure the dimensions of the MSFs, the samples were mounted normally on the aluminum stub using tape to facilitate imaging of the cross-section and subsequently coated with a layer of gold to render the samples conductive by a Hummer sputtering system (Anatech Ltd., Hayward, CA, USA). SEM images were obtained using either a Jeol JSM-840 Scanning Electron Microscope (Tokyo, Japan) or a FEI-MLA Quanta 650 Field Emission Gun-Environmental Scanning Electron Microscope (Hillsboro, OR, USA).

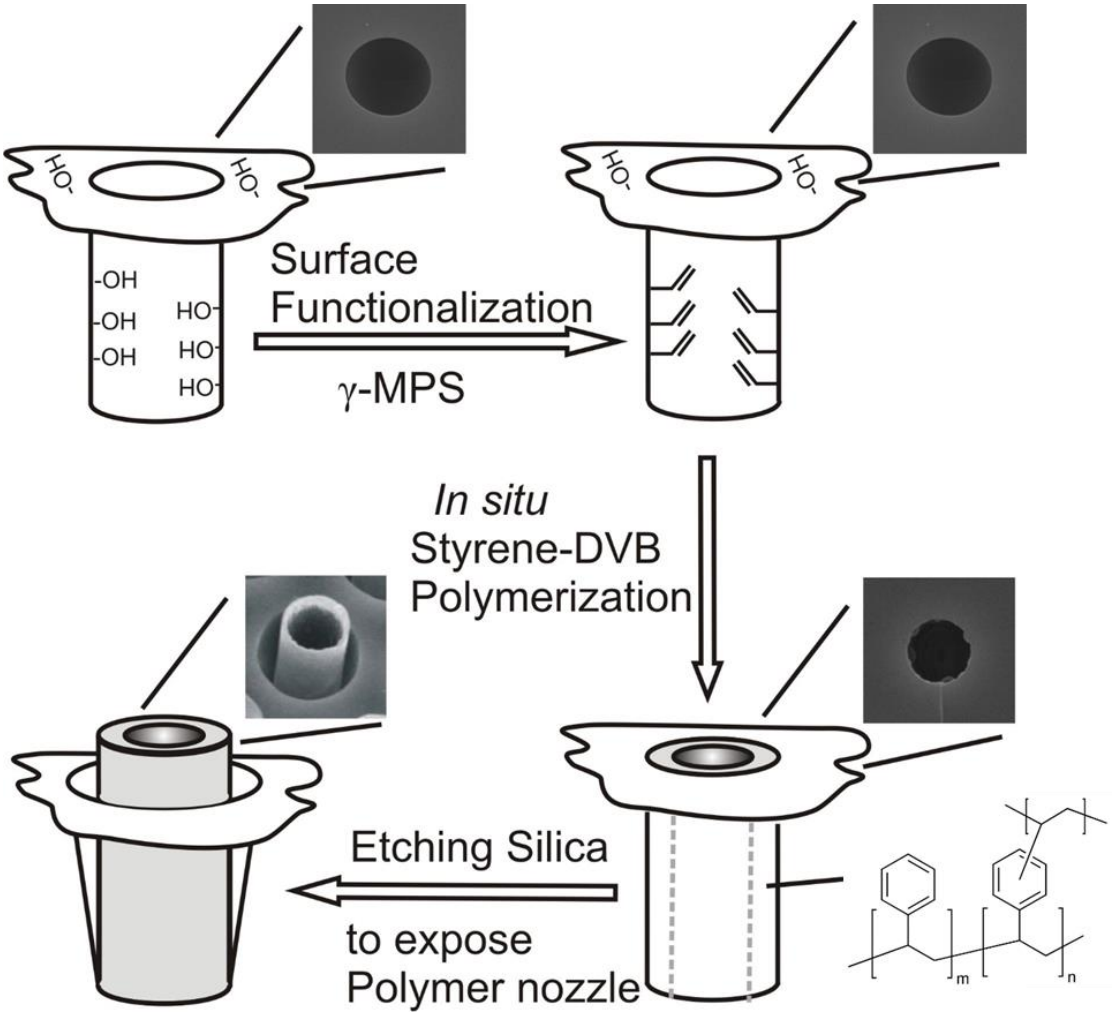

Figure 2.1 Schematic showing the fabrication PS-DVB nozzles in the channels of a MSF, and representative SEM image of a single channel at each step (inset).

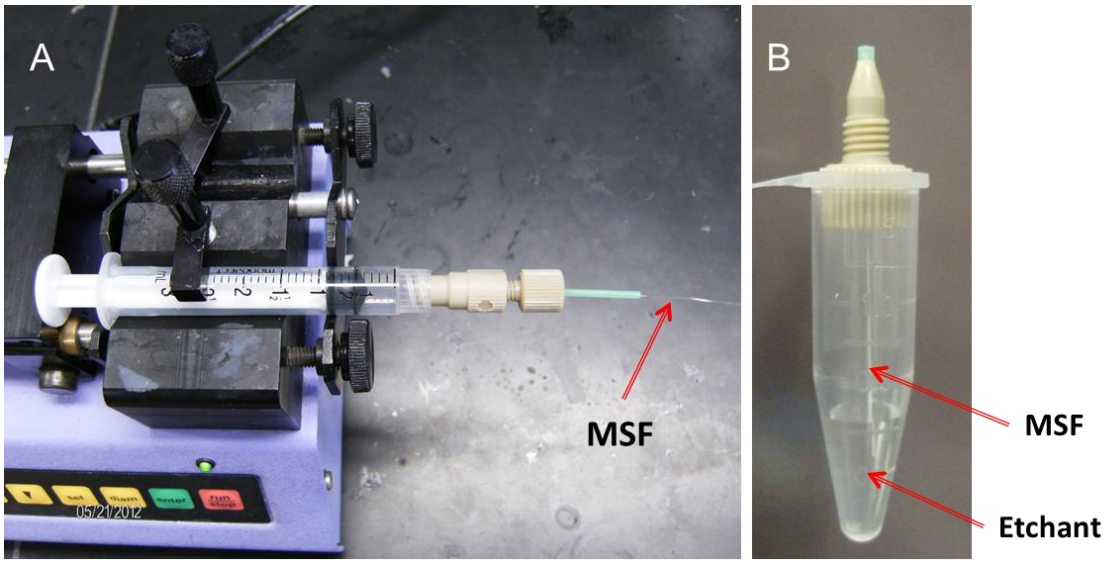

Figure 2.2 A) Photograph showing the introduction of a solution into the channels of a MSF using a syringe pump; B) Photograph showing the etching of a piece of MSF in an etchant contained in a microcentrifuge tube.

2.2.4 Offline electrospray

The electrospray behaviour of the multi-nozzle emitters was observed by *in-situ* microscope imaging and electrospray current measurement, the setup for which is shown in Figure 2.3. The spray solvent was composed of 79.2% water and 19.8% methanol and contained 1% acetic acid (v/v). The flow was generated using a prototype nano-flow gradient pump kindly provided by Upchurch Scientific (IDEX Health & Science LLC, Oak Harbor, WA, USA). Standard capillary tubing (Polymicro Technologies, Phoenix, AZ, USA) was used to connect the pump to the emitter, through a MicroTee (IDEX Health & Science LLC; Oak Harbor, WA, USA). Electrospray was generated via the MicroTee using a liquid junction with a platinum wire electrode, through which positive voltage was applied. The MicroTee was fixed such that the emitter was held in a horizontal position, facing toward an aluminum block electrode, which acted as the ground. The grounded electrode and the MicroTee were placed on the stage of an inverted microscope (Nikon

Eclipse Ti-S, Nikon Canada, Mississauga, ON, Canada), such that the objective was below them, looking up at the tip of the emitter. A transparency was positioned just above the stage to protect the objective lens from solvent and electrical arcing during experiments. The emitter tip was measured to be 2 ± 0.3 mm from the ground electrode by the Z-displacement of the microscope stage between the electrode being in focus and the tip being in focus. Images and videos were captured using a Nikon DS digital camera. Voltage for electrospray was supplied by a TriSep 2100 high-voltage module (Unimicro Technologies, Pleasanton, CA, USA). A Keithley 6485 picoammeter (Keithley Instruments Inc., Cleveland, OH, USA) was connected in this circuit. Current measurements consisted of averaging signals taken every 300 milliseconds for at least 5 minutes, the reported error being the standard deviation of this mean.

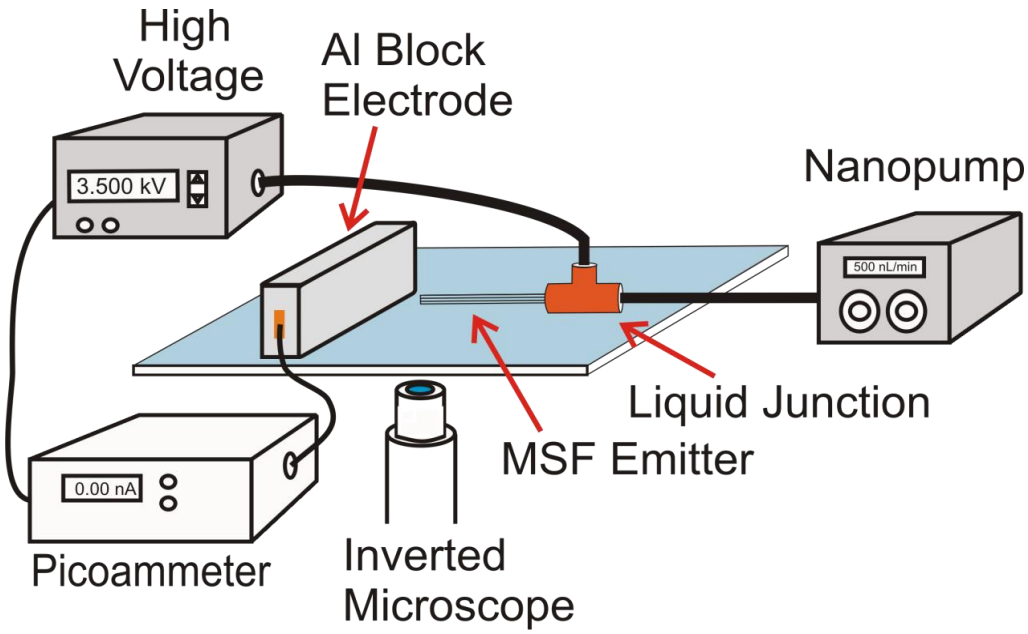

Figure 2.3 Schematic diagram showing the electrical current measurement/spray imaging apparatus for an offline electrospray test.

2.2.5 Online electrospray

Mass spectra were acquired over 400 to 800 amu (atomic mass units) on an API 3000 triple-quadrupole mass spectrometer (AB Sciex, Concord, ON, Canada) equipped with a nanospray interface (Proxeon, Odense, Denmark) and two CCD cameras to aid in positioning the micro-tee with an x-y-z stage. The first quadrupole (Q_1) was used for the MS full scan. The setup of electrospray ion source is shown in Figure 2.4. Voltage was applied to the micro-tee as described for offline experiments, and flow was provided by a nano-LC pump (Eksigent, AB Sciex). The curtain gas (99.998% pure N_2) flow rate was set at 0.3 L/min and both the declustering potential and focusing potential were kept at 60 V and 250 V, respectively. Quadrupole peak width (set to yield unit mass resolution of 0.7 amu at FWHM) and scan time (one spectrum per second, 1 Hz) were kept constant for all experiments. No additional desolvation methods were employed.

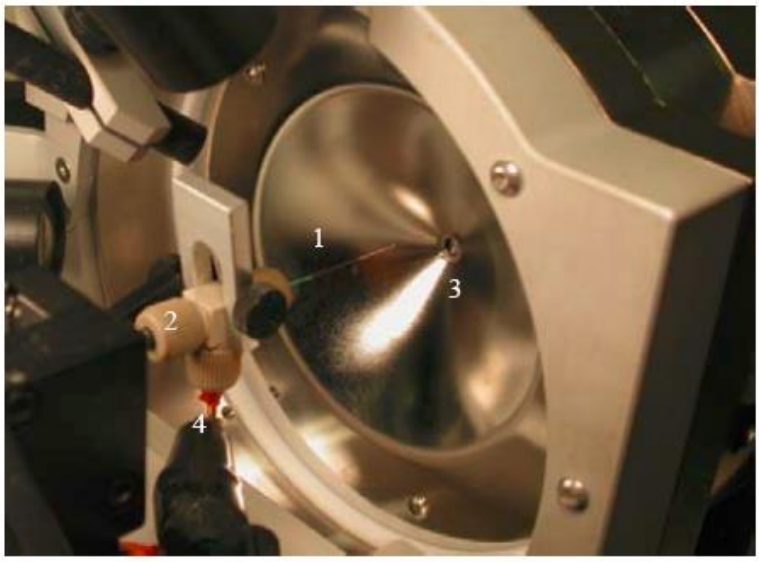

Figure 2.4 The configuration of electrospray ion source.[13]

2.3 Results and discussion

2.3.1 The architecture of MSF emitters

SEM images (Figure 2.5) show the cross-section of a commercial MSF investigated as a nanoelectrospray emitter. The commercial MSF (shown in Figure 2.5A with acrylate jacket/coating removed) has 126 independent channels arranged in a hexagonal pattern. The outer diameter of the MSF (~230 μm) can be easily matched with standard fluidic fittings and directly coupled to a liquid delivery pump (such as a syringe pump or higher pressure pumps used with typical nano-LC fluidic systems), allowing a facile way of introducing/pumping electrospray solvents or other reactants into the channels of the MSF. The Figure 2.5B shows that the fiber has a channel diameter of 5.58 ± 0.07 μm and the pitch (distance between adjacent air channels in the lattice[12]) of the channels is ~12.3 μm (12.28 ± 0.09 μm).

The channel dimension is consistent with the typical aperture sizes of tapered emitters used for flow rates as low as a few 10's of nL/min. This type of MSF emitter has the benefit of providing a much higher density of channels which could potentially translate into further enhanced spray current. It was found that minimization of edge effects is crucial for good emitter performance based on previous experiences developing non-tapered nanoelectrospray emitters.[18] Several capillary cutting methods were employed, and among them a precision fiber cleaver provided the best performance due to maintaining the integrity of the microstructured cladding. However, small cleavage artifacts at the tip face are not expected to significantly alter flow and electrospray characteristics.

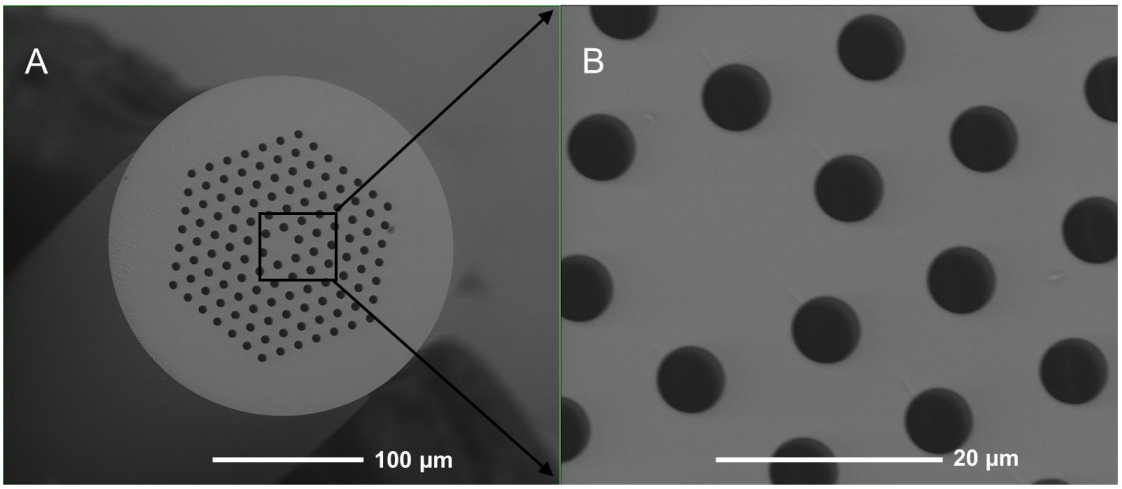

Figure 2.5 SEM images showing the cross-section of a commercial MSF with 126 channels in a hexagonal pattern at A) 400x magnification and B) 3000x magnification. Outer diameter of the MSF is ~230 µm and channel diameter is ~5.6 µm.

2.3.2 Optimizing fabrication conditions for MSF emitters with polymer nozzles

From early experiments it was clear that the fabrication process required optimization. As shown in Figure 2.6, polymer tubes were protruding from the surface of the etched end of the MSF based on the general fabrication procedures described on the section 2.2.2, but their protrusion length was not uniform and the inner wall of the polymer tubes contained nodules that could impede flow.[14] The channel diameter of the template MSF (~5.6 µm) expanded about 70% (~9.7 µm) following saturated AF etching of the tip, indicating that etching also occurred from inside the channels. As the morphology of an electrospray emitter tip significantly impacts its performance, several aspects of the fabrication process were optimized.

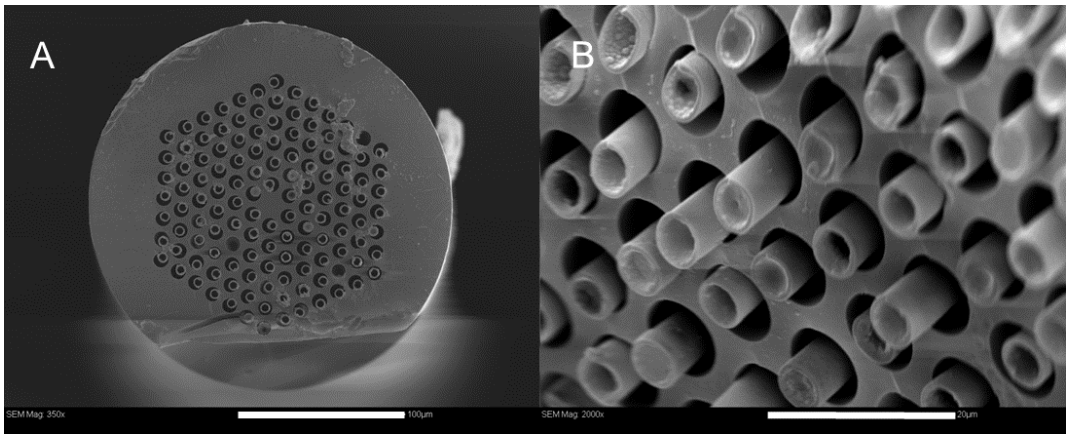

Figure 2.6 SEM images of a MSF emitter with polymer nozzles fabricated under general procedures from a top view A), and the nozzles from an enlarged tilt view B). Scale bar is 100 µm in image A, and is 20 µm in image B.[14]

2.3.2.1 Etching investigation

The function of the etchant is to chemoselectively react with the silica in order to remove the silica template from around the inert polymer tubes within its channels. When done only for a short time at the tip of the tube-containing MSF, the tubes will protrude from the surface and become nozzles from which liquid can be delivered, such as in ESI. Wet chemical etching in this way is an often-used, highly-controlled reaction that can provide homogeneous smooth surfaces. Etchants based on fluoride are well known to be selective for the etching of silica.[19, 20]

HF is the most commonly used for etching silica, but its toxicity led to the selection of AF for initial experiments, which is less threatening to human health but etches less quickly.[21, 22] The channels of the MSF were found to expand, however, due to etching from the channel outward. To investigate whether this effect was dependent on etching time, the faster etchant (HF, 48% (aq.)) was used for comparison. Between these two etchants for the etching of silica at the tip of MSFs, however, the morphology of the tip was identical, indicating that the mechanism of etching by both etchants is the same and that the channel

expansion rate is proportional to etching rate. In fact, a MSF etched for 12 minutes with AF was indistinguishable from one etched with HF for 1 minute. The similarity in etching between AF and HF is not surprising as these two etchants are in equilibrium in aqueous solutions and both are involved in the etching mechanism.[19] In the interest of time, HF was used for all further experiments.

In the etching of a MSF containing polymer tubes, the etchant uniformly removes silica from the tip face to reveal the polymer tubes raised above the tip surface. Etching occurs at the same rate from the outside of the fiber to reduce the outer diameter accordingly, and from the channel walls to increase the diameter of each channel accordingly. Presented in Figure 2.7 is a series of SEM images representing HF etching times explored from 30 seconds to 8 minutes. As the etching time increases, the linear depth of silica removal is proportional to etching time, as the reaction rate is not changing (HF concentration is high and reaction conditions do not significantly change during the reaction). The rate of silica loss between channels is the same as that from the tip face downward, but this etching has much greater impact on the tip morphology, as the distance between channels (the pitch) is relatively small. When the etching time is just 30 seconds, only a small part of the silica channels were etched away, leaving a pit around the polymer tubes. Therefore, no effective polymer nozzles were developed except a couple of abnormal ones (Figure 2.7A). By 2 minutes etching time (Figure 2.7C), the silica separating adjacent channels is gone and polymer nozzles are beginning to contact each other, while the tip face is only reduced by 6.1 μm (the pitch divided by 2). This means that the nozzles would protrude from the tip face a maximum of ~6 μm before nozzles interfere with each other, which puts a limit on the nozzle length for this type of MSF. As the etching time increases, the silica that makes

up the body of the MSF is removed linearly from the tip face and from the exterior, while the etchant continues to penetrate the thin silica walls between polymer tubes, leaving an array of free nozzles surrounded by an outer silica tube (Figure 2.7D and 2.7E). Eventually, the outer silica tube is etched away (by silica removal from either side), leaving an exposed array of long polymer nozzles (Figure 2.7F). The optimal etching time using 48% HF (aq.) was chosen to be 1 minute (Figure 2.7B), where nozzles protrude as far as possible while still confined to their channels.

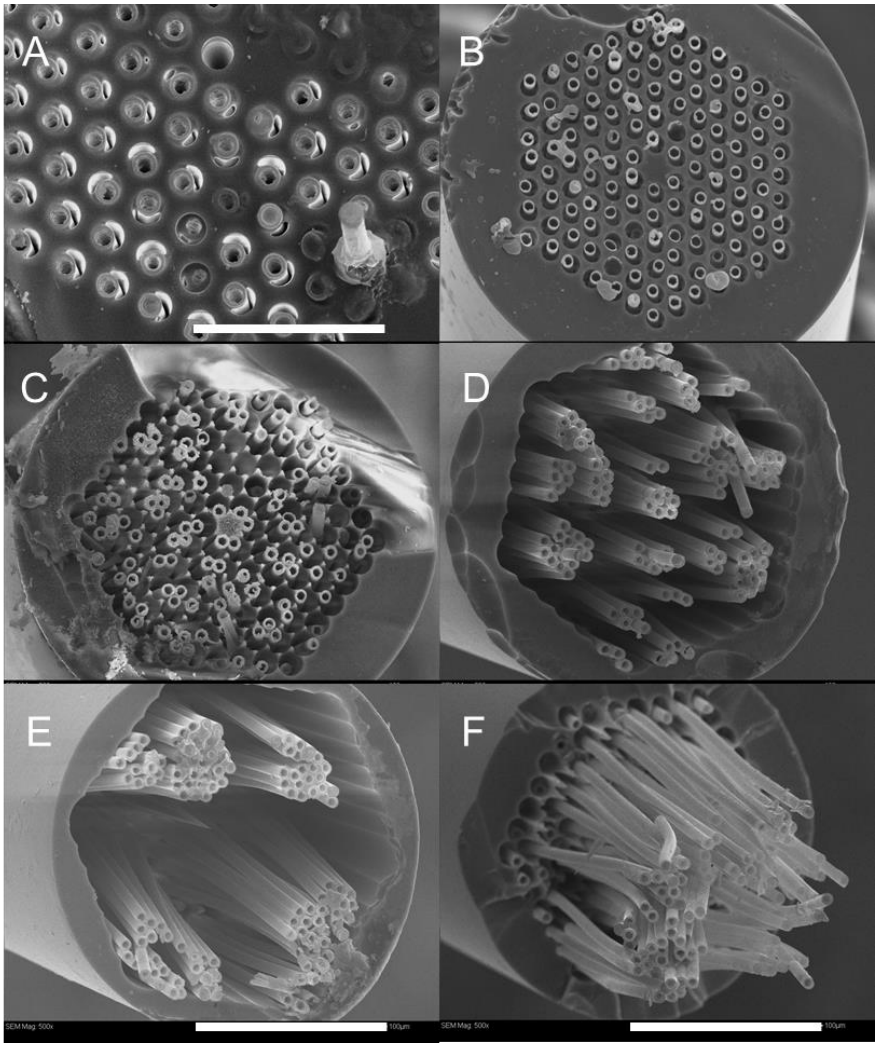

Figure 2.7 SEM images of MSFs containing polymer tubes after etching with HF for: A) 30 seconds (1000x magnification); B) 1 minute; C) 2 minutes; D) 4 minutes; E) 6 minutes and F) 8 minutes (500x magnification).

Ideally, the channels would not expand in this way during etching, where the tip face would be removed only in the axial direction allowing much better control over polymer nozzle length, the limit being set by the loss of silica from the fiber exterior inward. With the polymer tubes being chemically connected to the channel walls via γ-MPS (ultimately a Si-C linkage), this type of etching mechanism was anticipated. However, it became apparent that etchant was able to freely reach the silica of the channel walls and begin etching there. In fact, further examination suggested that etching along the silica-polymer interface may have been preferred. Using an optical microscope, the depth of etching in a given channel is observable from the side view as the expected "V" shape of the channel, as shown in Figure 2.8. The depth to which the trough surrounding the nozzles goes (the length of the "V" from the tip face) is much greater than the protrusion length of the polymer nozzles (which indicates bulk etching rate). This observation means that the etchant is able to penetrate the silica-polymer interface faster than it can etch through bulk silica, either by selectively etching at that interface or by accessing the channel walls through the polymer tube.

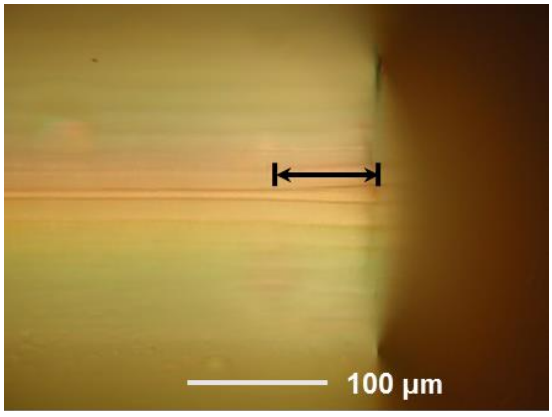

Figure 2.8 Optical microscope image of a MSF with polymer nozzles having been etched by HF for 1 minute, the double arrow line indicating the depth of etching as judged by the length of the channel that shows diameter expansion, from the tip face to the point where the channel diameter is uniform.

To explore the possibility of access through the polymer tube, the tubes were filled with Crystalbond™, a polyester that melts at about 120 ºC and is insoluble in water but easily removed in acetone. By filling the polymer tubes, access to the MSF silica through the tube wall is thoroughly blocked. The results after etching showed that whether the tubes were filled or not had no effect on the etching mechanism (see Figure 2.9), leading to the conclusion that etchant was not passing through the polymer tubes. Similar results were found when the tubes were filled with a non-volatile hydrophobic solvent such as 1-dodecanol instead of Crystalbond™.

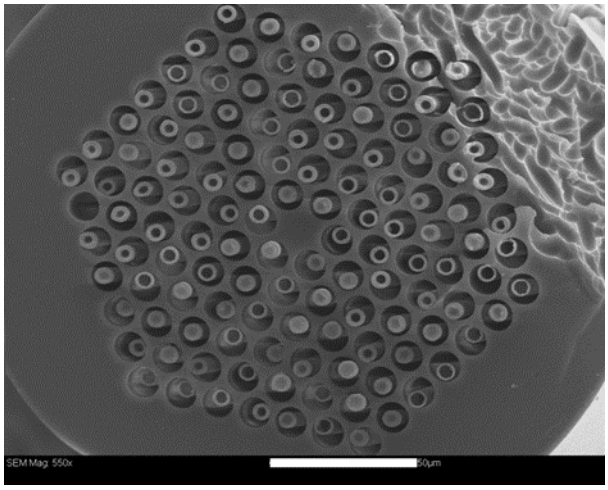

Figure 2.9 SEM image of a MSF with polymer tubes etched in HF for 1 minute while being filled with Crystalbond,™ a polyester used to block access to the channel walls by the etchant, the Crystalbond™ having been removed using acetone. Scale bar is 50 µm.

Another strategy was devised to investigate the etching process, whereby the etchant was passed through the polymer tubes in a MSF. Using plastic fittings and sleeves, AF solution was injected into one end of a 4-cm long MSF and collected from the opposite end, where etchant must travel only through the polymer tubes. After flowing for 12 minutes, the MSF was flushed with water. The MSF was then cleaved in the middle to examine the channels and tubes far from the point of injection. A SEM image of each cross-

section of that cleave is shown in Figure 2.10. Interestingly, the channels of the MSF were not found to have expanded to any appreciable extent, as the etchant was not present at that penetrated depth for long enough. However, the polymer tubes were found to have lost connection with the channel walls. Once cleaved, tubes were loose within their templates and in some cases pulled out of channels by up to 100 μm. On the opposite face, the inverted pattern is observed where empty channels match the protruding nozzles from the first face. Because access to the channels from inside the tube is ruled out, this evidence suggests that etchant can penetrate deeply and selectively along the polymer-silica interface all the way from the tip face, the effect presumably enhanced by the forced flow of etchant by the syringe pump. The ability of fluoride etchants to penetrate small cracks is known and leads to the cusp-like surface morphology of etched glass that initially appeared flat before etching.[19] The separation of the tube from the wall may also be aided by the selective breakage of the weaker Si-C bond of the organosilicon wall connections (bond dissociation energy of ~450 kJ/mol) relative to typical Si-O bonds on silica surfaces (bond dissociation energy of ~800 kJ/mol).[23] Furthermore, the Si-C connections at the interface are far fewer than the Si-O bonds of the silica matrix, greatly accelerating the rate of penetration along the interface.

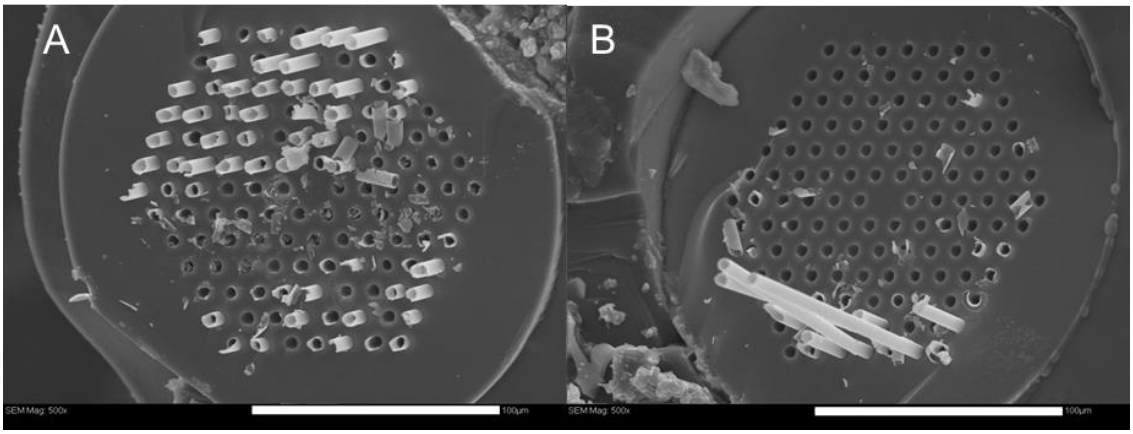

Figure 2.10 SEM images of cross-sections of a MSF with polymer tubes which had AF etchant passed through them for 12 minutes, where A) and B) are opposite faces of the same cleavage site, showing the loss of connection between the tubes and the wall despite the minimal expansion of the channels. Scale bar is 100 μm.

2.3.2.2 Optimization of polymer nozzles

One of the main goals for the etched multi-nozzle MSF is to have all of the nozzles be homogeneous, both in dimensions and morphology. In terms of dimensions, the diameter of the nozzles is defined by the channel diameter of the original template MSF, which is extremely uniform across all channels. Etching the tip to release the nozzles did not lead to any changes in polymer tube diameter, so this dimension remains very homogeneous. Nozzle length, on the other hand, was found to be quite variable between nozzles and difficult to predict. Interestingly, however, the disparity in nozzle length matches that of the tubes prior to etching. As shown in Figure 2.11A, for early experiments, the polymer tubes within the MSF template were not all flush with the cleaved MSF face. Following etching, the same pattern of varying nozzle lengths was found as that before etching, leading to a result like that shown in Figure 2.11B. This means that the nozzle length disparity does not arise from the etching process, but from the polymer tubes themselves. When cleaved, the MSF template is scored along the external diameter and

snapped such that the silica pulls apart and leaves a smooth, flat surface. While the channels in the MSF cleave with excellent fidelity with the fiber, the polymer tubes residing in those channels need to all be cleaved exactly at the plane of MSF cleavage. The tubes, unfortunately, were too elastic in nature and ultimately many stretched and snapped at some point after MSF cleavage. The point in the tube that eventually cleaved was thus not necessarily flush with the cleaved face of the MSF.

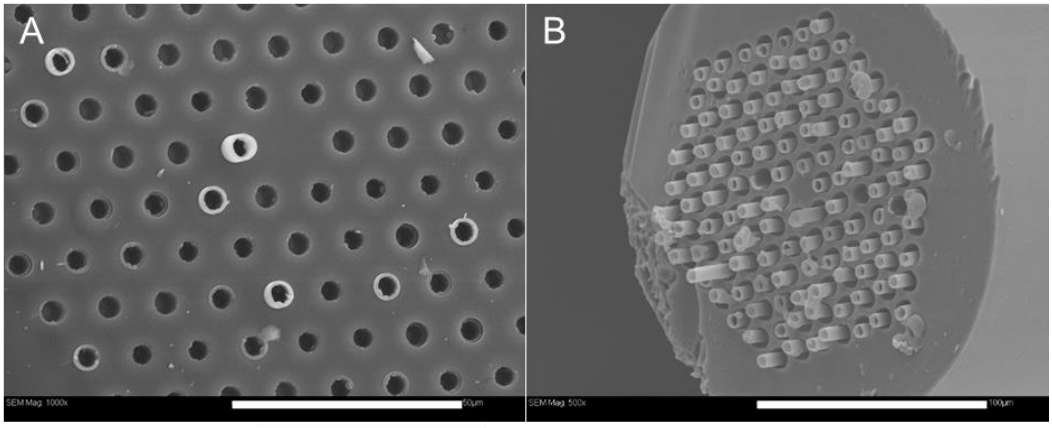

Figure 2.11 SEM images of the cleaved face of a MSF containing polymer tubes fabricated using the general composition A) before being etched and B) after being etched in HF for 1 minute. Scale bar is 50 μm in image A, and is 100 μm in image B.

In an effort to decrease the elasticity of the polymer tubes, the composition of the polymer (initially 20% styrene, 20% DVB, and 60% ethanol by volume) was altered. Specifically, the amount of crosslinker was increased to render the tubes more rigid and brittle.[24] To this end, the amount of DVB was varied from 50% to 100% of total monomer (DVB plus styrene) on a volume basis. Presented in Figure 2.12 is a series of SEM images of cleaved and etched MSF tips containing polymers comprising 75%, 67%, and 60% DVB by volume of total monomer. It was found that there was a direct correlation between the extent of crosslinker and nozzle length disparity, with tubes of ≥75% DVB being nearly perfectly aligned along the cleaved MSF face. Presumably, the rigidity of the highly

crosslinked tubes allowed cleavage in plane with the fiber without significant stretching. As no other disadvantage was observed with fully crosslinked polymer tubes, DVB was used as the sole monomer in any further formulations.

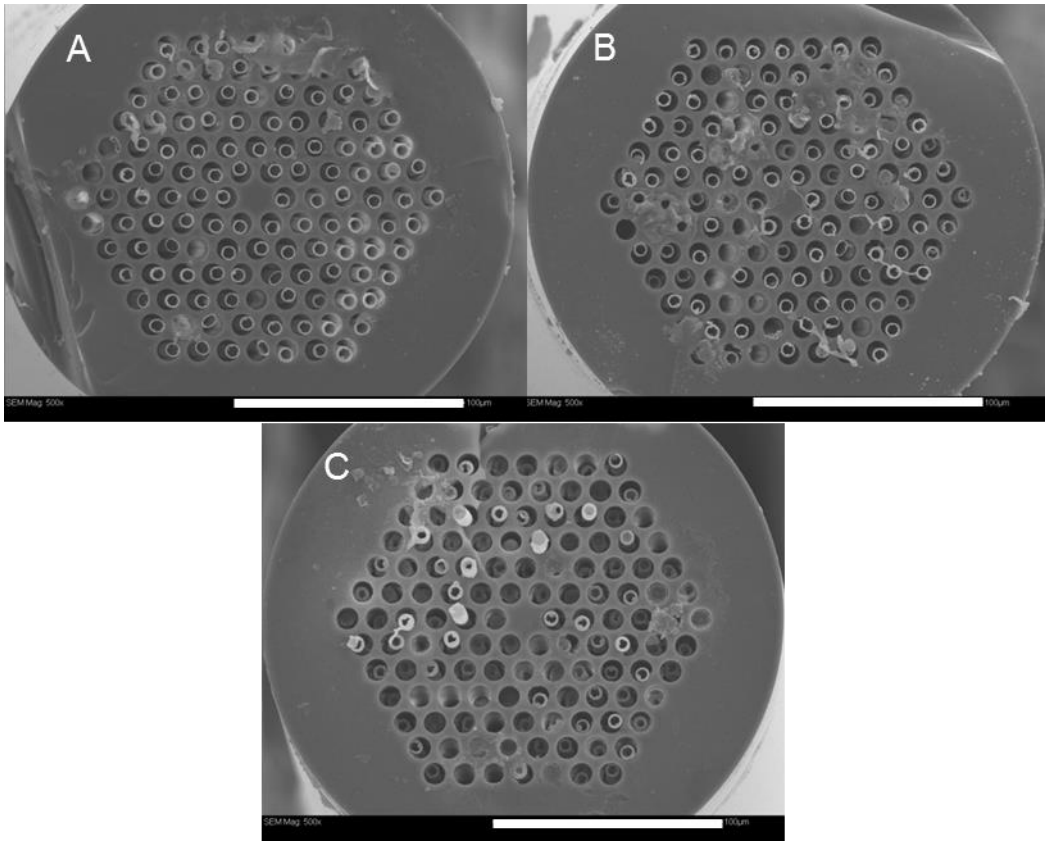

Figure 2.12 SEM images of MSFs containing polymer nozzles synthesized using different volume % of DVB in the total monomer (DVB plus styrene): A) 75% DVB; B) 67% DVB; C) 60% DVB. Scale bar is 100 μm.

The DVB concentration in the solvent ethanol was also optimized. Presented in Figure 2.13 is a series of SEM images showing cleaved and etched MSF tips containing polymer tubes formed from a polymerization solution comprising 30%, 40%, and 50% DVB in ethanol by volume. The formation of polymer tubes in channel templates, as it is done in this work, is accomplished by a partitioning mechanism whereby polymer forming during the polymerization reaction becomes insoluble in the solvent and partitions on the

hydrophobic channel walls.[25] While the DVB to styrene ratio does not significantly impact this mechanism, the concentration of DVB relative to ethanol does. As the concentration increases, the tube wall becomes thicker owing to the additional mass present, but the solubility is affected as well. Partitioning is weaker and polymer forms a less dense and more porous layer, including a greater incidence of polymer forming nodules extending into the tube interior. For this reason, the nozzles formed from the 50% DVB solution were found to be less tubular and more prone to fracture, with many breaking upon fiber cleavage (see Figure 2.13C). The nozzles fashioned from 30% DVB, on the other hand, were found to be uniformly tubular. With sufficient wall thickness and strength to resist breakage or deformity during use, this DVB concentration was chosen for all further experiments.

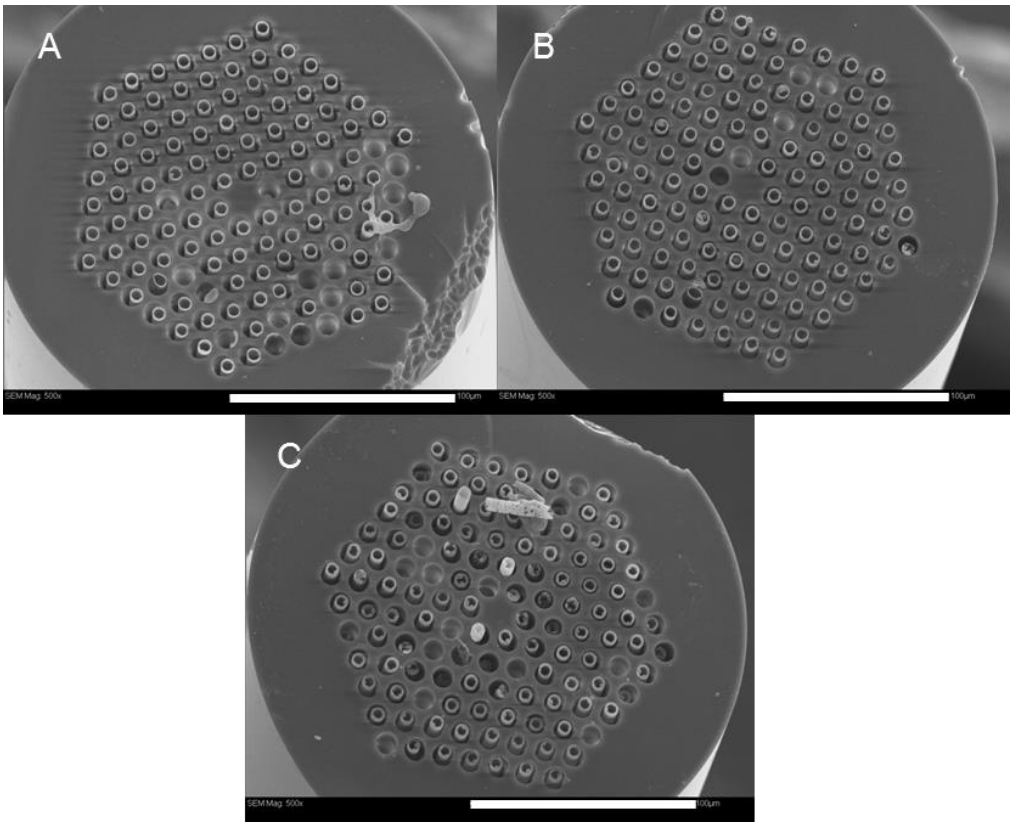

Figure 2.13 SEM images of MSFs containing polymer nozzles synthesized using different volume % of DVB in ethanol: A) 30% DVB; B) 40% DVB; C) 50% DVB. Scale bar is 100 μm.

Polymerization temperature was also explored. With thermal initiation of the free-radical polymerization, the rate of polymerization will increase with temperature in the expected way. However, the partitioning mechanism of tube formation is also affected, as the solubility of the forming polymer is higher at elevated temperatures. As a result, the polymer forms a less dense layer at the channel wall and more nodule features can be observed extending into the tube interior, getting closer in morphology to a porous polymer monolith.[25] Presented in Figure 2.14 of is a SEM image of polymer tubes formed at 100 °C, showing the large polymer nodules that formed inside of some polymer tubes. Such features may lead to tube clogging, increased flow-induced backpressure, and flow inhomogeneity among channels. Therefore, the lowest temperature that enabled reproducible thermal initiation in our system was used (80 °C), as these conditions lead to minimal nodule formation.

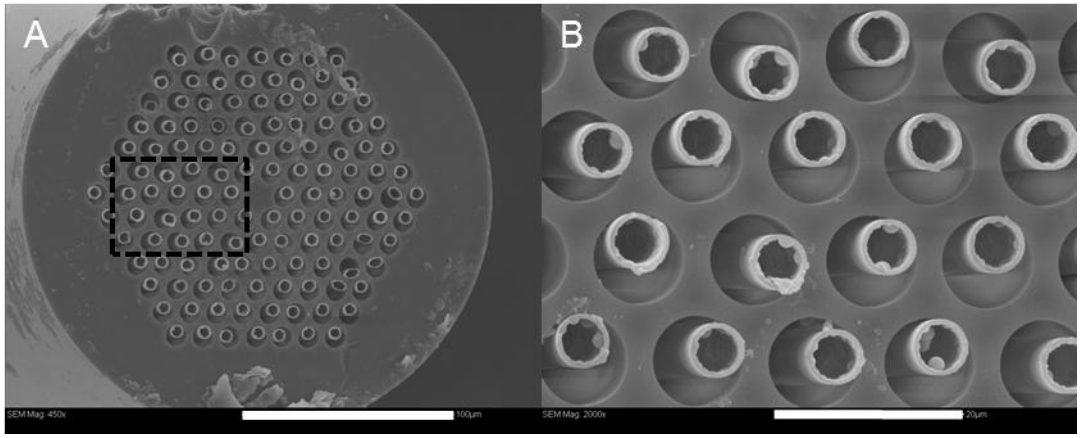

Figure 2.14 SEM images of a MSF containing polymer nozzles synthesized using the optimized polymer composition at 100 °C: A) top view and B) enlarged top view of the nozzles in the frame indicated in A). Scale bar is 100 μm in image A, and 20 μm in image B.

In summary, polymer nozzles were prepared at the face of a 126-channel commercial MSF using optimized polymerization and etching conditions, specifically a

prepolymer solution of 30% DVB in anhydrous ethanol with 5 % w/v AIBN, polymerized at 80 °C overnight, etched using 48 wt% HF for 1 minute, and rinsed in deionized water for 30 minutes. Each of the channels produced a polymer nozzle that showed high fidelity with the original channel and with each other. Every polymer nozzle was in good shape with similar wall thickness (0.53 ± 0.05 μm) and protrusion length (~5 μm), as shown in Figure 2.15.

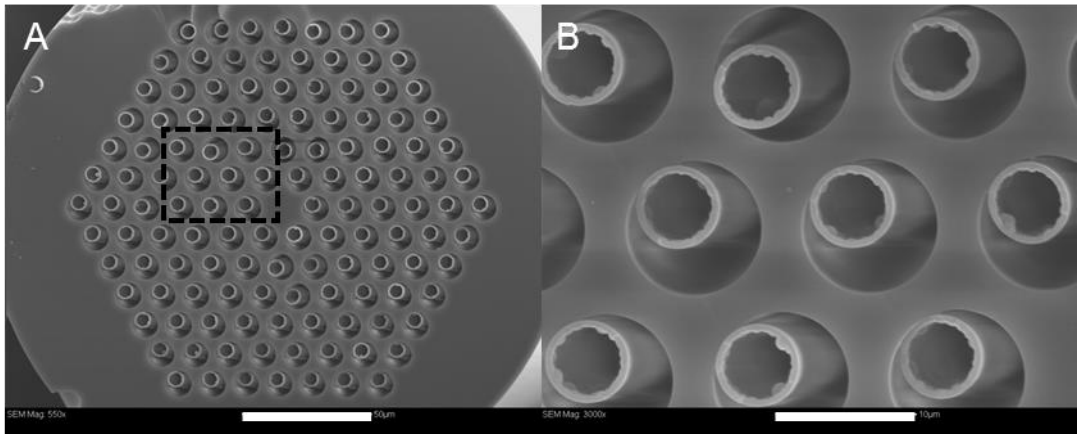

Figure 2.15 SEM images of a MSF containing polymer nozzles synthesized using the optimized procedure, showing excellent nozzle homogeneity in dimensions and in morphology: A) top view; B) enlarged top view of the nozzles in the frame indicated in A). Scale bar is 50 μm in image A and 10 μm in image B.

2.3.3 Electrospray testing of multi-nozzle MSF emitters

As outlined in the previous section, electrospray current increases with the square root of number of electrosprays, while sensitivity of the electrospray increases with smaller charged droplets that are emitted from smaller spray orifice. The multi-nozzle MSF emitters shown in the Figure 2.15 meet these criteria and were chosen in the current study. They have many nozzles and are therefore best suited to high total flow rates. As well, the nozzle diameter small is at ~5 μm and individual nozzle flow rate is low. Measurements of

electrospray current and imaging the spray behaviour are necessary to demonstrate the capabilities of this type of emitters.

The emitters were first tested offline, using an ammeter as a detector to measure the electrospray current. The apparatus appears in Figure 2.3, constructed directly on the stage of an inverted microscope so that the electrospray behaviour could be closely monitored in a side-on fashion. Shown in Figure 2.16A is an optical image of a multi-nozzle MSF emitter obtained using this set-up. For a solvent of 79.8% water/19.2% methanol with 1% acetic acid (v/v) and working distance of 2.0 mm from the counter electrode,[26] the multi-nozzle MSF emitters were optimized to determine the range of voltage and flow rate to obtain cone-jet mode operation.[27] Shown in Figure 2.16B is a stable Taylor cone obtained at 200 nL/min total flow rate and with a 3.2 kV applied potential. Under these conditions, the relative standard deviation (RSD) of the electrospray current signal is less than 3% for over 5 minutes (data not shown). A stable Taylor cone was formed over a wide range of applied voltage (2.2-3.5 kV) and total flow rate (100-1000 nL/min). These emitters, similar to the blunt MSF emitters,[13] showed excellent resistance to clogging relative to commercial tapered ESI emitters, and good electrospray stability over a wide range of conditions in the direct infusion mode. It is worth noting that the flow rate per channel of a multi-nozzle MSF emitter with 200 nL/min flow rate is only 1.6 nL/min, which is very low even in the nanoelectrospray regime.

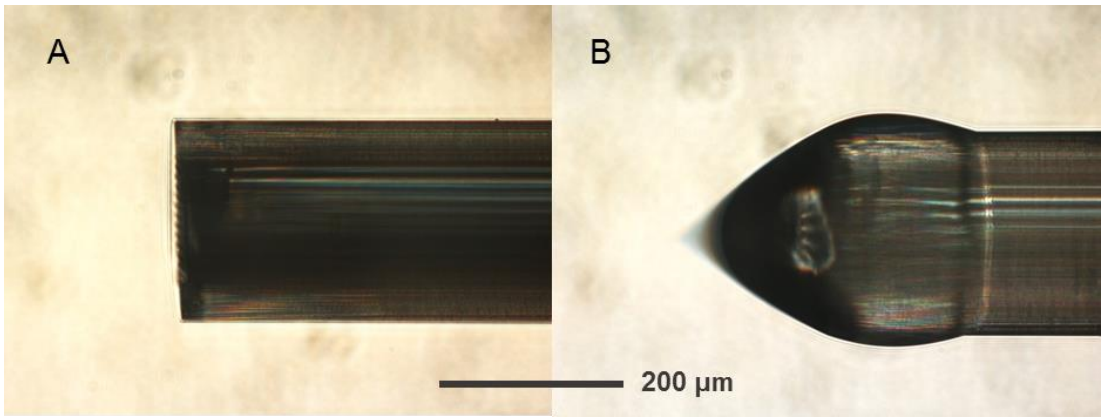

Figure 2.16 Photomicrographs (100×magnification) of a multi-nozzle MSF emitter with polyDVB nozzles in each channel viewed from the side A) before spraying and B) forming a stable Taylor cone from the tip surface by spraying 79.8% water/19.2% methanol (with 1% acetic acid) at 200 nL/min flow rate, 3.2 kV applied potential and 2 mm working distance.

The multi-nozzle MSF emitters were also tested online, coupled to a triple-quadrupole mass spectrometer. Sensitivity and stability of the electrospray from an emitter could be probed using total ion current (TIC) or extracted ion current (XIC) generated by the constant infusion of an analyte into the mass spectrometer. The intensity of these traces was used to represent sensitivity, and the RSD of the signal was a measure of electrospray stability. The performance of the emitters was tested by infusion a model peptide, leucine enkephalin (LE), which is a small and hydrophobic peptide that presents good sensitivity and generates a single ion at *m/z* 556 in a positive ion mode. Different concentrations of LE solutions were prepared in a standard ESI solution: 1:1 (v/v) water/ACN with 0.1% formic acid. The electrospray tests of the MSF emitters were conducted using standard conditions, which were established early based on previous nanoelectrospray work.[14] The conditions were then tuned to achieve the most stable ion current for a certain test. During the tests, air bubbles were always observed to pass through the emitters and disturb the Taylor cone, resulting in an unstable ion current. This issue severely impacted the

performance tests of the emitters. Therefore, the electrospray experiments could only be conducted with no or undetectable air bubble.

MSF emitters from the same batch possessing the best morphology (nozzles protrusion length and uniformity and number of nozzles) were evaluated, whose polymer nozzles are all in good shape before the electrospray tests. After analyzing the standard ESI solution for an extended period (*e.g.* 2 minutes), LE solution was directly infused in the sample loop (5 μL) that is connected to the emitter and pumped at 200 nL/min flow rate, 3.0 kV applied potential and at a 7 mm working distance between the tip of the emitter and the spectrometer orifice. Based on the XIC trace of LE (545-565 *m/z*), the analyte was detected after infusion for ~9 minutes, and the analyte was measured for ~30 minutes before it was completely consumed. TIC and XIC traces for the direct infusion of 5 μM LE are shown in Figure 2.17. The RSD of the TIC signal is less than 5% for a relatively long period of time, which is comparable to that of a standard tapered emitter.[28] The RSD of the most stable 2 minutes of the TIC signal is ~3%. Although the RSD of the XIC (545-565 *m/z*) is higher than that of the TIC, it is still acceptable for a nanoelectrospray emitter. More stable signals can be obtained by the infusion of less concentrated LE (1 μM), which has around one fifth of XIC intensity of that for the 5 μM LE (Figure 2.18). The RSD of the TIC signal is less than 3% for 9 minutes. This electrospray stability would not be possible for a blunt-ended capillary, and is adequate for most ESI-MS applications.

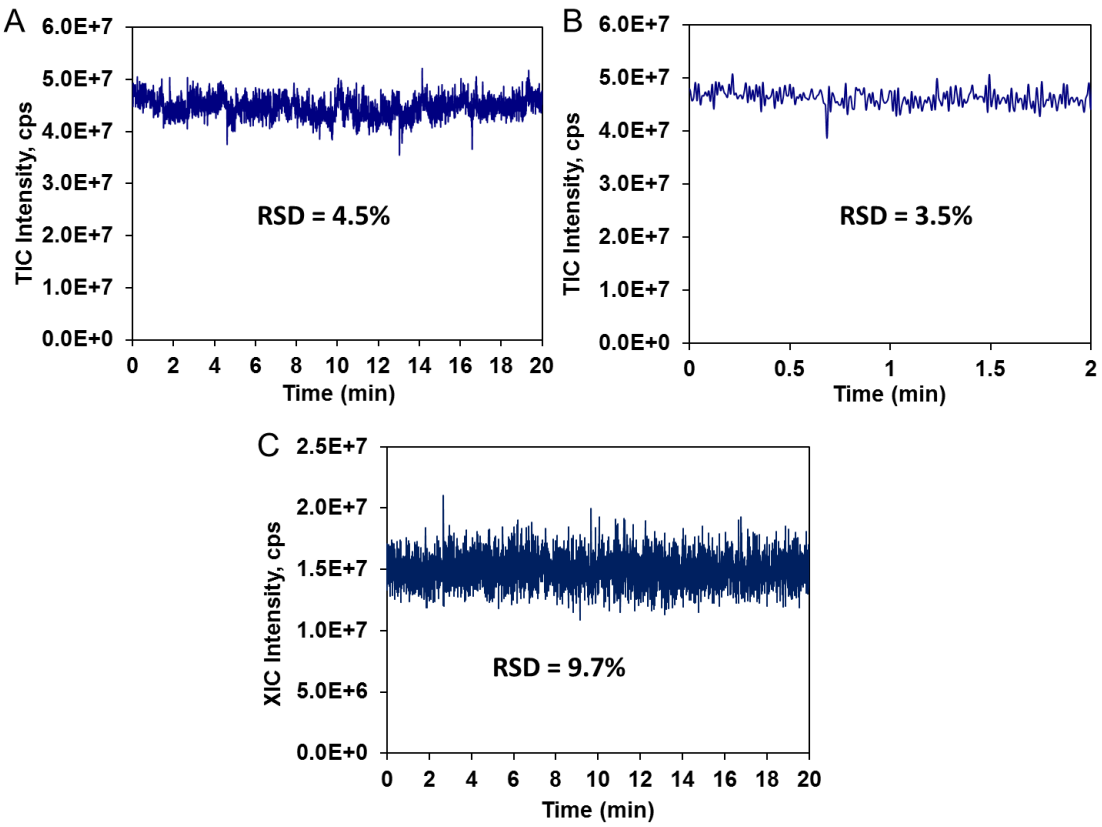

Figure 2.17 TIC and XIC traces showing signal stability for a MSF emitter, obtained by infusion of 5 µM LE prepared in 1:1, (v/v), water/ACN (with 0.1% formic acid) with 200 nL/min flow rate, 3.0 kV applied potential and 7 mm working distance: A) 20 minutes and B) the most stable 2 minutes of the TIC trace; C) 20 minutes of the XIC trace (545-565 *m/z*). RSD is shown for each of the trace.

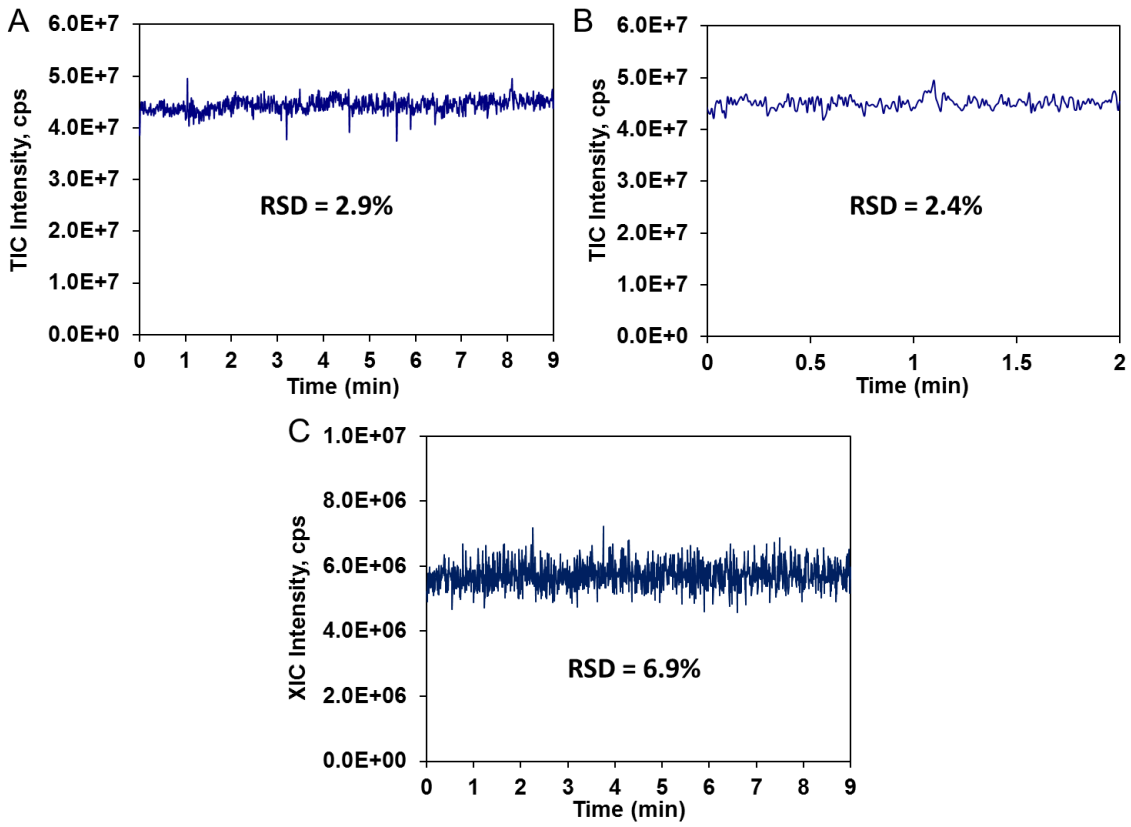

Figure 2.18 TIC and XIC traces showing signal stability for a MSF emitter, obtained by infusion of 1 μM LE prepared in the same ESI solution and sprayed under the same conditions: A) 9 minutes and B) the most stable 2 minutes of the TIC trace; C) 9 minutes of the XIC trace (545-565 *m/z*). RSD is shown for each of the trace.

The multi-nozzle MSF emitters provided a single Taylor cone encompassing all nozzles over all conditions where stable spray was observed. Ultimately, the fluid coming from the nozzles was able to wet the entire tip face and coalesce into a single electrospray. This result arises from the fact that the channels in the MSF template were too close together, which led to a variety of phenomena. First, the fact that the polymer nozzles were so close together in the final emitter decreased the physical barrier between fluids from adjacent nozzles. Second, the short spacing between channels (pitch) also limited the depth to which the tip face could be etched away, and hence the protrusion length of the nozzles. Because of the unavoidable etching of the channels from the inside, the nozzle length could

be a maximum of half the pitch before the silica separating the nozzles was completely removed. Third, the dense array of nozzles on the surface had a large effect on the electric field experienced by the individual nozzles. It is known that electrical shielding causes significant differences in the electric field felt by the nozzles near the fiber axis relative to those near the outer edge, effectively ensuring that no set of electrospray conditions allows both types of nozzles to support Taylor cones simultaneously.[29] Stable electrospray from each nozzle independently is necessary to achieve the enhancement in signal offered by MES, and so further effort should be made to reach this goal.

The approach presented in this chapter, whereby a MSF containing polymer tubes which are exposed as nozzles at one end of each channel following wet chemical etching, is capable of generating an emitter with true MES ability. What is ultimately required is a new MSF template design more conducive to MES, *i.e.* one that solves the problems associated with the commercial MSF template presented here. First, the channels need to be farther apart to reduce the chances of interference between nozzles and subsequent flow coalescence. With greater inter-nozzle distance, the length of protrusion from the tip face can also be improved. Second, the channels should be arranged in a radial pattern, all having the same distance from the fiber axis. This pattern eliminates inhomogeneities in the electric field experienced by each nozzle, allowing Taylor cone stability from each nozzle under the same conditions. A design based on these premises was tested for MES in a polymer prototype MSF.[26]

2.4 Summary

Commercially available MSFs, typically used for fiber optic applications, have been used as templates to form polymer tubes. The MSFs were then etched at one end to reveal an array of nozzles raised above the tip surface. Polymerization conditions for the formation of the tubes were optimized to promote homogeneity between nozzles, in terms of both tubular shape and nozzle protrusion length, the latter arising from elasticity of the polymer. Conditions for wet chemical etching by fluoride etchants were optimized to achieve the longest polymer nozzles without interference between adjacent nozzles. For the densely packed channel array of the 126-channel MSF in this study, only 1 minute of etching with 48% HF (aq.) was needed before the silica separating channels was removed, effectively limiting the nozzle protrusion length. After optimization, MSFs could be consistently fabricated with nozzles having uniform shape and length in every channel.

The resulting multi-nozzle MSF emitters were demonstrated as efficient nanoelectrospray emitters, both offline and coupled to a mass spectrometer for the detection of a peptide. The fiber is easily coupled to conventional nano-LC equipment due to its dimensional similarity with commonly used capillary tubing and can be directly used with standard nano-ESI-MS interfaces. A stable electrospray in cone-jet mode showing comparable performance to that of standard tapered emitters was observed over a wide range of applied voltage (2.2-3.5 kV) and total flow rates (100-1000 nL/min). Furthermore, the MSF emitters are highly resistant to clogging due to their multiple untapered channels. However, as the nozzles were too close together and their protrusion length was limited, independent electrosprays from individual nozzles were not observed under any of the conditions tested. To achieve the sensitivity enhancement of multiple electrospray, the

nozzles need to be farther apart and arranged in a circle to avoid flow coalescence and electric field inhomogeneity, respectively. Commercial MSFs are designed for optics applications, thus a custom silica MSF must be designed and fabricated. The study of custom-designed MSFs as MES emitters will be discussed in the following chapters.

2.5 References

[1] M. Wilm, A. Shevchenko, T. Houthaeve, S. Breit, L. Schweigerer, T. Fotsis, M. Mann, *Nature* **1996**, *379*, 466-469.

[2] A. El-Faramawy, K. W. M. Siu, B. A. Thomson, *Journal of the American Society for Mass Spectrometry* **2005**, *16*, 1702-1707.

[3] G. T. T. Gibson, S. M. Mugo, R. D. Oleschuk, *Mass Spectrometry Reviews* **2009**, *28*, 918-936.

[4] K. Tang, Y. Lin, D. W. Matson, T. Kim, R. D. Smith, *Analytical Chemistry* **2001**, *73*, 1658-1663.

[5] B. Lojewski, W. Yang, H. Duan, C. Xu, W. Deng, *Aerosol Science and Technology* **2012**, *47*, 146-152.

[6] P. Mao, R. Gomez-Sjoberg, D. Wang, *Analytical Chemistry* **2013**, *85*, 816-819.

[7] B. Q. T. Si, D. Byun, S. Lee, *Joural of Aerosol Science* **2007**, *38*, 924-934.

[8] R. T. Kelly, J. S. Page, R. Zhao, W.-J. Qian, H. M. Mottaz, K. Tang, R. D. Smith, *Analytical Chemistry* **2008**, *80*, 143-149.

[9] P. Russell, *Science* **2003**, *299*, 358-362.

[10] J. C. Knight, T. A. Birks, P. S. J. Russell, D. M. Atkin, *Optics Letters* **1996**, *21*, 1547-1549.

[11] P. J. Bennett, T. M. Monro, D. J. Richardson, *Optics Letters* **1999**, *24*, 1203-1205.

[12] A. S. Cerqueira, Jr., *Reports on Progress in Physics* **2010**, *73*, 024401-024421.

[13] S. Su, G. T. T. Gibson, S. M. Mugo, D. M. Marecak, R. D. Oleschuk, *Analytical Chemistry* **2009**, *81*, 7281-7287.

[14] R. D. Oleschuk, G. Gibson, R. Wright, *US 8373116 B2*, **2013**.

[15] Q. Luo, G. Yue, G. A. Valaskovic, Y. Gu, S.-L. Wu, B. L. Karger, *Analytical Chemistry* **2007**, *79*, 6174-6181.

[16] J. Courtois, M. Szumski, E. Bystroem, A. Iwasiewicz, A. Shchukarev, K. Irgum, *Journal of Separation Science* **2006**, *29*, 14-24.

[17] S. M. Ngola, Y. Fintschenko, W.-Y. Choi, T. J. Shepodd, *Analytical Chemistry* **2001**, *73*, 849-856.

[18] M. F. Bedair, R. D. Oleschuk, *Analytical Chemistry* **2006**, *78*, 1130-1138.

[19] G. A. C. M. Spierings, *Journal of Materials Science* **1993**, *28*, 6261-6273.

[20] Y. Kunii, S. Nakayama, M. Maeda, *Journal of The Electrochemical Society* **1995**, *142*, 3510-3513.

[21] J. Buehler, F. P. Steiner, H. Baltes, *Journal of Micromechanics and Microengineering* **1997**, *7*, R1-R13.

[22] D. M. Knotter, *Journal of the American Chemical Society* **2000**, *122*, 4345-4351.

[23] http://web.chem.ucsb.edu/~zakariangroup//11---bonddissociationenergy.pdf.

[24] F. Rietsch, D. Froelich, *Polymer* **1975**, *16*, 873-878.

[25] G. T. T. Gibson, S. M. Mugo, R. D. Oleschuk, *Polymer* **2008**, *49*, 3084-3090.

[26] G. T. T. Gibson, R. D. Wright, R. D. Oleschuk, *Journal of Mass Spectrometry* **2012**, *47*, 271-276.

[27] I. Marginean, R. T. Kelly, J. S. Page, K. Tang, R. D. Smith, *Analytical Chemistry* **2007**, *79*, 8030-8036.

[28] G. A. Schultz, T. N. Corso, S. J. Prosser, S. Zhang, *Analytical Chemistry* **2000**, *72*, 4058-4063.

[29] R. T. Kelly, J. S. Page, I. Marginean, K. Tang, R. D. Smith, *Analytical Chemistry* **2008**, *80*, 5660-5665.

Chapter 3 Polymer Micro-nozzle Array for Multiple Electrospray Produced by Templated Synthesis and Etching of Custom-designed Microstructured Fibers

3.1 Overview

Multiple electrospray (MES) emitters function to increase electrospray current and mass spectrometry sensitivity through independently spraying elements while making the ion plume as compact as possible to enable efficient accumulation of the ions in the spray.[1] MES emitters have been successively fabricated by various methods,[2-5] however, these emitters have several limitations including that some emitters are complicated to fabricate and some are too large to enable efficient ion collection, and have typically been difficult to couple with conventional analytical separation methodologies. Microstructured fibers (MSFs), which have many channels built into the same fiber and possess dimensional similarity with conventional capillary tubing, can be fabricated with a wide variety of channel numbers, patterns, and shapes. This flexibility offers a customizable solution to practical MES emitter fabrication.

Commercial MSFs typically contain a large number of channels within a fiber having a diameter similar to common fused-silica capillary. The high density of channels makes these materials ideal candidates for MES. When tested for MES generation, however, several such commercial MSFs were found to be incapable of supporting independent electrospray from individual channels.[6] With only flat silica separating channel openings, and with a pitch of <20 μm, the fluid emanating from the channels tended to wet the surface and coalesce to form a single spray. It was found that functionalizing the silica tip face with

a hydrophobic group, *e.g.* with chlorotrimethylsilane, helped to prevent wetting by hydrophilic electrospray solvents, but regardless of conditions MESs could not be generated.[6]

A raised nozzle at the channel exit would help prevent fluids from wetting the tip face and coalescing with fluids from nearby channels. Furthermore, by forming a nozzle with a sharp point, the electric field that generates electrospray is concentrated at the tip of the nozzle and helps support spray at lower voltages.[7] A similar approach using wetted carbon fibers at the exit of standard capillary tubing was modeled and found capable of supporting MESs.[8] In an effort to form nozzles at the emitter tip, polymer tubes were formed within the channels using an *in-situ* polymerization technique developed previously. The silica MSF can then be selectively etched at the tip, leaving behind the inert polymer tubes as raised nozzles protruding above the tip surface, retaining the exact shape of the channel templates in which they were formed.

Unfortunately, when polymer nozzles were formed within the channels of a commercial MSF as shown in Chapter 2, the short pitch of the channels led to complete etching of the silica between nozzles before they could protrude very far from the tip surface. As a result, electrosprays coalesced into a single Taylor cone and MES was still not achieved. In order to generate MES from a MSF of similar diameter, a much greater inter-nozzle distance is required.

The customizable nature of MSFs allows alternative channel patterns and spacing to be tested for applications like MES. Prototype MSFs with several channel designs were fabricated from polycarbonate and tested for MES.[9] MES was observed for some of the

designs under some conditions, but the fluids wetted the MSF surface and the base of each Taylor cone was large and variable relative to the channel openings.

In this chapter, custom-designed silica MSFs are used as templates for the fabrication of MES emitters featuring an array of polymer micro-nozzles. Polydivinylbenzene (polyDVB) tubes are formed within each of the channels of the MSF, which is then partially etched away to yield an array of protruding micro-nozzles independently capable of electrospray. Microscope imaging, electrospray current measurement, and ESI-MS detection of a model analyte all confirm the MES behaviour of the multi-nozzle MSF emitters, showing significant signal enhancement relative to a single-nozzle emitter at the same total flow rate. LC/MS data from a protein digest obtained at an independent laboratory demonstrates the applicability and robustness of the emitter for real scientific challenges using modern LC/MS equipment.

3.2 Experimental

3.2.1 Reagents and Materials

All chemicals and solvents were obtained from Sigma-Aldrich or Fisher Scientific and used without purification unless stated otherwise. See details in section 2.2.1. Custom silica MSFs were designed in our laboratory and fabricated by INO (Quebec, Canada), using a “Stack-and-Draw” technique.[10] Nine silica capillaries and eighteen silica were disposed around a central silica rod to form the inner assembly, which was inserted in an outer tube. This preform was then drawn into a fiber having nine air channels arranged in a radial pattern. In the similar way, a fiber having six air channels was also fabricated, where preform was produced with six silica capillaries and twelve silica rods disposed around a central silica rod.

3.2.2 Fabrication of polymer micro-nozzles on MSFs

Micro-nozzles on MSFs were fabricated using four steps as shown in Figure 2.1 in the previous chapter with optimized polymerization and etching conditions: a polymerization mixture is composed of divinylbenzene (monomer/crosslinker, 30% v/v), anhydrous ethanol (porogenic solvent, 70% v/v) and 2,2'-azobisisobutyronitrile (AIBN, initiator, 0.5% w/v). The MSF was heated in an oven at 80 °C overnight with both ends sealed after every channel of it was filled with the mixture using a syringe pump. The MSF, now containing a polymer layer (polyDVB) along the wall in each channel (*i.e.* a polymer tube), was flushed with acetonitrile (95% in water) to remove any residual polymerization reagents. Furthermore, nozzles with double polymer layer were also fabricated to enhance the robustness of the emitters.

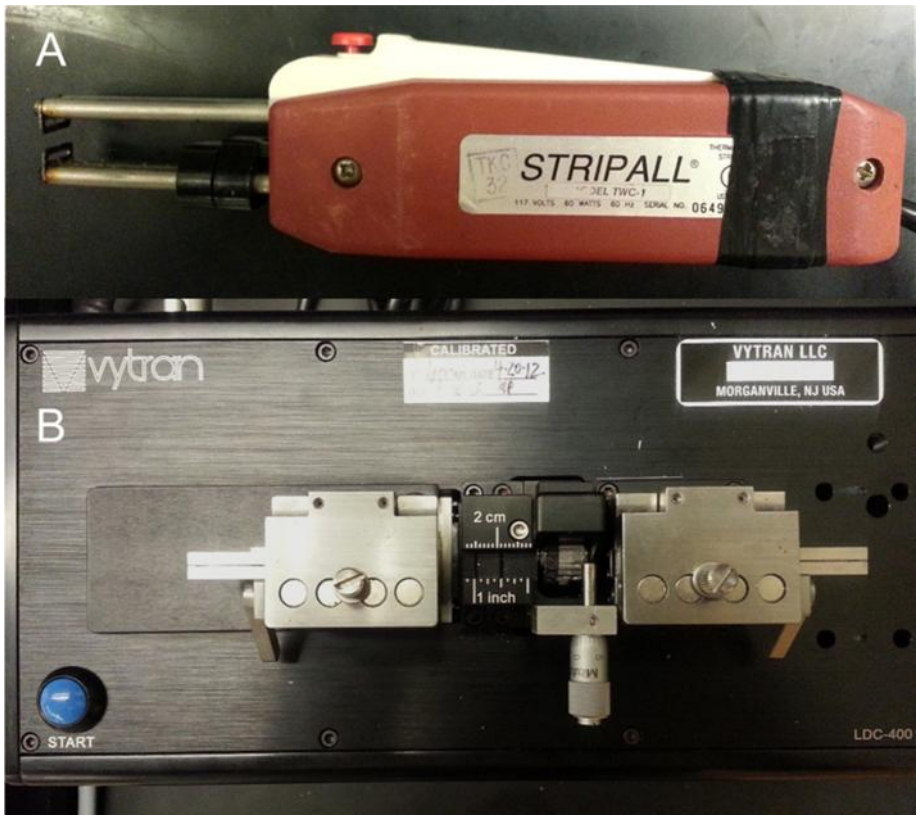

Figure 3.1 Pictures of A) the fiber coating remover: Stripall® and B) the precise fiber cleaver: Vytran LDC-400.

Before cleaving, the fiber's protective polyacrylate coating needs to be removed; this was done by using a handhold thermal wire stripper (Stripall® TWC-1 Teledyne Impulse, Figure 3.1A). The MSFs with polymer tubes were then cut into 4-5 cm long pieces using a ceramic cleaving stone or a precision fiber cleaver (LDC-400, Vytran LLC, Morganville, NJ, USA, Figure 3.1B) to produce a straight cut. One end of each piece was then immersed in concentrated hydrofluoric acid (HF) (300 µL of 48 wt % HF in water) to etch away the silica at the end of the emitter to expose the polymer micro-nozzles. Finally, the etched end of the fiber was rinsed with water to remove the HF and any debris from the emitter end.

3.2.3 Chemical modification of MSF emitters

For comparison, MSFs were also prepared having no nozzles. These MSFs, however, were chemically modified as the emitting end of a MSF was found to require hydrophobic modification to support stable electrospray.[6] One end of the MSF emitters was immersed into a solution of chlorotrimethylsilane (CTMS) (20% v/v in toluene) overnight to render the emitter face hydrophobic. Following silylation, the emitters were rinsed/cleaned with an acetonitrile/water solution (80%/20% v/v) using a Nano-LC-1D pump (Eksigent, AB Sciex, Redwood City, CA, USA).

3.2.4 Offline electrospray current measurement

The experimental setup for measuring the electrospray current was shown in Figure 2.3 in the previous chapter. See details in section 2.2.4. The working distance of the tip of the nozzles to the counter electrode block was investigated and the optimal distance was chosen as 2 mm. The current was smaller and less stable when the emitter was farther away from the electrode while droplets would gradually accumulate on the electrode when the

emitter was closer to the electrode. On the other hand, there was no significant change in current caused as a result of altering the vertical position of the emitter relative to the electrode (data not shown).

Flow-induced back pressure of the emitters was determined using the nano-flow pump in conjunction with these experiments. The back pressure was measured at each flow rate and a linear plot was constructed as shown in Figure 3.2, the slope being used to calculate the back pressure of the emitter at any given flow rate. The back pressure for a 9-nozzle emitter was found to be 160 psig (11 bar) at 1 μL/min for the 5 cm long emitter, or 32 psig (2.2 bar) per centimeter as back pressure is also linearly dependent on length.

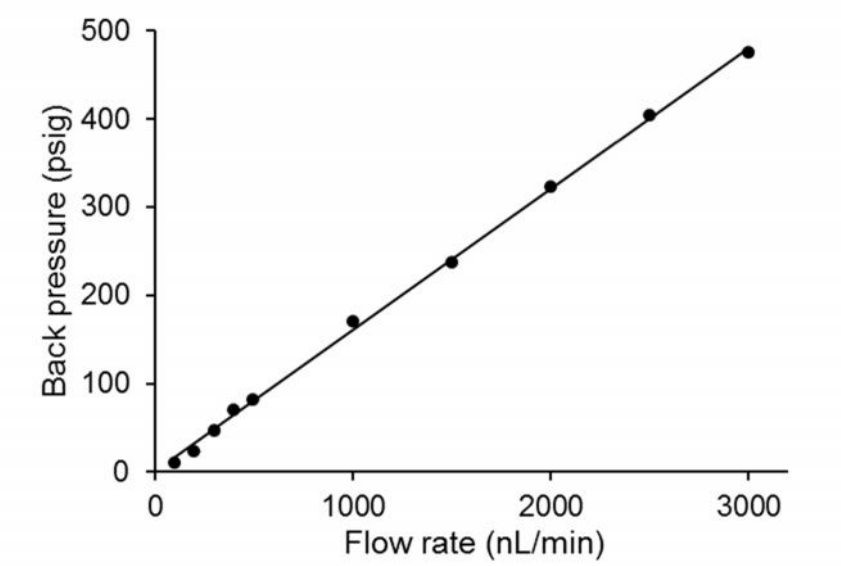

Figure 3.2 Flow-induced backpressures at different flow rates from a 5 cm long 9-nozzle emitter.

In some cases, some channels were deliberately blocked to investigate the effect of the number of working nozzles on the electrospray current. A two-part epoxy (AB9123, Fiber Optic Center, Inc., New Bedford, MA, USA) was applied to the head of the fiber with a sharp stainless steel needle and cured in an oven at 110 °C for 15 minutes. The

number of blocked channels was observed using an optical microscope, and confirmed by visualizing the number of individual electrosprays while collecting spray current data.

3.2.5 Online electrospray ionization mass spectrometry

Emitters were tested online using a Thermo Scientific LTQ Orbitrap Velos hybrid FT mass spectrometer with a nanoelectrospray source, connected via a liquid junction to a syringe pump, which delivered electrospray solution at a given flow rate, through a transferring capillary (360 µm o.d. and 75 µm i.d.). The on-line setup for testing the emitters is shown in Figure 3.3. The electrospray solution was 1 µM leucine enkephalin (LE), a peptide with 5 amino acids, in 50% water/50% acetonitrile (v/v) containing 0.2% formic acid (v/v). Electrospray potentials were optimized for total ion current (TIC) and spray stability for the multi-nozzle and the commercial tapered emitters, respectively. Positive mode was employed. TIC was monitored from 400 to 800 *m/z*, while extracted ion current (XIC) for LE was monitored from 555 to 560 *m/z*. The emitter tip was measured to be 4 ± 0.3 mm from mass spectrometer orifice, capillary temperature was set at 200 ºC and S-lens (ion guide) was set as 60%. No additional desolvation methods were utilized. Emitter performance was evaluated by the intensity and stability of the XIC signal of the analyte ion peak of the mass spectrum.

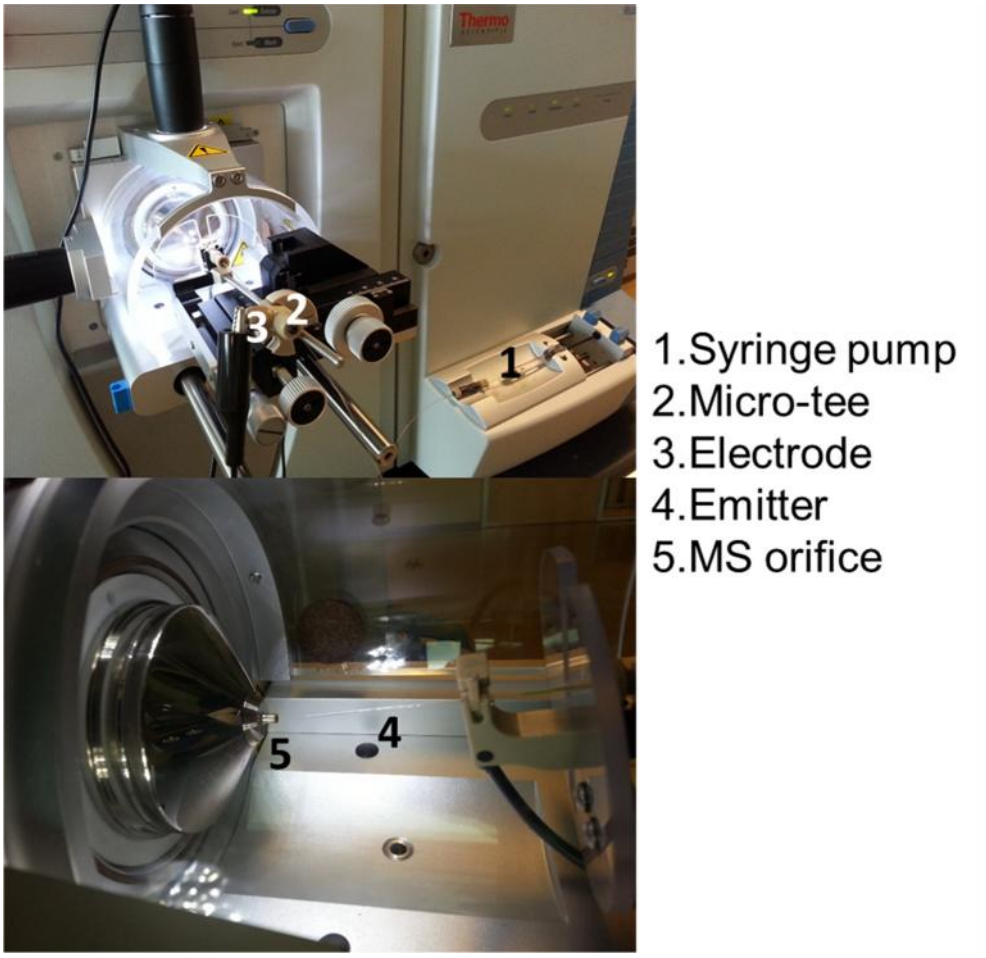

Figure 3.3 Experimental on-line setup for the emitters.

For comparison, a commercial tapered capillary emitter having a 50 μm capillary inner diameter (i.d.) tapered to an 8 μm i.d. orifice was obtained and used as directed by the manufacturer (SilicaTip™, New Objective, Woburn, MA, USA).

3.2.6 Liquid chromatography/mass spectrometry evaluation

LC/MS data was collected at AB Sciex research facilities using a QTRAP 5500 Linear Ion Trap Quadrupole LC/MS/MS mass spectrometer. A solution of bovine serum albumin (BSA) was digested in a batch using sequencing grade trypsin (V5111, Promega, Madison, WI, USA). Briefly, 2 mg BSA is boiled with 100 μL of 20 mM dithiothreitol for 15 minutes, the mixture being afterward treated with 100 μL of 55 mM iodoacetamide for

30 minutes in the dark. A 600 μL aliquot of 50 mM ammonium bicarbonate buffer was added, followed by 195 μL of 200 μg/mL trypsin, and the mixture was incubated overnight at 37 °C. Various volumes of the aqueous digest sample were injected to evaluate the sensitivity of the system. The protein fragments were separated using a reversed-phase capillary column (Eksigent, AB Sciex) with a 75 μm i.d. and length of 15 cm, packed with 5 μm silica-based particles. The solvent gradient was as follows: 98% A (v/v) for 2 minutes, to 20% A over the next 8 minutes, to 2% A over the next 0.2 minute, holding for 1.8 minutes, then returning to 98% A over the next 0.2 minute and holding for 7.8 minutes (20 minutes total), where solvent A is water and B is acetonitrile, both containing 0.1% formic acid. A set of 14 representative peptides were detected using XIC for their respective *m/z* peaks in the mass spectrum.

3.2.7 Scanning electron microscopy (SEM)

See details in section 2.2.3.

3.3 Results and discussion

3.3.1 The architecture of MSF emitters

The nature of the methods employed for MSF fabrication enables significant flexibility in size, composition and channel layout.[10] Several design elements identified with lower-cost polymer prototypes,[9] such as fiber diameter, channel diameter, and pitch, were considered to design a custom silica MSF to promote MES. The ability of an emitter to support nanoelectrospray at a particular flow rate is based in part on the dimensions of the nozzle/emitter; for example, 5 μm and 30 μm diameter single emitters are compatible with a flow rate range of ~60 and ~600 nL/min, respectively.[11] In this work, the channel

diameter was chosen to be ~9 µm for the 9-channel MSF or ~5 µm for the 6-channel MSF, which is small enough to support nanoelectrospray, but not so small that clogging or flow-induced back pressure becomes a concern. Furthermore, the channels should be separated to minimize the interaction among electrosprays emanating from adjacent channels, so the pitch of the channels was chosen to be ~100 µm based on our computational and experimental studies.[9, 12] A radial channel pattern was chosen to minimize differences in electric field between the nozzles arising from electrical shielding of the nozzles closer to the axis.[13] The custom-designed MSFs for MES are shown in Figure 3.4A and 3.4B. The 9-channel MSF has an outer diameter of ~460 µm with nine channels (9.1 µm in diameter) arranged radially with a pitch of ~115 µm residing on a centered circle with a diameter of 327 µm. The 6-channel MSF has an outer diameter of ~280 µm with six channels (5.2 µm in diameter) arranged radially with a pitch of ~90 µm residing on a centered circle with a diameter of 178 µm.

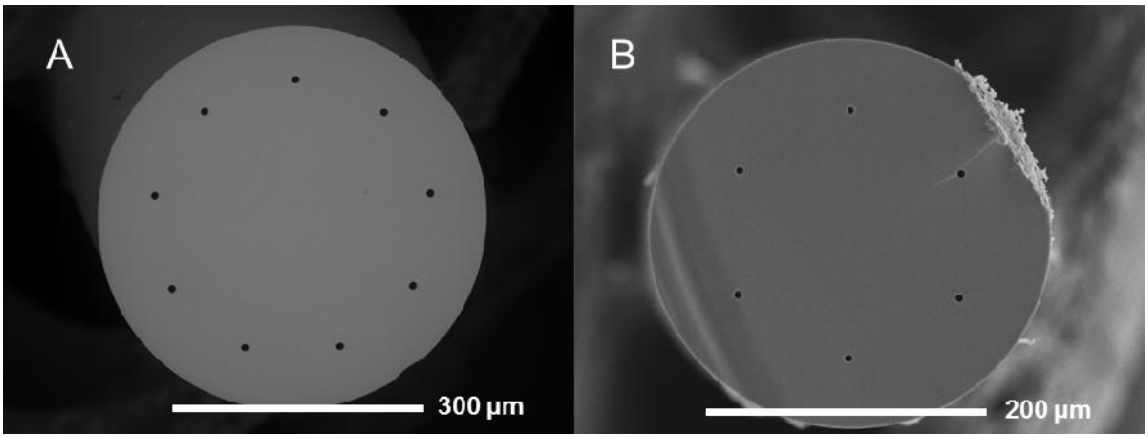

Figure 3.4 SEM images showing A) a custom-designed MSF with nine channels in a radial pattern, where outer diameter is ~460 µm and channel diameter is 9.1 µm and B) custom-designed MSF with six channels in a radial pattern, where outer diameter is ~280 µm and channel diameter is 5.2 µm. Scale bars are labeled on the images.

3.3.2 Electrospray characteristics of hydrophobic modified MSF emitter

To improve the ionization efficiency when spraying highly aqueous solutions the silica MSF emitter can be modified with a number of silylation reagents to alter its wetting characteristics. Electrospraying aqueous analytes is important for reversed-phase LC separation gradients. Moreover, in proteomics, some analytes cannot bear significant organic solvent content without denaturation, therefore aqueous working environment is necessary.

CTMS can effectively modify the surface wetting characteristics of glass. The water contact angle is increased from 50º to 127º for CTMS-derivatized fused silica by the contact angle experiments conducted in our laboratory.[14] To prevent tip surface wetting and promote individual electrosprays, the tip surface of the 9-channel MSF emitters was modified using CTMS to render it hydrophobic as shown in Figure 3.4A.

The emitters were tested using the apparatus for monitoring the electrospray behaviour and measuring the electrospray current under various conditions. Voltage and flow rate were optimized to provide electrosprays operating in a cone-jet mode.[15] The hydrophobically-modified flat-tip emitter showed small and unstable droplets emanating from each channel. Space-charge effects caused the positively-charged droplets to migrate toward the outside edge of the tip face, although the droplets eventually coalesce into several larger droplets that wet the entire face resulting in a single electrospray as shown in Figure 3.5. Even with the significantly large pitch (~115 μm), radial channel distribution and hydrophobic treatment, the lack of a physical barrier isolating the fluid to the channel still resulted in flow coalescence.

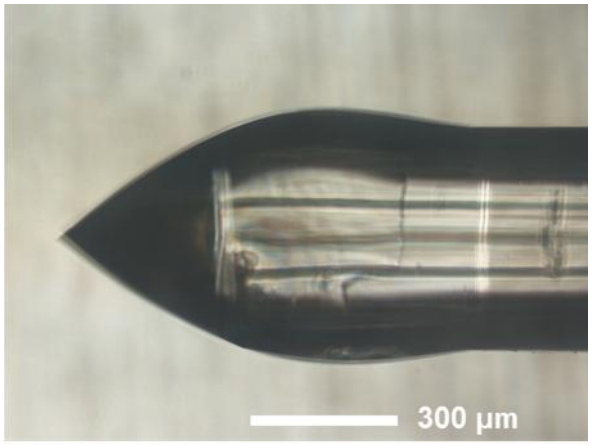

Figure 3.5 Photomicrograph (100×magnification) of an electrospray with a single Taylor cone from a custom-designed 9-channel MSF emitter with CTMS coating on the tip surface viewed from the side under the spray conditions of 500 nL/min of 79.2% water/19.8% methanol/1% acetic acid with 3.5 kV applied potential and working distance of 2 mm.

3.3.3 Electrospray characteristics of MSF emitters with polymer micro-nozzles in the channels using off-line apparatus

Alternatively, polymer micro-nozzles can be utilized to effectively elevate and isolate each individual channel above the fiber face to promote the formation of individual electrosprays. To fabricate the nozzles, a layer of polymer is formed at the inner wall of each channel of the MSF by thermally initiated free-radical polymerization.[16] The channel surface of the silica MSF is first functionalized with a vinyl-containing reagent γ-MPS,[17] thus the polyDVB layer will be covalently attached to the silica surface. The tubular morphology of the formed polymer is developed through a partitioning phenomenon where the growing polymer preferentially forms at the hydrophobic wall to minimize contact with the "poor" polar porogenic solvent.[14] The silica template is then rapidly etched leaving the individual polymer tubes exposed to form the micro-nozzles on the MSF emitters. An interesting etching pattern is evident where the etch rate is faster at the polymer tube/silica fiber contact point compared to the bulk silica regions. The result is a deep "trench" that surrounds and further isolates the polymer nozzle.

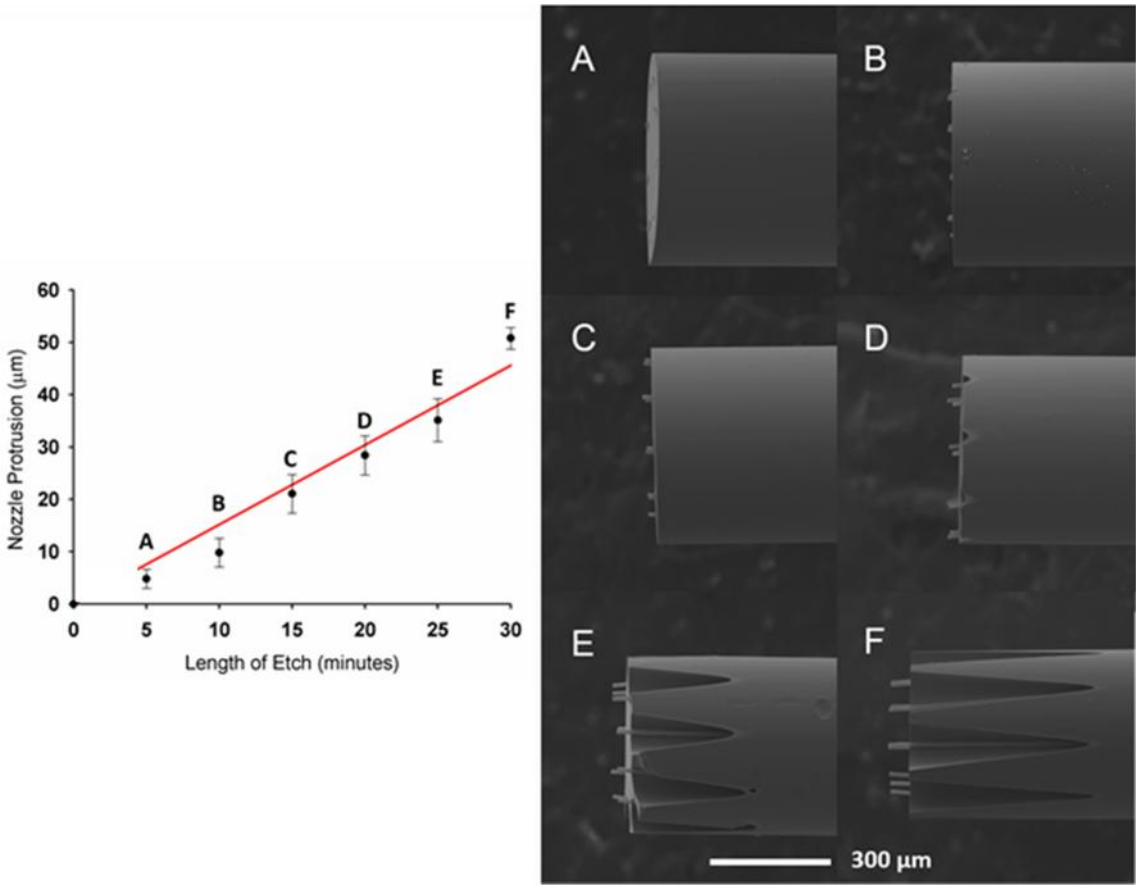

Figure 3.6 Plot showing a linear relationship between the protrusion length of the micro-nozzles from the fiber face and the etching time in 48% HF solution. Letters on the plot correspond to the matching SEM images.

The protrusion length of the nozzles above the tip face for the 9-channel MSF emitters was found to be linearly dependent on the time the tip spent in the HF etchant, as shown in Figure 3.6. An etching time of 30 minutes was chosen for the electrospray experiments as presented in Figure 3.7, giving a protrusion length of 51 ± 2 μm. Additional etching time led to complete loss of the silica between the polymer nozzles, eliminating any structural control over the position of the nozzles. Figure 3.8 shows a MSF emitter etched for 40 minutes, where the polymer tubes have too much freedom of movement and some have overlapped.

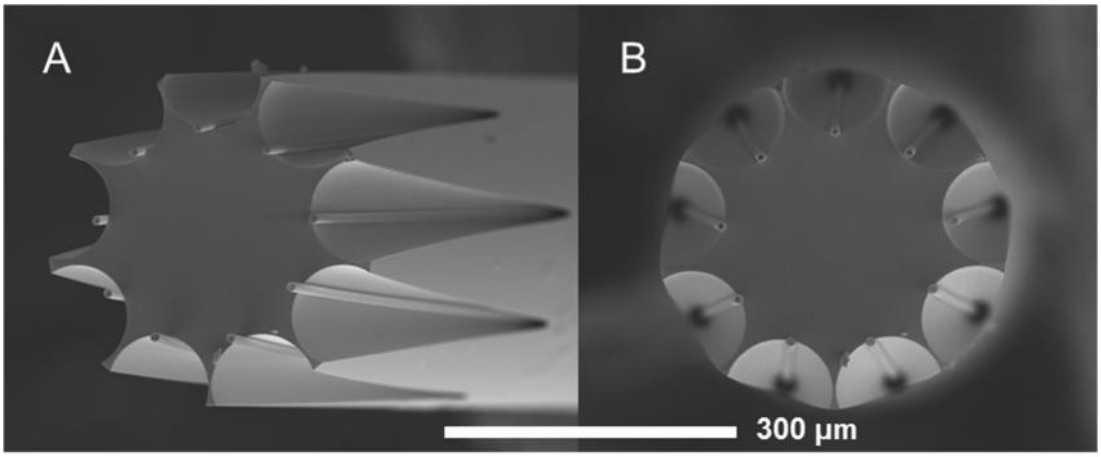

Figure 3.7 SEM images of a MSF emitter following in-channel polymerization and HF etching with nine micro-nozzles protruding 51 ± 2 µm from the tip of the emitter: A) tilt view and B) top view.

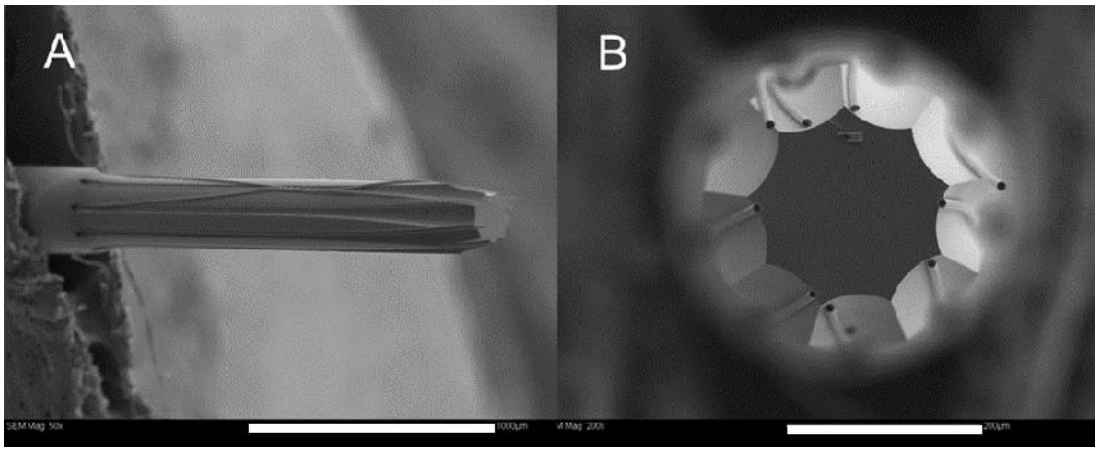

Figure 3.8 SEM images of a MSF emitter having been etched for 40 minutes, showing the lack of silica near the tube to control the tube's position: A) side view, scale bar is 1000 µm; B) top view, showing the overlap of adjacent tubes, scale bar is 200 µm.

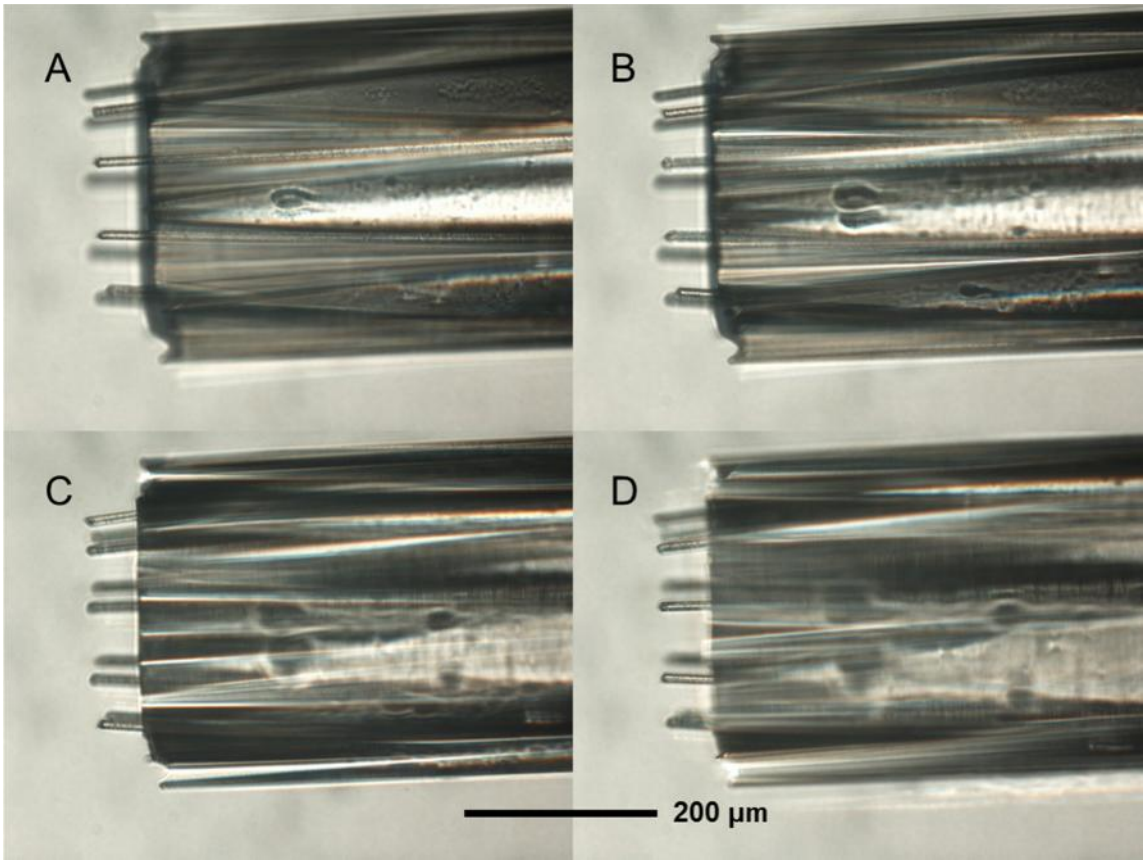

Figure 3.9 Photomicrographs (200×magnification) of nine stable individual electrosprays generated from the MSF emitter with polymer micro-nozzles in each channel viewed from the side using the same spray conditions (500 nL/min of 79.2% water/19.8% methanol/1% acetic acid with 3.5 kV applied potential) as in Figure 3.5, the depth of focus is successively changed to visualize each electrospray from A) front nozzles to D) back nozzles.

Unlike the dense array of short polymer nozzles in the commercial MSF emitter, the nine nozzles of the custom-designed MSF emitter produce nine individual Taylor cones that emanate directly from the tip of each nozzle as presented in Figure 3.9, each having an approximate volume of 5-10 pL (a factor of roughly 2500-5000 less volume than the same emitter without nozzles generating a single large Taylor cone). Individual Taylor cones can be seen in Figure 3.9A to 3.9D, in which the depth of focus is successively changed to visualize each electrospray, demonstrating the MES behaviour of this type of emitter which can be referred as a MES emitter. The shape, chemical properties, and raised profile of the polymer micro-nozzles help to enhance the electric field at the nozzle tip, avoid wetting,

and minimize the interference among the sprays.[7] Although the Taylor cones are deflected off axis due to the electrostatic repulsion among the sprays, the nozzles in a radial arrangement experience the same electric field and operate in the same electrospray regime.[13]

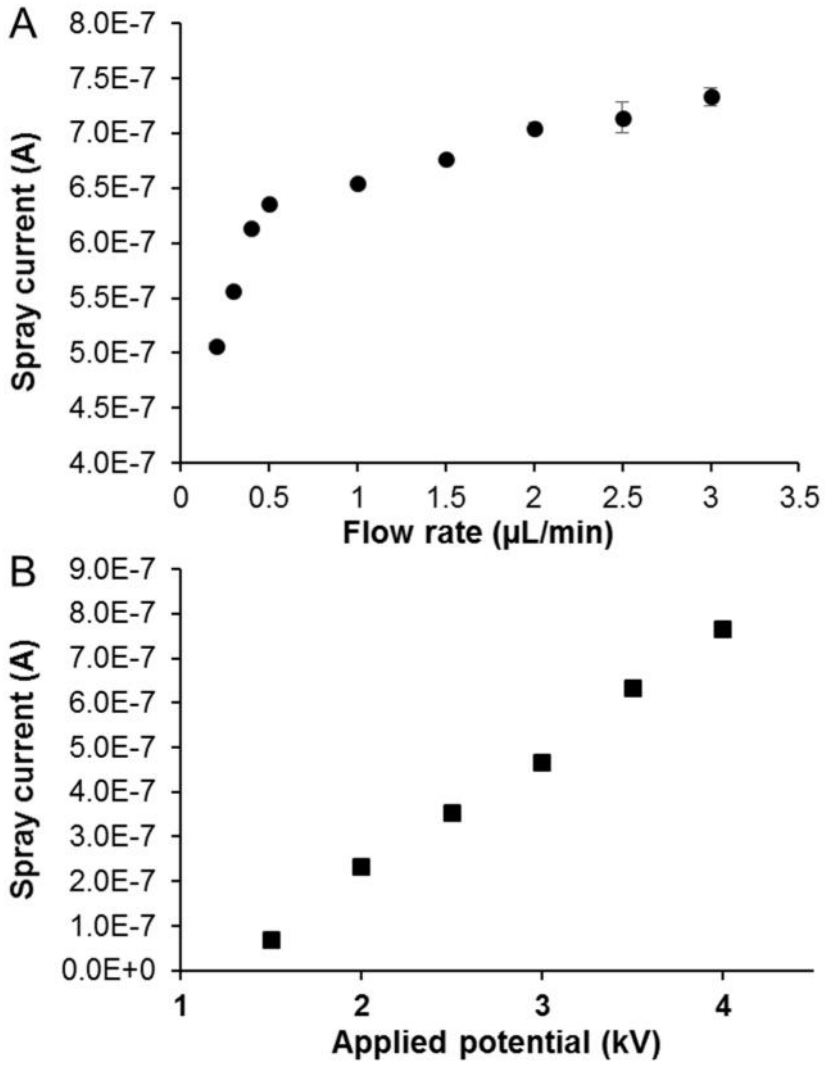

Figure 3.10 Spray current as a function of A) flow rate for 9-nozzle MES emitters under optimized voltages 3.5 kV, showing the expected square root dependence under lower total flow rate (1 µL/min) and of B) applied potential for the emitters at total flow rate of 0.5 µL/min, showing a linear dependence between the current and applied potential. Electrospray solution was 79.8% water/19.2% methanol/1% acetic acid.

Nine stable individual electrosprays were observed for the emitter over a wide range of total flow rate (0.3-3.0 μL/min at 3.5 kV), and applied voltage (1.5-4.0 kV at 0.5 μL/min). The small electrical current generated by the electrospray was measured for all conditions tested, with the value for a particular condition being the mean current over at least 5 minutes acquisition time and the uncertainty being the standard deviation of the mean. The spray current was first plotted as a function of total flow rate at a particular voltage (3.5 kV), presented in Figure 3.10A. The plot follows the well-known square root dependence on flow rate under 1 μL/min, which arises from the increased supply of charged species at higher flow rates counteracted by poorer ionization efficiency which is exaggerated due to the limitation of the off-line testing apparatus.[18] When the flow rate is held steady, the dependence of the spray current on applied potential is linear (Figure 3.10B). As all the nozzles of the emitter are spraying in the same cone-jet regime over all conditions in the plot, and the working distance defines the constant resistance of the system, this linearity is predicted by Ohm's law. These results indicate that each of the nozzles of the emitter are behaving independently as single Taylor cones, without apparent cooperative or interference effects among electrosprays.

To further investigate the MES behaviour the of polymer nozzle emitters, the offline electrospray current was measured as a function of the number of individual electrosprays. Using only the 9-channel custom-designed MSF, the number of working nozzles was varied by deliberately blocking some of the channels with epoxy at the head of the MSF. Flow and electrospray from each nozzle was easily observed by microscope imaging. Presented in Figure 3.11A is a plot of electrospray current relative to the square root of the number of working nozzles, obtained at 500 nL/min flow rate and 3.5 kV applied

potential. The linear relationship (linear regression shows $R^2 = 0.98$) of the plot indicates that the nozzles are independently electrospraying, demonstrating the expected enhancement of spray current due to MES. The spray current for 1 working nozzle (square root of 1) closely matches that obtained from a commercial tapered emitter with 8 μm i.d. tip diameter under similar conditions ($1.1 \pm 0.1 \times 10^{-7}$ A). Similar plots constructed using data obtained at 400 nL/min flow rate and 3.5 kV (Figure 3.11B), at 300 nL/min and 3.5 kV (Figure 3.11C), and at 200 nL/min flow rate and 3.5 kV (Figure 3.11D) also show a linear relationship, with R^2 values of 0.99, 0.98 and 0.97, respectively. This relationship is expected to hold for all electrospray conditions as long as all nozzles produce individual electrosprays in the cone-jet mode under those conditions, which was observed over a wide range of flow rate and voltage as discussed above. Ultimately, a 9-nozzle MES emitter was tested and monitored for several days spanning an 82-day period, the electrospray performance of it showed no change as the relative standard deviation (RSD) of the spray current signal is only 4% under the same conditions during the test period, demonstrating its longevity and robustness.

The channels of the 6-channel MSF were also arranged in a radial pattern, so that the resulting electric field would be equivalent at each nozzle. A cross-section of the drawn MSF appears in Figure 3.4B. From this and similar images, the outer diameter of the MSF was measured to be 280.2 ± 7.6 μm, and the channel diameter was 5.2 ± 0.3 μm.

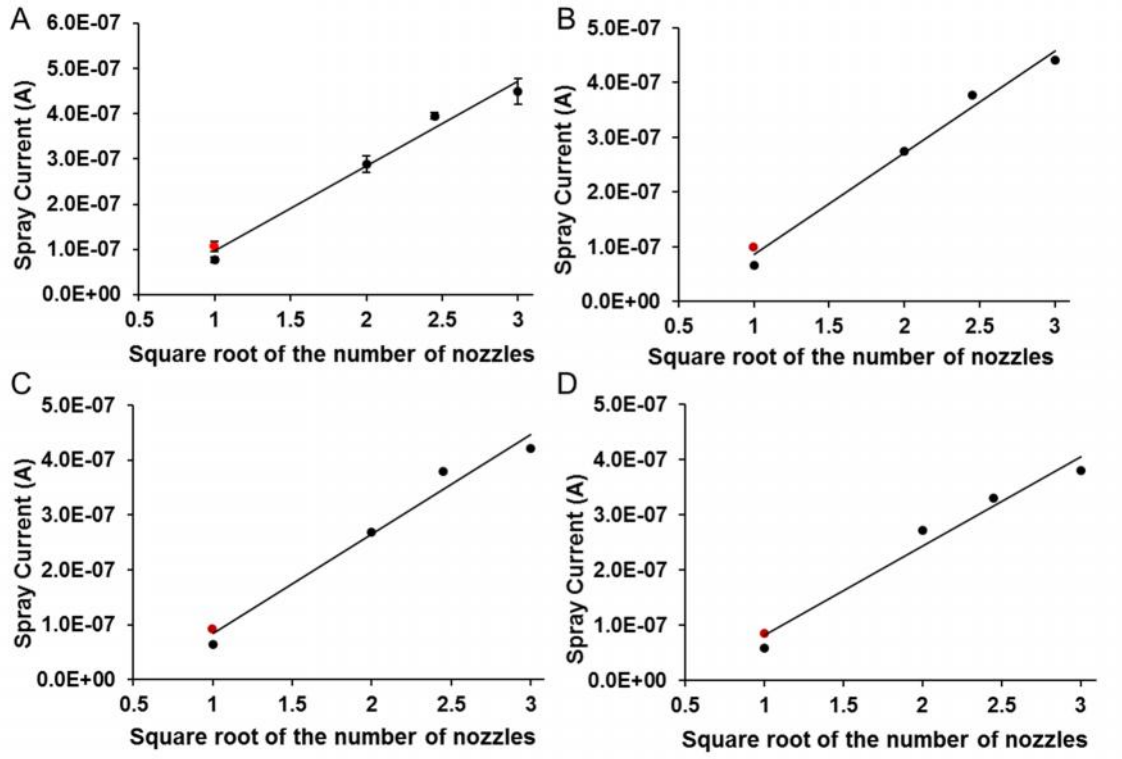

Figure 3.11 Electrospray current measured for a 9-nozzle MES emitter as a square root function of the number of working nozzles, the linearity of which demonstrates the theoretical signal enhancement of MES emitters. Conditions: A) 500 nL/min flow rate; B) 400 nL/min flow rate; C) 300 nL/min flow rate and D) 200 nL/min flow rate with the same applied potential (3.5 kV). The red data point in each plot indicates the spray current produced by an 8 μm SilicaTip™ emitter under the same conditions.

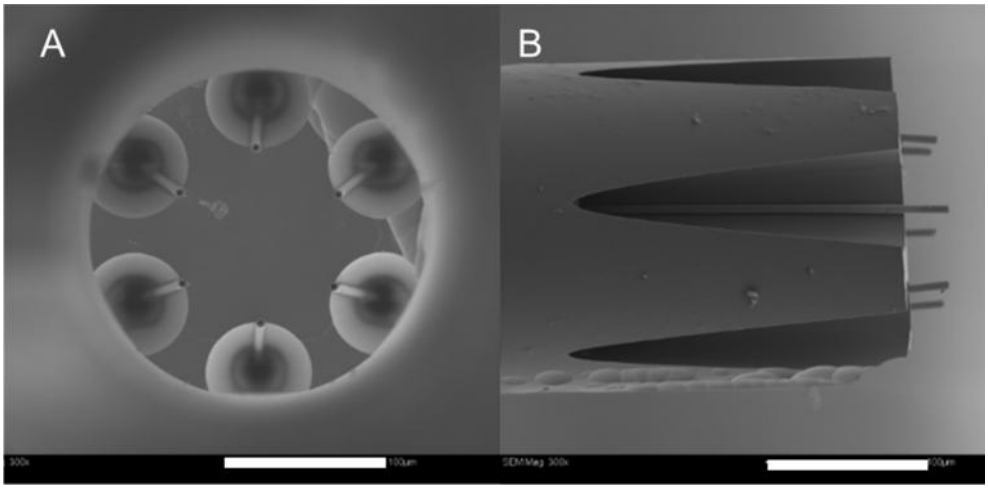

Figure 3.12 SEM images of a custom-designed 6-channel MSF after polymer tube formation and HF etching for 20 minutes: A) top view and B) side view. Scale bar is 100 μm in the images.

The optimized polymerization conditions from the commercial MSF template experiments were also used to form polyDVB tubes in the custom-designed 6-channel MSF. The HF etching time of the new fiber was re-optimized, having different channel number and spacing. It was determined that, after 20 minutes, the silica between adjacent channels had not yet been removed, but the polymer nozzles were becoming exposed from the outside of the MSF. This represents the etching limit, as the nozzles can be kept separated from each other, but still held within the MSF. SEM images of the MSF with six nozzles after 20 minutes of etching in HF from the top and side views appear in Figure 3.12A and 3.12B, respectively. The nozzle protrusion length under these conditions was measured to be 25.7 ± 2.8 μm.

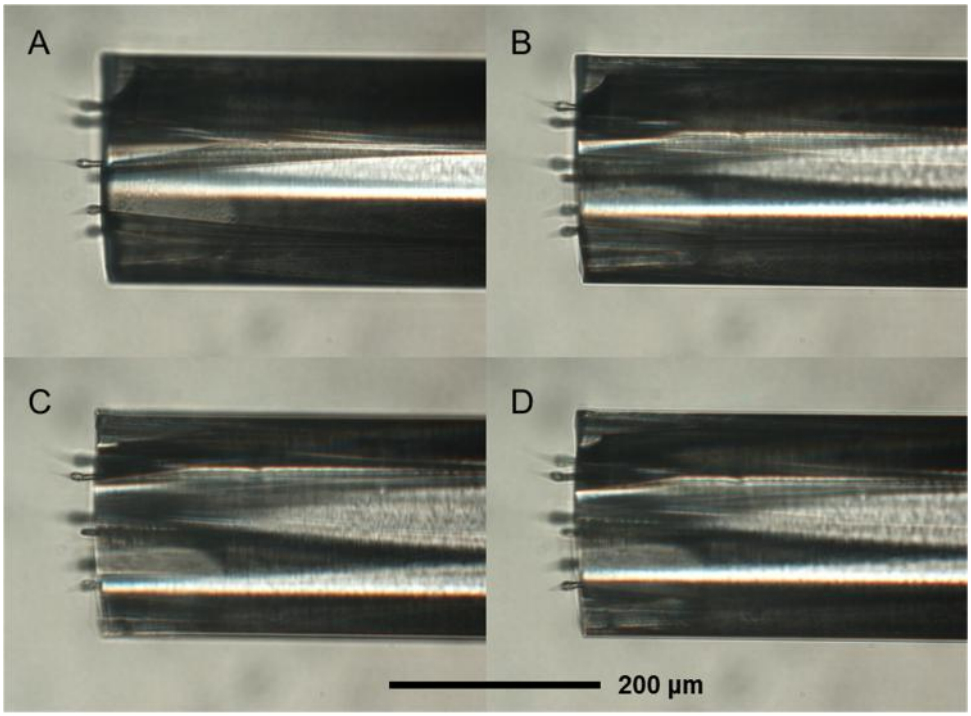

Figure 3.13 Photomicrograph (200×magnification) of a 6-channel MSF emitter with polyDVB nozzles in each channel viewed from the side, showing the formation of a stable Taylor cone from each of the nozzles while spraying 79.2% water/19.8% methanol (with 1% acetic acid) at 400 nL/min flow rate, 3.5 kV applied potential and 2 mm working distance. The depth of focus is successively changed to visualize each electrospray from A) front nozzles to D) back nozzles.

The emitters were tested for electrospray performance using the same apparatus. Shown in Figure 3.13 are optical images of the 6-nozzle MSF emitter with six independent electrosprays while flowing 79.2% water/19.8% methanol (with 1% acetic acid) at 400 nL/min under 3.5 kV applied potential. Individual Taylor cones can be seen in Figure 3.13A to 3.13D on this type of emitter, conforming the stable MES by focusing on each nozzle as it sprays. Under these conditions, the RSD of the electrospray current signal is less than 1.2% for over 10 minutes (data not shown). Stable MESs were observed over a wide range of applied voltage (2.4-5.9 kV) and total flow rate (100-1000 nL/min).

The offline electrospray current was also measured as under a given set of conditions for a series of emitters with different numbers of spraying nozzles with some channels blocked by epoxy at the end of the 6-channel MSF. Shown in Figure 3.14 is a plot of electrospray current relative to the square root of the number of working nozzles, obtained at 100 nL/min flow rate and 3.5 kV applied potential. The strong linearity of the plot demonstrates the true MES behaviour of the 6-nozzle emitter, where the enhancement of the electrospray current matches the theoretical value very well (linear regression shows $R^2 = 0.98$). Due to the fewer number of channels and the higher back pressure of the 6-nozzle MES emitters, only the 9-nozzle MES emitters were used in the following on-line MS measurements.

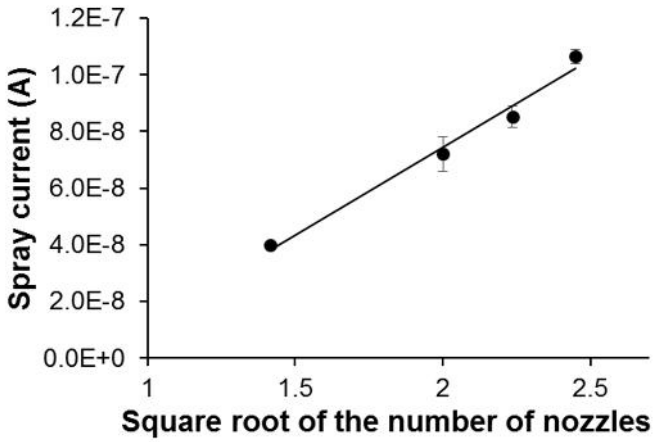

Figure 3.14 Plot of the electrospray current measured for a 6-nozzle MES emitter relative to the square root of the number of working nozzles, showing the theoretical enhancement of current predicted for MES behaviour. Conditions: 79.2% water/19.8% methanol (with 1% acetic acid) at 100 nL/min flow rate, 3.5 kV applied potential.

3.3.4 Electrospray characteristics of MSF emitters with polymer micro-nozzles in the channels using mass spectrometers

To demonstrate the practical benefits of MES, the polymer nozzle MES emitters were connected online with a Thermo Scientific Orbitrap mass spectrometer. The electrospray current enhancement of MES is derived from the increased ionization efficiency resulting from the smaller initial droplets in the lower flow spray of the individual nozzles relative to the total flow rate. In theory, the enhancement should be observed in a mass spectrometer as an increase in a given ion signal by the spectrometer, assuming efficient transmission of the additional ions into the mass analyzer. In this experiment, continuous 500 nL/min flow of 1 μM leucine enkephalin (LE) in 50% acetonitrile (v/v in water) was electrosprayed using 1) a 9-nozzle MES emitter with 9 working nozzles, 2) one with a single working nozzle, and 3) a commercial SilicaTip™ emitter with 8 μm tip diameter. Presented in Figure 3.15A is the XIC for the LE peak over a 10-minute period for each emitter. The XIC intensity for the 9-nozzle emitter (1.79 ± 0.03

$\times 10^7$ cps) was found to be 2.5 times greater than that for the 1-nozzle emitter ($0.71 \pm 0.03 \times 10^7$ cps). The signal enhancement is close to the expected factor of 3, which corresponds to the square root of the number of emitters. The full theoretical signal enhancement was likely not realized because of inefficiencies in ion transmission, as the electrospray plume generated by the MES emitter is far wider than for a single nozzle owing to electrostatic repulsion of the high ion density. As a result, some ions fail to enter the mass spectrometer orifice and are thus not detected. This drawback of MES emitters is known, and engineering solutions to the problem have been presented in the literature.[19] In fact, for previously reported MES emitters where the individual nozzles were separate capillary-based emitters,[19] the inter-nozzle distance of 500 µm (center to center) greatly exacerbated the ion transmission problem. Modification of the mass spectrometer inlet with an ion funnel[20] is expected to capture more of the plume and allow achievement of the full MES effect, but because near-theoretical signal enhancement is already achieved, it is unlikely to be worth the additional cost to install an ion funnel. Also shown in Figure 3.15A is the XIC trace for the commercial tapered emitter ($0.82 \pm 0.01 \times 10^7$ cps), closely matching that of the MES emitter with one nozzle working. This result implies that the electrospray behaviour of a single polymer nozzle is comparable to that of the commercial emitter of similar tip diameter. The voltage applied to the tapered capillary emitter (1.2 kV) is much lower than that applied to the MSF-based emitters (3.5 kV), which is attributed to the electric shielding experienced by the nozzles in the vicinity of the MSF tip face. The LE mass spectra accumulated for 74 scans (averaged 1 minute) for each of the tapered, 1-nozzle, and 9-nozzle emitters in Figure 3.15A are presented in Figure 3.15B, 3.15C and

3.15D, respectively. The background noise is low, with the signal-to-noise ratio of the LE molecular ion peak being at least 5110 for these mass spectra.

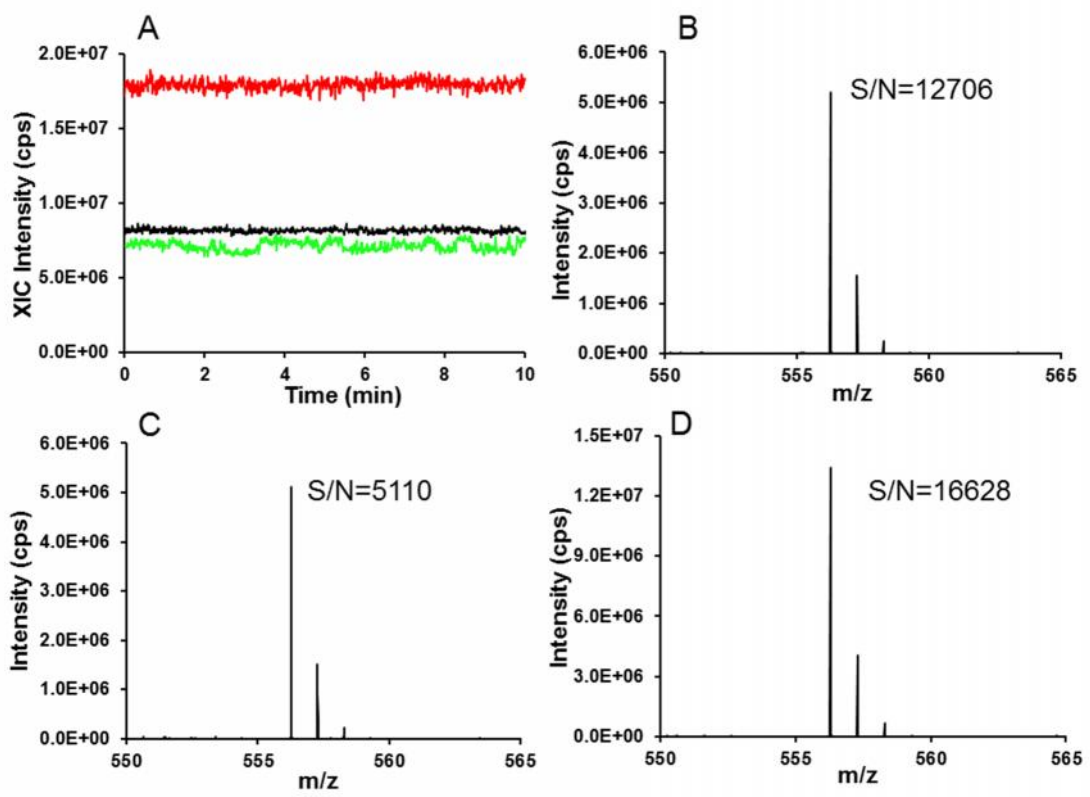

Figure 3.15 A) XIC intensity for the LE peak when using a 9-nozzle MES emitter (top, red), an 8 μm SilicaTip™ emitter (middle, black), and a 9-channel MES emitter with only 1 working nozzle (bottom, green). Mass spectra for LE ($M + H^+ = 556.28$ amu) associated with the B) SilicaTip™, and C) 1-nozzle D) 9-nozzle, emitters in A), with signal-to-noise ratios calculated for the molecular ion as indicated in each case. Noise was measured as the standard deviation of the background signal. Conditions: 500 nL/min, 1 μM LE in 50% ACN/water with 0.2% formic acid, 3.5 kV applied voltage for the MES emitters and 1.2 kV for the tapered emitter.

Another way of thinking about the online signal enhancement of MES is to consider the signal arising from a given number of analyte molecules, *e.g.* the XIC intensity for the LE peak divided by its molar concentration, as a function of flow rate. Consistent with nanoelectrospray theory,[21] as the flow rate drops, the initial electrospray droplets get smaller and ionization efficiency increases. The XIC signal per mole LE sprayed from a given solution from the emitter, then, increases sharply as the flow rate drops,

demonstrating the efficiency of sample utilization at low flow rates.[6] As seen in Figure 3.16A, the signal per mole is much greater for the 9-nozzle MES emitters than it is for a commercial fused-silica emitter having an 8 μm tip diameter at any given total flow rate for the 1 μM LE solution, this effect diminishing as flow rate increases. Recalling that the signal enhancement arises from the benefits of nanoflow electrospray from individual nozzles while the emitter is spraying at a higher total flow rate, the data in Figure 3.16A was re-plotted in Figure 3.16B with flow rates reflecting those from individual nozzles, *i.e.* flow rate per nozzle. In this sense, emitters behave as though their flow rate is high while enjoying the excellent ionization efficiency associated with much lower flow rates. The consistency of the plot in Figure 3.16B with a hypothetical plot describing signal intensity per mole for a single emitter as a function of flow rate further demonstrates the MES nature of the emitter, and that the signal enhancement is primarily attributable to flow rate.

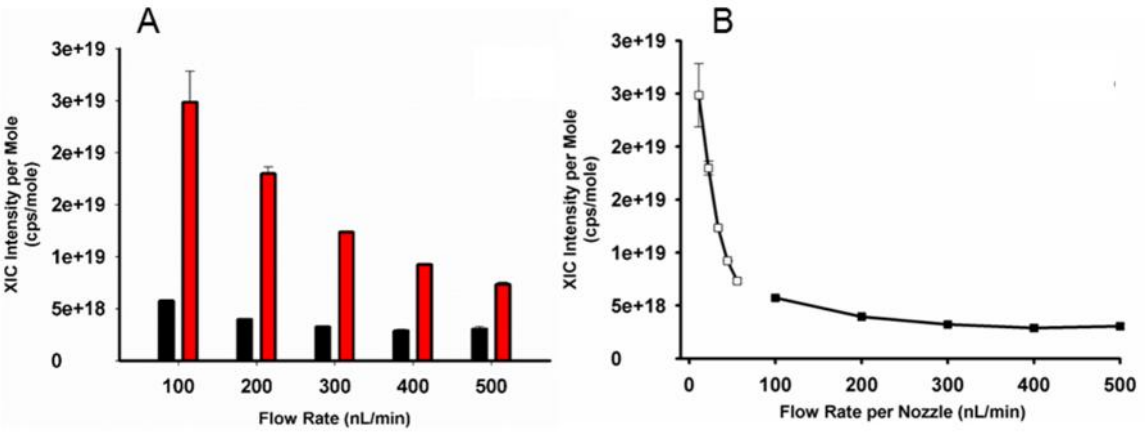

Figure 3.16 XIC intensity relative to the number of moles of analyte as a function of flow rate, showing the sharp increase in sample utilization efficiency as flow rate drops. A) comparing sample utilization efficiency of the 9-nozzle MES emitter (red) and a commercial 8 μm tip diameter SilicaTip™ emitter (black) relative to the total flow rate applied experimentally. B) the same data as in A) for the MES emitter (open squares) and SilicaTip™ emitter (dark squares) relative to the flow rate coming from each emitter, which represents the ionization efficiency the emitter enjoys as a result of multiplying the electrospray. The electrospray solution in all cases was 1 μM LE in 50% water/50% acetonitrile (v/v) containing 0.2% formic acid (v/v).

To further demonstrate the applicability of the 9-nozzle MES emitters, samples were sent to an independent laboratory for testing. A tryptic digest of bovine serum albumin (BSA) was separated by nano-LC at 400 nL/min using an established method and coupled online to a QTRAP 5500 mass spectrometer using a MES emitter. A representative chromatogram showing overlaid XIC traces for selected diagnostic *m/z* peaks resulting from the injection of peptides from a tryptic digest of 1 fmol BSA appears as Figure 3.17A. Peak widths and separation efficiency are indistinguishable from chromatograms obtained using commercial electrospray emitters, and no obvious signs of sample carry-over were observed (data not shown). This result is particularly important as it shows that the polymeric material of the nozzles does not interfere with the retention times or peak shape of the eluting analytes, as might be expected when a phenyl-based polymer is in contact with hydrophobic analytes. The organic content required to elute the peptides from the reverse phase column was high enough to prevent adsorption to the polymeric nozzle material. Furthermore, the multi-channel nature of the emitter may also be anticipated to contribute to band broadening or tailing peak shapes if flow amongst the channels is not homogeneous, but this effect was not observed either.

Chromatographic data for a series of 54 injections using this set-up is presented in Table 3.1. For the set of 14 diagnostic peptides over the *m/z* range 450-723 amu, peak area standard deviation is no greater than 30% (<21% for all peptides except one) and retention time standard deviation is no greater than 0.05 minute for any given peak. Presented in Figure 3.17B is a chromatogram obtained for the same sample under the same conditions, with a sample injection from the digestion of only 10 amol BSA. The chromatogram is nearly identical to that in Figure 3.17A, but with lower signal intensity. Signal-to-noise

ratio, however, is still over 140 for the peak representing the peptide at *m/z* 461.8 amu (peak in red), for example, demonstrating the excellent sensitivity of the emitter when used in conjunction with the system at the external research facility.

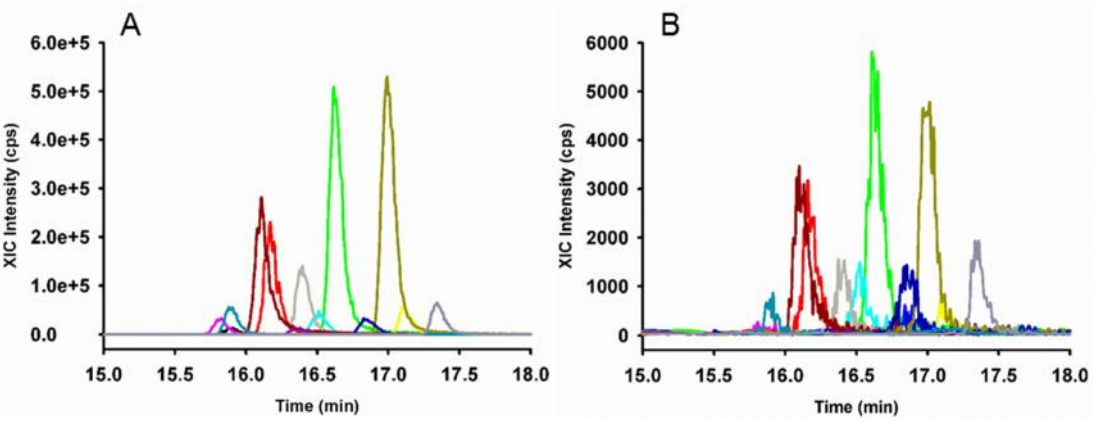

Figure 3.17 LC/MS chromatogram showing 14 representative peptides from the tryptic digestion of A) 1 fmol BSA and B) 10 amol BSA using a 9-nozzle MES emitter.

Table 3.1 Chromatographic data for the analysis of 54 injections of tryptically digested BSA (10 fmol injected) using a LC/MS system and a 9-nozzle MES emitter.

Peptide (*m/z*)	**Peak Area (counts)**	**RSD (%)**	**Retention Time (min)**	**Retention Time Standard Deviation**
450.2	551635	16	15.867	0.039
461.8	3832490	15	16.166	0.034
464.3	8322063	16	16.63	0.046
474.2	2144762	29	17.109	0.028
480.6	3381617	20	16.595	0.034
487.7	1070608	18	15.802	0.04
547.3	4487451	17	16.468	0.031
554.8	2684630	9.9	16.398	0.032
570.7	9995829	8.4	16.123	0.035
571.9	152714	21	16.8	0.03
582.3	11232597	19	16.998	0.047
628	6515428	17	16.846	0.029
653.4	1104590	14	16.336	0.032
722.8	3589601	8.6	15.9	0.038

Given the size of the polymer micro-nozzles and their precarious position above the MSF tip face, the MES emitters have remarkable stability and robustness. The repeated injections for the LC/MS experiments did not lead to deterioration in performance, either from the perspective of signal intensity or chromatographic reproducibility. These experiments also showed excellent electrospray stability over a wide and rapidly changing solvent composition, performing well even while going from 98% acetonitrile to 98% water in 0.2 minute. Furthermore, online constant infusion experiments in our lab (Figure 3.15A) showed excellent electrospray stability, as judged by the XIC intensity of the LE peak. The RSD for the 9-nozzle MES emitter over 10 minutes of spraying was only 1.8%, comparable to the best commercial emitters, such as a SilicaTip™ emitter having 8 μm tip diameter, which was found to have a RSD in XIC intensity of 1.7% over the same time under similar conditions.

3.4 Conclusions

In summary, MSFs offer a convenient, highly customizable template material to fabricate MES emitters capable of enhancing the signal in the nanoelectrospray regime and increasing sample throughput. MES, however, was not obtained with the commercial MSFs as the small pitch contributes to spray coalescence. Custom silica MSFs with a larger pitch and nine or six channels arranged in a radial pattern were designed and fabricated to minimize inter-channel electric field inhomogeneities and promote MES. Polymer micro-nozzles produced by an optimized polymerization/etching procedure were required to prevent the sprays from coalescing and minimize the interference. Nine or six individual electrosprays operating in the cone-jet mode were generated from a single emitter. Offline electrospray experiments showed a square root relationship between the electrospray

current and the number of nozzles, confirming MES behaviour. When coupled online with a mass spectrometer, the spray current enhancement provided by the 9-nozzle MES emitter translated into a near-theoretical enhancement in the extracted ion current measured for a model peptide. Signal variations with flow rate demonstrated that the signal enhancement from MES arises from the benefits of using lower (nano) flow rates for electrospray, whereby smaller initial electrospray droplets lead to much improved ionization efficiency. The MSF-based emitter enables the generation of multiple Taylor Cones with a very small footprint producing both higher electrospray current and ion intensity compared to a single-channel emitter. Furthermore, the cylindrical MSF patterned with polymeric nozzles enable facile coupling with standard fluid delivery methodologies and compatibility with existing ion sources. The number of nozzles in the radial array may be expanded to increase the nozzle density to further enhance spray current in future designs. The simplicity of the design and fabrication combined with the convenience of coupling to conventional equipment make the MES emitters more readily applicable across many fields, particularly for applications where sensitivity is most important, such as in the study of proteomics.

3.5 References

[1] G. T. T. Gibson, S. M. Mugo, R. D. Oleschuk, *Mass Spectrometry Reviews* **2009**, *28*, 918-936.

[2] B. Lojewski, W. Yang, H. Duan, C. Xu, W. Deng, *Aerosol Science and Technology* **2012**, *47*, 146-152.

[3] P. Mao, R. Gomez-Sjoberg, D. Wang, *Analytical Chemistry* **2013**, *85*, 816-819.

[4] B. Q. T. Si, D. Byun, S. Lee, *Joural of Aerosol Science* **2007**, *38*, 924-934.

[5] R. T. Kelly, J. S. Page, R. Zhao, W.-J. Qian, H. M. Mottaz, K. Tang, R. D. Smith, *Analytical Chemistry* **2008**, *80*, 143-149.

[6] S. Su, G. T. T. Gibson, S. M. Mugo, D. M. Marecak, R. D. Oleschuk, *Analytical Chemistry* **2009**, *81*, 7281-7287.

[7] S. B. Q. Tran, D. Byun, V. D. Nguyen, H. T. Yudistira, M. J. Yu, K. H. Lee, J. U. Kim, *Journal of Electrostatics* **2010**, *68*, 138-144.

[8] A. K. Sen, J. Darabi, D. R. Knapp, *Microfluidics and Nanofluidics* **2007**, *3*, 283-298.

[9] G. T. T. Gibson, R. D. Wright, R. D. Oleschuk, *Journal of Mass Spectrometry* **2012**, *47*, 271-276.

[10] J. C. Knight, T. A. Birks, P. S. J. Russell, D. M. Atkin, *Optics Letters* **1996**, *21*, 1547-1549.

[11] N. B. Cech, C. G. Enke, *Mass Spectrometry Reviews* **2001**, *20*, 362-387.

[12] X. Wu, R. D. Oleschuk, N. M. Cann, *Analyst* **2012**, *137*, 4150-4161.

[13] R. T. Kelly, J. S. Page, I. Marginean, K. Tang, R. D. Smith, *Analytical Chemistry* **2008**, *80*, 5660-5665.

[14] G. T. T. Gibson, S. M. Mugo, R. D. Oleschuk, *Polymer* **2008**, *49*, 3084-3090.

[15] I. Marginean, R. T. Kelly, J. S. Page, K. Tang, R. D. Smith, *Analytical Chemistry* **2007**, *79*, 8030-8036.

[16] Q. Luo, G. Yue, G. A. Valaskovic, Y. Gu, S.-L. Wu, B. L. Karger, *Analytical Chemistry* **2007**, *79*, 6174-6181.

[17] S. M. Ngola, Y. Fintschenko, W.-Y. Choi, T. J. Shepodd, *Analytical Chemistry* **2001**, *73*, 849-856.

[18] R. Bocanegra, D. Galan, M. Marquez, I. G. Loscertales, A. Barrero, *Journal of Aerosol Science* **2005**, *36*, 1387-1399.

[19] R. T. Kelly, J. S. Page, K. Tang, R. D. Smith, *Analytical Chemistry* **2007**, *79*, 4192-4198.

[20] R. T. Kelly, A. V. Tolmachev, J. S. Page, K. Tang, R. D. Smith, *Mass Spectrometry Reviews* **2010**, *29*, 294-312.

[21] M. S. Wilm, M. Mann, *International Journal of Mass Spectrometry and Ion Processes* **1994**, *136*, 167-180.

Chapter 4 Fabrication of Silica Multi-nozzle Emitters for Multiple Electrospray Ionization by Selective Etching of a Custom-designed Microstructured Fiber with Doped Regions

4.1 Overview

Microstructured fibers (MSFs) represent a class of optical fiber that features an array of air channels as part of a cladding designed to guide light through the core by total internal reflectance.[1] Typically, these fibers are composed of silica and the channels are evenly spaced and homogeneous in diameter. The construction of MSFs starts with a preform at a manageable scale, either a disc through which holes are drilled or, more often, an assembly of tubes and rods, where the holes/tubes are carefully places according to a design. This preform is then drawn, sometimes in steps, at high temperatures to a thin fiber that retains the pattern of the preform.[2]

Additionally, the preform can have regions of different properties, such as doped regions of silica.[3] An example of this type of MSF is a polarization-maintaining photonic crystal fiber with doped regions. It is known from solid silica fibers, that birefringence may be introduced by stress-applying parts (SAPs). That is, a part of the fiber consists of a material with a different thermal expansion coefficient than that of silica resulting in a stress field in the fiber when it is cooled below the softening temperature of silica during fabrication. In this way the fiber is given a built-in stress field and, because of the elasto-optic effect, the glass becomes birefringent.[4] An example of the polarization-maintaining silica MSF (Figure 4.1A), which was obtained from NKT Photonics (LMA-PM-15,

Birkerød, Denmark) contains boron-doped silica on either side of the 54 channels (cladding) as SAPs.

Wet chemical etching, particularly by hydrofluoric acid (HF), is a commonly used approach to remove silica in a predictable and well-controlled manner. It is well known that different types of silica are etched by HF at different rates, which allows the fabrication of structure at the tip of a MSF after etching if that fiber is comprised of more than one type of silica.[5-7] Selective etching of these doped regions is demonstrated in Figure 4.1B and 4.1C, where HF etches these regions faster than silica to leave depressions and ammonium bifluoride (AF), another commonly-used etchant, etches these regions slower than silica to leave raised plateaus.[8] With the versatility imparted in the patterning of MSFs by preform drawing methods, coupled with the flexibility in etching selectivity of various doped silica materials and with etchant pH, the shape, size, and pattern of surface structures is extremely variable and precisely controlled.

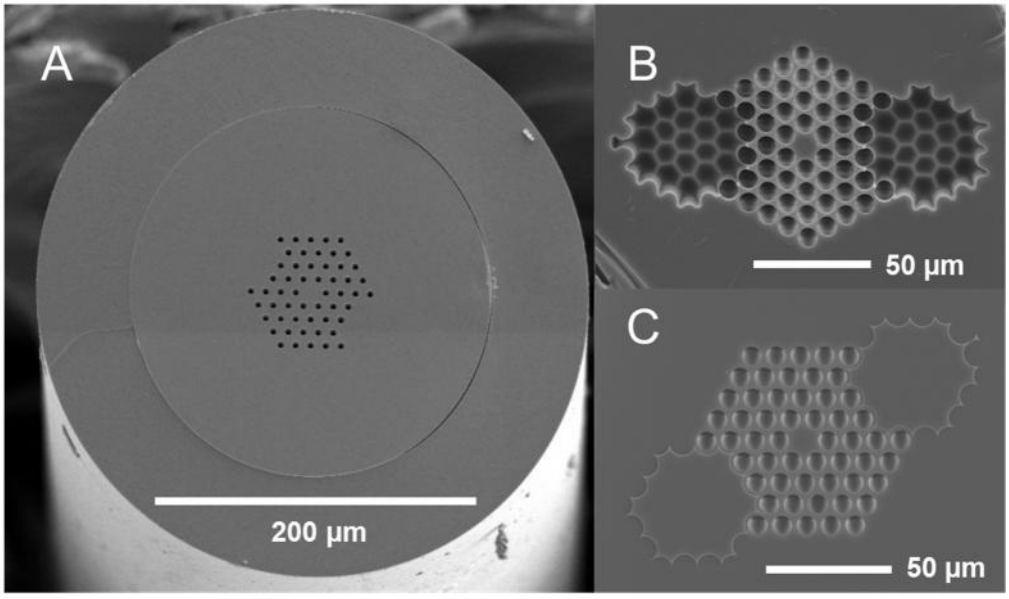

Figure 4.1 Scanning electron microscopy (SEM) images of the cross-section of MSF with 54 channels and SAPs: A) bare fiber with protective coating; B) fiber after etched in AF for 12 minutes; C) after etched in HF for 1 minute. Scale bars are labelled on the images.

One application of this approach to materials fabrication is the development of multiplexed emitters for electrospray ionization (ESI). In ESI mass spectrometry, the effects of multiple electrospray (MES) impart a major advantage in the analysis of ions, particularly for biological samples such as proteins.[9] Much of the benefit is associated with the dependence of ESI on solution flow rate. As the flow rate drops, especially to the nL/min range, the charged droplets that are ejected from the electrospray plume become smaller and the efficiency of charge transfer to analyte molecules in solution improves.[10] A variety of MES emitters have been developed,[11] including examples fabricated by microchip fabrication techniques, laser ablation, or simply assembling an array of conventional fused-silica capillary-based emitters.[12, 13] These emitters are typically large and do not couple well with traditional mass spectrometer inlets,[13, 14] are complicated to fabricate,[15, 16] or usually both.[12, 17]

MSFs present an interesting alternative approach to MES emitters, as they can be fabricated to any design having dimensions compatible with conventional LC and MS equipment. However, commercially available MSFs have channels that are too close together to enable MES, even with the assistance of polymer nozzles.[18] Specially designed polymer MSFs without nozzles were found to be limited in conditions where MES was possible.[19] When polymer nozzles were fabricated in the channels of a custom-designed silica MSF, while MES was successful, the nozzles need to be more easily produced and more robust to supplant those fashioned in silicon and stainless steel.

The study in this chapter seeks to improve on previous work involving MSF by utilizing a fiber custom designed with 9 channels positioned in a radial fashion with a diameter of 360 μm which allows for use with conventional ESI apparatus. This fiber has

a structure inspired by polarization-maintaining photonic crystal fibers with channels of pure silica surrounded by doped regions to facilitate nozzle formation promoted by differing etch rates. This study demonstrates a procedure to produce multiple silica nozzles which protrude from the tip of the fiber by protecting the inner channel with flowing water as has been previously demonstrated by Kelly *et al.* for a single channel.[20] Additionally, this study shows that the produced multi-nozzle emitters are able to function effectively as nano-ESI emitters, demonstrating the expected trend for MES with current increasing with the number of spraying nozzles at a given flow rate.

4.2 Experimental

4.2.1 Reagents and Materials

(Tridecafluoro-1, 1, 2, 2-tetrahydrodecyl)dimethylchlorosilane (TFDCS, **1**) and (heptadecafluoro-1, 1, 2, 2-tetrahydrodecyl)dimethylchlorosilane (HFDCS, **2**) were purchased from Gelest Inc. (Morrisville, PA,USA). All other chemicals and solvents were obtained from Sigma-Aldrich or Fisher Scientific and used without purification unless stated otherwise. Electrospray solvents were degassed and filtered prior to use. See details in section 2.2.1. The pulled-tip nanoelectrospray emitters (non-coated 8 or 10 μm internal tip diameter, SilicaTip™) were purchased from New Objective (Woburn, MA, USA).

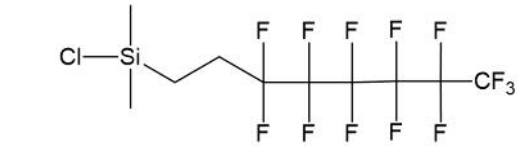

1

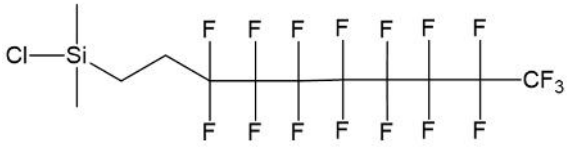

2

4.2.2 Fiber design and fabrication

Custom silica MSF was designed in our lab to have channels made from a different preform material than the bulk of the fiber, such that selective etching could be used to make a nozzle at each channel exit. In the design (Figure 4.2), 9 channels were set 100 µm apart (pitch) to prevent interference between electrosprays, and arranged in a radial pattern to ensure electrical shielding effects are equivalent for all channels.[14, 19, 21] The outer diameter (o.d.) of the fiber was 360 µm to match standard fused-silica capillary, for which plastic fittings are commercially available (standard Upchurch Microtight fittings (0.014”)). The 9 capillaries that form the channels are made of pure silica while the large center rod and 36 small filler rods that fill the space around the 9 silica capillaries are doped by 9 mol% boron (grey regions shown in Figure 4.2). Because these doped regions are etched faster than pure silica by HF, the silica immediately surrounding the channels protrudes from the fiber tip following etching to form micro-nozzles.[8] The capillaries having thick walls ensure the nozzles are protruding long enough above the emitter tip after the etching process. Channel inner diameter (i.d.) is 10 µm, which is similar to the aperture diameter of standard tapered nano-ESI emitters and all channels reside on a centred circle with a diameter of 275 µm. Design was fabricated by Canada’s Excellence Research Chair in photonics innovations (CERC) (Québec City, Canada). The macroscopic preform of the MSF was first constructed, by stacking the rods and capillaries together followed by drawing down to a fiber at high temperature (a technique commonly referred to as ‘‘stack and draw’’).[1] The arrangement and diameters of the tubes and rods were chosen by CERC based on experience such that the target dimensions will be met upon drawing.

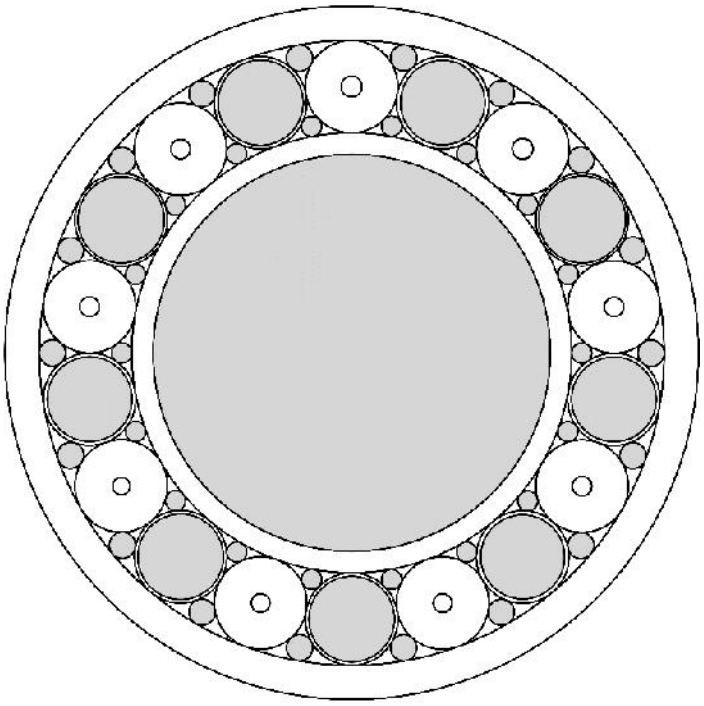

Figure 4.2 Design for the silica MSF with boron-doped regions (9 mol% boron) in grey color having nine channels arranged in a radial array. The o.d. of the fiber is 360 µm and the channels i.d. is 10 µm with a pitch of 100 µm.

4.2.3 Emitter preparation

Prior to etching, part of the MSF's protective polyacrylate coating was removed thermally using a wire stripper (Stripall TWC-1, Teledyne Impulse, San Diego, CA, USA). A fiber cleaver (LDC-400, Vytran, Morganville, NJ, USA) was then used in the stripped area to produce a straight cleave for etching. The fiber was connected to a syringe filled with deionized water via plastic fittings (IDEX, PK-120BLK with an F-185x sleeve). A syringe pump (Harvard Apparatus Pump 11 Plus, Holliston, MA, USA) was used to control the rate of flow. The other end was observed under an optical microscope (Nikon Eclipse ME600, Nikon Canada, Mississauga, Canada) or a USB microscope (Veho VMS-004D) to ensure all 9 channels had water flowing at the desired rate. After confirmation of flow, the etching end was placed into a 1.5 mL microcentrifuge tube containing 350 µL of 48 wt%

HF (aq.) such that the tip of the MSF was suspended in etchant. The fiber was etched with constant flow of 75 nL/min water for 14 minutes, and then transferred to a microcentrifuge tube containing water to quench further etching and clean the tip of debris. The fiber was left in the water with a high flow rate of flushing water for 25 minutes. The etched fiber was cleaved at a length of ~5 cm, and the remaining protective coating was removed to give a final emitter, which was examined by a microscope to determine if all nozzles were generated evenly by the etching process. A schematic of the apparatus is shown in Figure 4.3.

To make the surface of the emitter less wettable by the electrospray solvent, it was chemically modified by a hydrophobic group through a silanization reaction.[18] After drying the emitters at 150 °C for >6 hours, the tip of an emitter was immersed into the silanization solution, comprising 3:1 (v/v) toluene:HFDCS (totaling 400 µL), in the same manner as for etching (Figure 4.3C). This reagent was chosen for its highly hydrophobic properties with an observed contact angle of 111°.[22-24] The emitters were left in the solution overnight, at which time the emitters were rinsed with acetonitrile (95% in water) using an HPLC pump for 20 minutes and stored in a desiccator until needed.

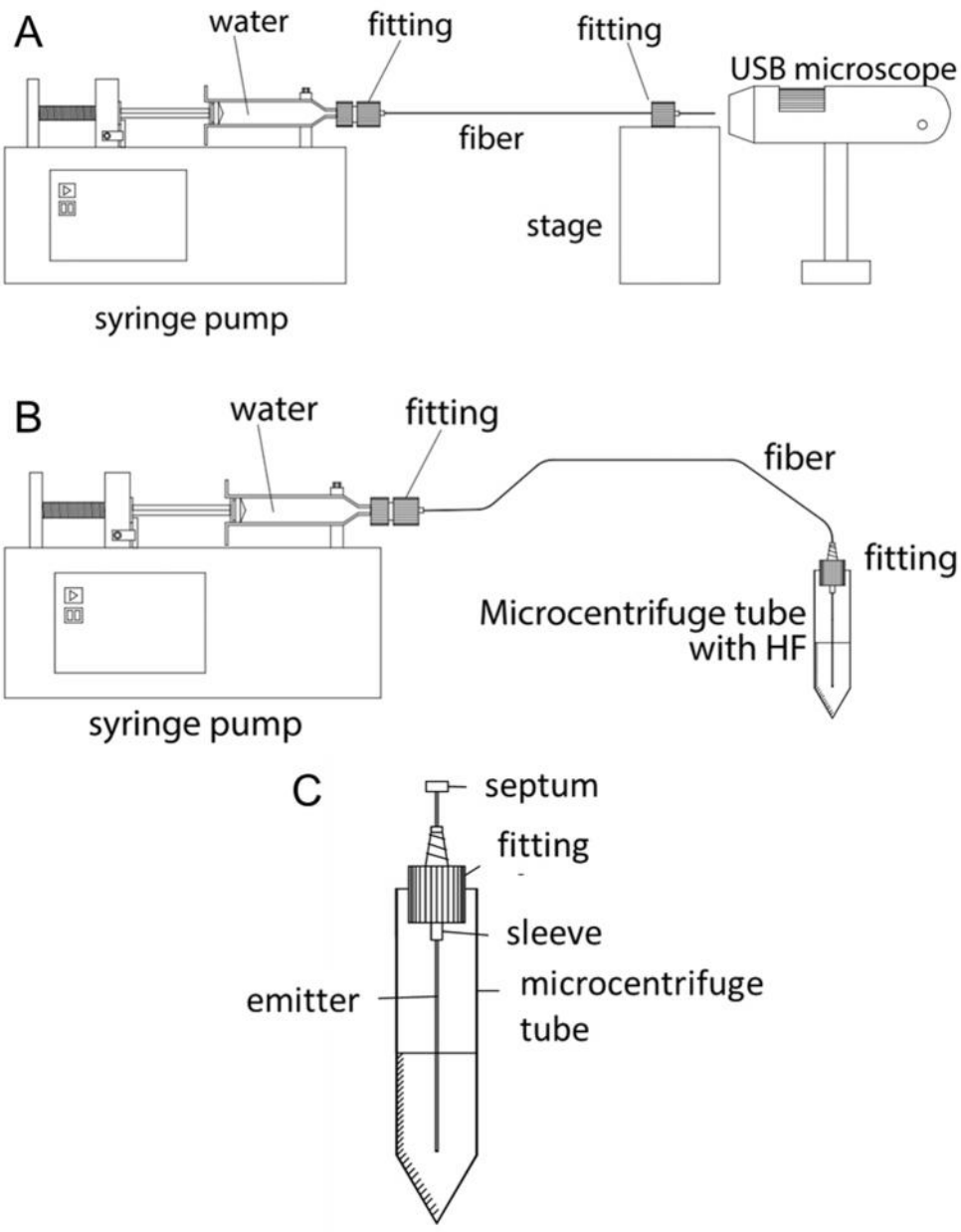

Figure 4.3 Schematic setups of A) a USB microscope and a syringe pump for confirmation of water flow from all 9 channels of the MSF, B) etching MSF end in concentrated HF with water flow and C) silanization step showing immersion of etched tip of an emitter into the reagent solution.

4.2.4 Offline electrospray current measurement and spray imaging

The experimental setup for measuring the electrospray current was shown in Figure 2.3 in Chapter 2. See details in section 2.2.4. Electrospray current was measured for 5 minutes for each run and the mean and standard deviation were used as the data point and

uncertainty. Additionally, a solvent gradient was used to test the multi-nozzle emitters for their performance under typical LC conditions using offline conditions in two cycles with a change in composition from 1% methanol to 50% methanol and back. This cycle was done twice, the first time holding at 50% methanol for 1 minute followed immediately by a second cycle which was held at 50% methanol for 5 minutes.

4.2.5 Online electrospray ionization mass spectrometry

See details in section 3.2.5.

4.2.6 Scanning electron microscopy (SEM)

See details in section 2.2.3.

4.3 Results and discussion

4.3.1 The architecture of MSF with doped regions

The aim of the study is to design and fabricate MSF with doped regions which have different etch rate to directly form nozzles promoting MES by etching process. Several design elements are similar to the custom-designed MSF with polymer micro-nozzle array as MES emitters discussed in the previous chapter. The o.d. of the fiber was reduced to 360 μm in order to be more compatible with the small circular mass spectrometer orifice. The fiber design (Figure 4.2) was assembled into the preform in Figure 4.4A, which was drawn into the fiber shown in Figure 4.4B and 4.4C. The SEM image (C) shows the simple surface structure of the cross section of the MSF, but the optical image (B) shows the nature of the silica composition due to the different refractive indexes of the pure silica and boron-doped regions, which appear darker. From this image it can be seen that the boron-doped silica rods lose their shape and fill in the space around the pure silica tubes, owing to the lower

temperature at which the doped silica melts. The dimensions of the drawn MSF were measured to be: o.d. of the fiber is 363.7 ± 0.8 µm, channel diameter is 8.2 ± 0.1 µm and the pitch of the channels is 96.3 ± 1.0 µm residing on a centered circle with a diameter of 281.5 ± 2.0 µm based on measurements using SEM images. The dimensions of the final MSF fulfill the design.

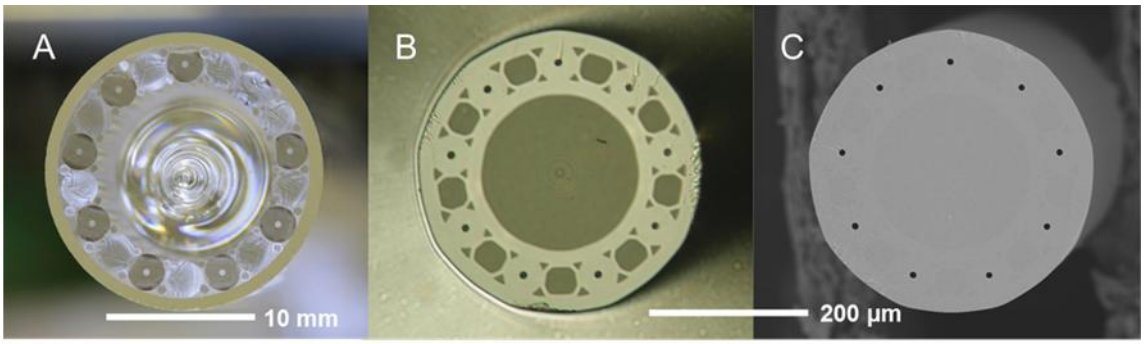

Figure 4.4 A) Optical image of the MSF preform as constructed by CERC; B) optical image of the drawn fiber (boron-doped regions are darker); and C) SEM image of the drawn fiber. Scale bars are labeled on the images.

4.3.2 Fabrication of multi-nozzle MES emitters

Based on our experience on the emitters fabricated by pure silica MSF with similar dimensions, the blunt face of the MSF with doped regions would not support MES without nozzle formation. Nozzles at the channel exits would provide a better barrier between channels, less surface area to wet, and a finer point closer to the counter electrode upon which the electric field is concentrated leading to stable electrospray at lower voltage.[25] When a similar MSF was modified to have polymer nozzles at the channel exits, independent electrosprays were observed at each nozzle over a wide range of conditions. To avoid the issues associated with polymer nozzles, however, including fragility of the polymer tubes and potential incompatibility with certain analytes, all-silica nozzles built in to the MSF would be a major advantage.

To this end, the new MSF was designed to possess channels made of pure silica which have slower etch rate surrounded by boron-doped regions which have faster etch rate in HF to facilitate nozzle formation.[8] After etching the MSF tip with HF, the optical image in Figure 4.4B gives a good indication of what the final structure will look like and where the nozzles will appear. SEM imaging was used to determine the degree of nozzle protrusion and the channel diameter altered by the etching procedure.

A series of fibers were etched in the HF solution for various times from 6 to 17 minutes, with representative SEM images shown in Figure 4.5. As time passes, the pure silica regions are etched at the same rate over the face of the fiber tip, while the boron-doped regions are etched more quickly and occupy a deeper plane (Figure 4.5B). The silica features, such as the rims defined by the inner and outer silica tubes in the design, are also etched laterally as etchant is able to access the sides of these features after the surrounding borosilicate is removed. At some point, the surface area of these rims is reduced to zero and they become sharp ridges with a defined height relative to the borosilicate plane (Figure 4.5C). As etching continues, lateral etching eventually removes all the silica features at the outside of the MSF and channels are no longer enclosed (Figure 4.5F). An important consequence of this lateral etching is the widening of the channels as etchant enters the tubes and etches the silica there. The diameter of the channels increased to 29 ± 0.5 μm from 8.2 μm after only 6 minutes of etching (Figure 4.5B). Not only does the change in channel diameter affect the electrospray performance, but this etching of the silica that forms the nozzle greatly limits the nozzle's protrusion length. From the measurements of the channel diameter, the etch rate of the pure silica parts is calculated to be 1.7 μm/min.

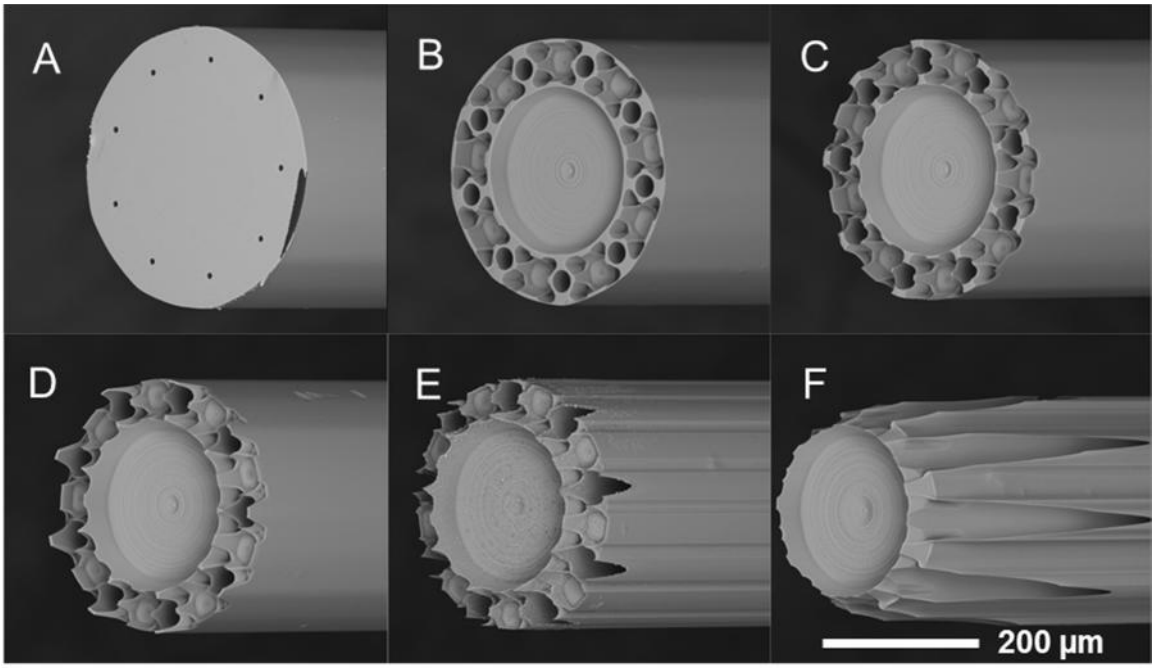

Figure 4.5 Tilted SEM images of a MSF A) before etched and after etched in HF without running water for B) 6 minutes, C) 8 minutes, D) 10 minutes, E)12 minutes and F)17 minutes. Scale bar is labelled on the images.

In order to prevent the etchant from entering the channels and widening the openings, the channels can be filled with a material inert to the etching process and subsequently removed to restore the channels. The simplest way of accomplishing this in a continuous fluid conduit like a MSF is to flow water through the channels from the other end, at a linear velocity that overcomes the diffusion of HF into the channels. Ultimately this approach will dilute the etchant near the tip surface, so the lowest possible flow rate should be used. Indeed, effective results have been observed for the etching of a single-channel capillary.[20, 26] The SEM image in Figure 4.6 demonstrates the effectiveness of water flow in a MSF, where 5 channels having no water flow due to blockage show channel widening from 8 to 38 µm while 4 channels protected with flowing water show negligible widening over 8 minutes of etching time with HF. The partial channel blockage resulted from the dissolved gasses in the water. It was found that the presence of bubbles can block

multiple channels on one side of the fiber in an unpredictable manner. To prevent this effect and ensure all the channels have water flowing through them, the deionized water was degassed by boiling for 15 minutes to keep bubbles from forming.

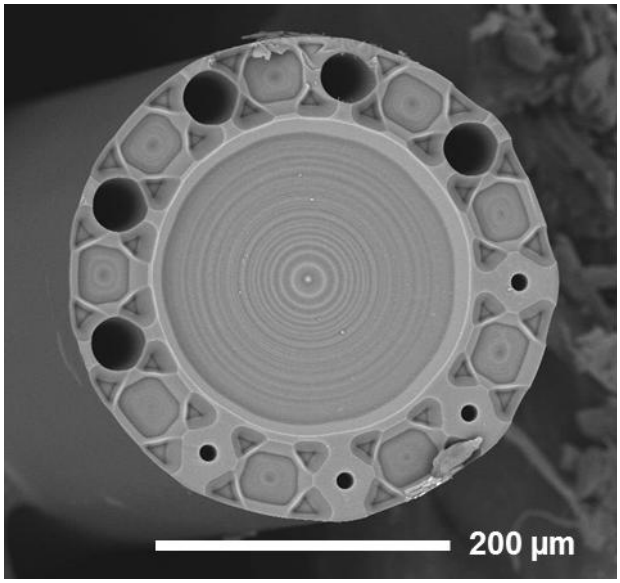

Figure 4.6 SEM image of a fiber etched in HF for 8 minutes with 90 nL/min water flow rate. Bubbles in the water caused partial blockage of the channels during etching process resulting in 4 channels protected while 5 channels did not, demonstrating the importance of water protection and degassing procedure. Scale bar is labelled on the image.

The etching time for the MSF immersed in HF etchant with 75 nL/min water flow was optimized for nozzle shape and protrusion length. This low flow rate was found to give reproducibly negligible channel widening and not to significantly affect the etch rate over the etching times studied, so this water flow rate was used for all further etching. As etching time increases, the lateral etching of the silica tubes that form the nozzles causes the silica surrounding the channels to be removed. While the channels are no longer etched from the inside in the presence of flowing water, etching time is essentially limited by the time it takes for the loss of silica to reach the channel. This etching time was found to be 14 minutes for the fiber design in this work (Figure 4.4), where the silica remaining around a given channel is only ~10 µm thick, ultimately defining the nozzle tip. Presented in Figure

4.7A and 4.7B are SEM images showing the front and side views of a MSF face after etching for 14 minutes in HF with 75 nL/min water counter flow. Measurements indicate that the channels are equivalent in diameter to those prior to etching (8.3 ± 0.2 μm vs. 8.2 ± 0.1 μm, respectively). The nozzle protrusion length, defined as the distance from the tip of the nozzle to the bottom plateau comprised of borosilicate glass (see Figure 4.7B), was found to be 60.8 ± 1.2 μm. This translates to borosilicate parts etching 4.3 μm/min faster than silica parts over the 14 minutes, or about 6.0 μm/min (1.7 + 4.3 μm/min). The o.d. of the fiber decreased from 363.7 ± 0.8 μm to 310.3 ± 1.6 μm. These measurements can be compared to another segment of the same fiber etched for 14 minutes which show no protrusion as the walls of each channel etched away without water protection causing the formation of a recessed area. Additionally, the channel diameter of the fiber was found to dramatically increase from 8.3 ± 0.2 μm to 48.8 ± 0.9 μm as seen in Figure 4.7 C and 4.7D. The observed etch rates (1.7 μm/min for pure silica parts and 6 μm/min for borosilicate parts) are similar to previous literatures on concentrated HF etching which show ~1.5 μm/min etch rate on pure silica and ~6 μm/min etch rate for Corning Pyrex 7740 glass which also has boron-doped regions.[8, 27]

For the MSF design in this work, therefore, the best possible nozzles are those shown in Figure 4.7A. To increase nozzle protrusion, the pure silica tubes that define the channels would need to have walls of initially greater thickness, allowing longer etching time before the nozzle tip diameter is minimal. From Figure 4.7A it can also be seen that the outer silica tube has been completely removed at this etching time, although etching from the outside of the fibre has not yet reached the channel. Thus, the initial wall thickness

of the outer tube (at the MSF perimeter) should also be increased accordingly so that its removal by etching does not expose the channel from the side at the desired etching time.

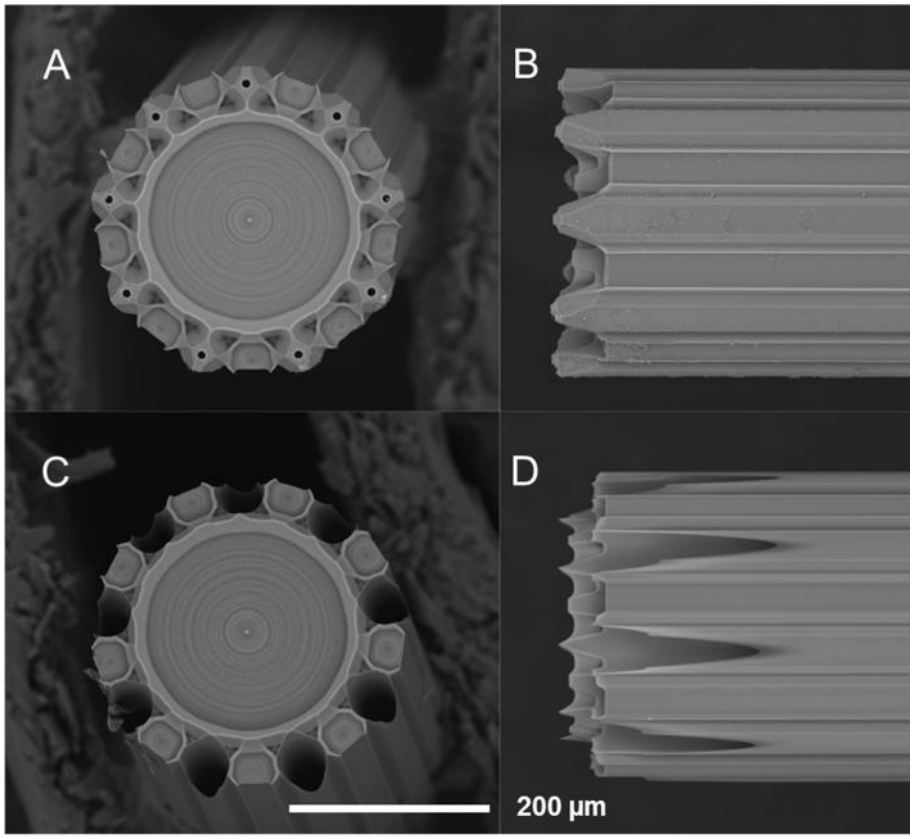

Figure 4.7 SEM images of multi-nozzle emitter generated by etched in HF for 14 minutes with a water flow rate of 75 nL/min, having nozzle protrusion length of 60.8 µm and channel diameter of 8.3 µm: A) top view and B) side view; and images of emitter etched in HF for the same period of time without water flow for comparison, having a channel diameter of 48.8 µm with no effective nozzle formation: C) top view and D) side view. Scale bar is labelled on the images.

The chosen flow rate value is near the maximum allowable to only protect the channel region from the etching effect producing the longest nozzles without channel expansion. Higher flow rate will affect efficient nozzle formation and dilute the etchant quickly, while lower flow rate will not effectively prevent the etchant from flowing into the channels resulting in increased channel diameter. Even assuming complete dissociation

and using fluoride ion diffusion constants found by Li *et al.* the concentration at a given distance after a given time is given by Fick's law:[28]

$$C = n_0\left(\mathrm{erf}\left(\frac{x}{2\sqrt{Dt}}\right)\right) \qquad \textbf{Equation 4.1}$$

Where n_o is the concentration at the interface of the acid and water, C is the concentration at a given distance, x is the distance from origin, D is the diffusion coefficient, t is time, and *erf* is the error function. When the interface is between a solution with some concentration and a pure solvent, the Equation 4.1 has an approximation:

$$C = n_0\left(1 - \left(\frac{x}{2\sqrt{Dt\pi}}\right)\right) \qquad \textbf{Equation 4.2}$$

The concentration at the origin was taken to be 28 molal, obtained from a previous study of activities in concentrated HF. For simplicity, the activity of F^- was assumed to be equal to that of H_3O^+, and D is 13.1 × 10^{-6} cm^2/s.[29] In Fick's law the theoretical flow rate needed to dilute the HF in the channels to less than 0.1 M is calculated by Equation 4.2 when the distance of the etchant into the channel is set as 1 μm (0.0001 cm):

$$. \mathrm{M} = 28\mathrm{M}\left(1 - 2\left(\frac{0.\quad 01\,\mathrm{cm}}{2\sqrt{13.2 \times \quad^{-6}\,\mathrm{cm\ s^{-}\ t\ \pi}}}\right)\right)$$

t is calculated as 0.000243 second and this translates to a linear velocity of 0.411 cm/s, or 24.7 cm/min. For each channel with a diameter of 8.2 μm (radius is 4.1 μm or 0.00041 cm), this translates into a volumetric flow rate of 13.04 nL/min. therefore, total flow rate would be 117 nL/min for 9 channels, which is similar to the actual water flow rate used in the study.

4.3.3 Electrospray testing and MES behaviour

Offline electrospray testing was conducted on the multi-nozzle MSF emitters by measuring electrospray current under a variety of conditions and visually monitoring the electrospray mode using the set-up described in Figure 2.3. For emitters without chemical modification at the emitting end, stable individual Taylor cones were not formed with the highly aqueous spray solvent (79.2% water, 19.8% methanol and 1% acetic acid, v/v). With the newly etched silica having an exceptionally clean surface with many exposed hydroxyl groups, the water contact angle is low and the associated surface wetting is considerable.[30] Rapid wetting of the surface was observed within 5 seconds despite the nozzles being raised from the MSF tip surface, and the formation of a single large Taylor cone covering the entire tip face was unavoidable.

To counteract this, the emitters were functionalized with various silanizing agents to render the tip surface hydrophobic. Using an emitter functionalized using 3-(trimethoxysilyl)propyl methacrylate (γ-MPS), stable MES behaviour was observed for <1 minute before failure led to complete wetting of the fiber tip, an irreversible effect that prevented future MES from that emitter. Stable MES was observed for up to 1 hour using an emitter treated with the fluoroalkyl chlorosilane TFDCS, although this level of robustness is still insufficient. The longer-chain silane HFDCS, used as a hydrophobic coating on many substrates,[24] was used for all further experiments as it was able to last between 5 and 15 hours of offline testing under acidic (1% acetic acid) conditions. It was also found that using di- and tri-chlorosilanes for the surface functionalization suffered from crosslinking siloxane polymerization reactions and undesirable rough surfaces, leading to the use of mono-chlorosilanes in this work.[23] It is likely that acid-catalyzed

hydrolysis of the siloxane bonds that hold the hydrophobic groups to the surface is the cause of this failure, and indeed the use of less concentrated acid solutions in other testing did appear to improve the longevity of MES for these emitters. In all cases, re-functionalizing an emitter after tip wetting was able to renew MES ability with no apparent deterioration of performance or longevity. Hydrophobic surface functionalization is well studied, and it is anticipated that a more robust coating, such as the polymeric coatings typically used in HPLC stationary phases, would greatly improve the robustness and versatility of these MES emitters.

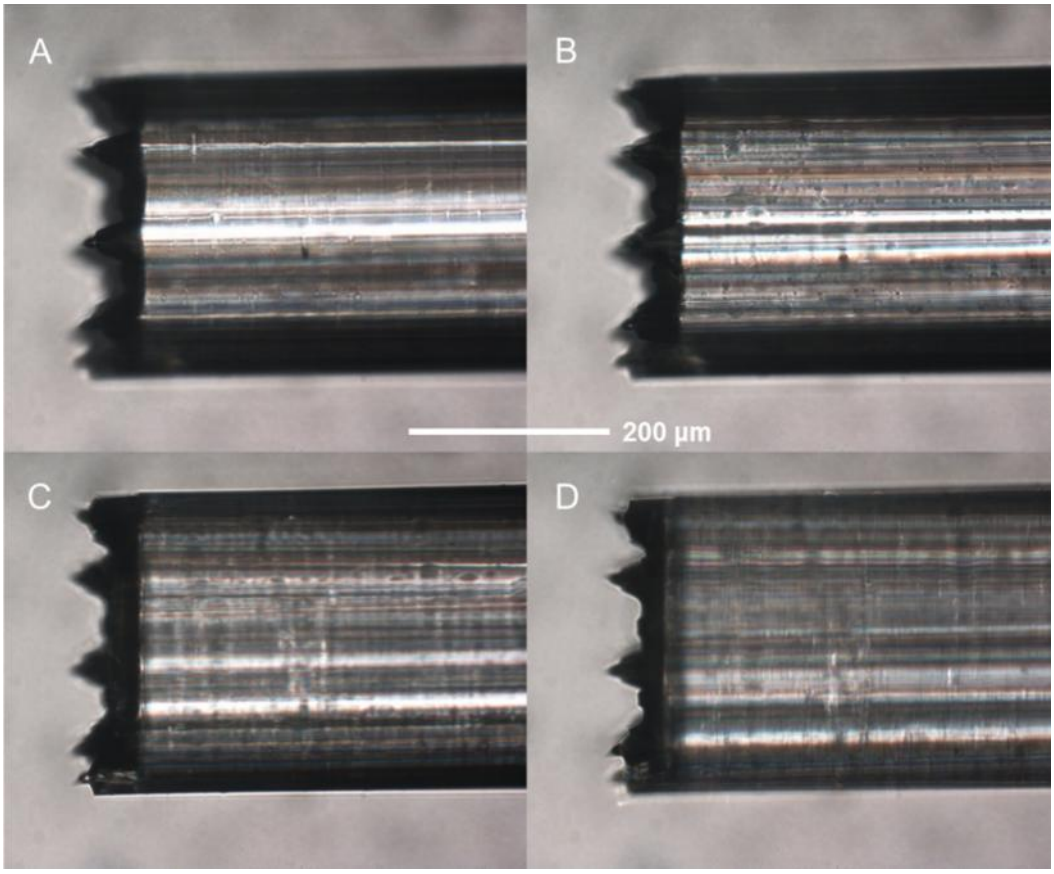

Figure 4.8 Photomicrographs (200x magnification) of 9 individual electrosprays in stable cone-jet mode generated from the multi-nozzle emitter with a hydrophobic coating (HFDCS) with the plane of focus successively changing to visualize of all 9 individual Taylor cones from A) front nozzles to D) back nozzles. Conditions: 79.8% water/19.2% methanol/1% acetic acid at 300 nL/min total flow rate, 2.8 kV applied potential and 2 mm working distance.

A series of photos exhibiting stable, independent electrosprays in cone-jet mode coming from each nozzle of the emitter with a hydrophobic coating (HFDCS) are shown in Figure 4.8A to 4.8D, with the plane of focus changing to allow clear visualization of all 9 individual Taylor cones, demonstrating the MES behaviour of this type of emitter. The chemical functionalization of the surface and elevation of the nozzles relative to the tip face help to avoid wetting of the face and eventual loss of MES. The pointed shape of the nozzles also helps to concentrate the electric field at the nozzle tip, allowing more stable electrosprays at lower voltage.[25] The radial pattern of the nozzles around the emitter axis positions the nozzles to experience equivalent electric field by equalizing the effects of shielding,[14] but it is apparent from Figure 4.8 that electrostatic repulsion of the positive ions in the electrospray plumes causes them to orient themselves off axis.

Further testing revealed that the emitters support MES over a wide range of operating conditions. Nine individual electrosprays were observed for applied voltages of 2.2-3.4 kV (at 0.3 µL/min), with stable cone-jet mode for all nozzles consistently and for extended periods being practically limited to 2.6-3.2 kV. While the voltage is high compared to a single tapered emitter (typically 1-2 kV), it is a known consequence of electrospray from multiple nozzles on a planar emitter face that shielding raises the applied voltage required to invoke a particular electric field at each nozzle.[12, 17] Full MES behaviour was also observed at 2.8 kV for total flow rates from 100 nL/min to 3.0 µL/min (data not shown). These conditions represent a remarkably wide range over which these emitters generate stable MES, and while full characterization of spray conditions was not explored,[31] it is anticipated that stable MES can be achieved outside of these ranges if other conditions, such as solvent, working distance, voltage or flow rate, are changed.

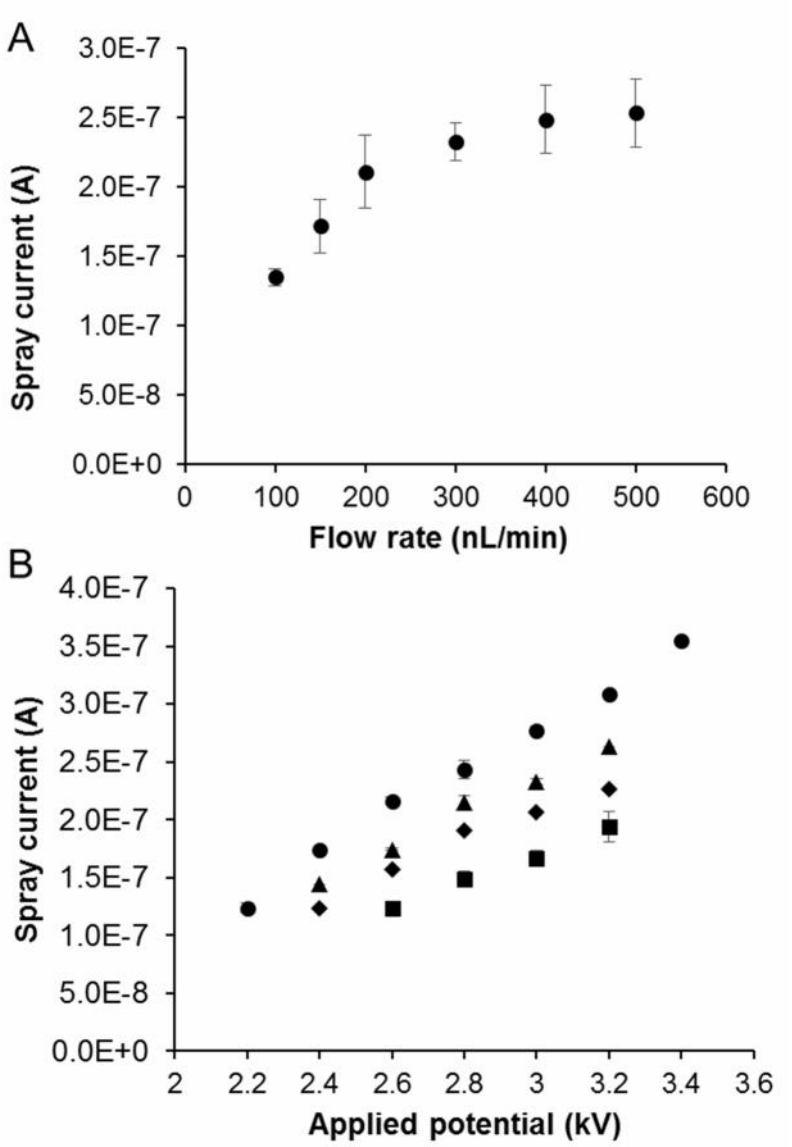

Figure 4.9 Spray current as a function of A) flow rate for 9-nozzle MES emitters showing expected square root dependence across a total flow rate range from 100 to 500 nL/min under the applied potential of 2.8 kV and B) applied potential for the emitters at the same total flow rate of 300 nL/min, showing a linear response to potential across entire tested voltage range indicating stable Taylor cone formation throughout for various number of working nozzles (circle: 9 nozzles; triangle: 8 nozzles; diamond: 6 nozzles; square: 4 nozzles) spraying 79.8% water/19.2% methanol (with 1% acetic acid).

The small electrical current generated by the electrospray was measured for all conditions tested, with the value for a particular condition being the mean current over at least 5 minutes acquisition time and the uncertainty being the standard deviation of the mean. The spray current was first plotted as a function of total flow rate at a particular

voltage (2.8 kV) from 100 to 500 nL/min, presented in Figure 4.9A. The plot follows the well-known square root dependence on flow rate, which arises from the increased supply of charged species at higher flow rates counteracted by poorer ionization efficiency.[16] When the flow rate is held steady (300 nL/min), the dependence of the spray current on applied voltage is linear (Figure 4.9B). As all the nozzles of the emitter are spraying in the same cone-jet regime over all conditions in the plot, and the working distance defines the constant resistance of the system, this linearity is predicted by Ohm's law. These results indicate that each of the nozzles of the emitter are behaving independently as single Taylor cones, without cooperative or interference effects among electrosprays.

The most interesting consequence of the MES behaviour exhibited by the multi-nozzle MSF emitters is the dependence of the spray current on the number of nozzles. At a given total flow rate, the spray current is enhanced by a factor of $\sqrt{n}$ relative to a single electrospray, where *n* is the number of times that flow is split into individual electrosprays. For the multi-nozzle MSF emitters in this study, fabricating prototypes of a series of designs having more or fewer nozzles was not cost-effective. Instead, some of the channels can be blocked from the inlet end of the MSF such that a fewer number of nozzles are in use. In this way, the same total flow rate and otherwise equivalent electrospray conditions can be applied to the same type of emitter with a variable number of working nozzles. Presented in Figure 4.10 is a plot of spray current, collected at 300 nL/min total flow rate and 2.8 kV applied potential, as a function of the square root of the number of working nozzles. The linear dependence (linear regression shows $R^2 = 0.98$) is definitively indicative of true MES behaviour, demonstrating the greatest advantage of MES emitters, that the current signal is enhanced by a factor of $\sqrt{n}$ relative to that of the commercial

single-channel emitters at the same total flow rate. A manifestation of the spray current dependence on the number of working nozzles appears in the Ohm's law plots in Figure 4.9B, where emitters having more working nozzles exhibited straight lines at higher currents as expected under the same testing conditions.

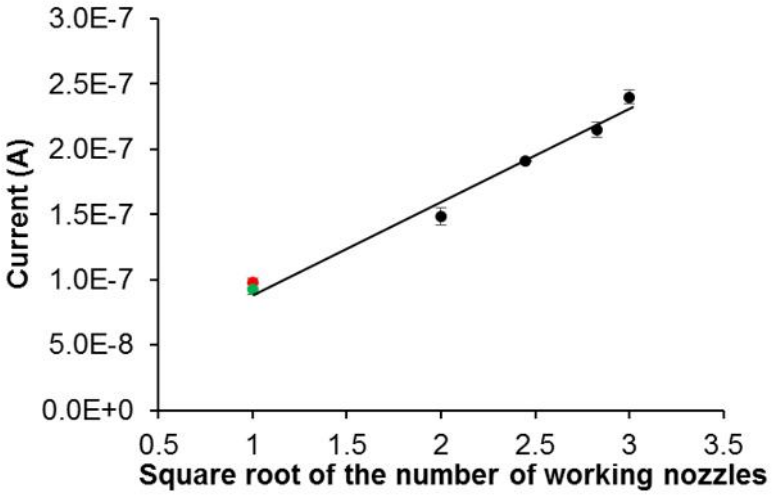

Figure 4.10 Spray current measured for multi-nozzle MES emitters as a function of the square root of the *n* (the number of spraying nozzles), showing good correlation with the theoretical current enhancement predicted by splitting the flow into *n* independent electrosprays and demonstrating MES behaviour of the multi-nozzle MSF emitter. Conditions: 79.8% water/19.2% methanol/1% acetic acid at 300 nL/min total flow rate, 2.8 kV applied potential. The red and green data point in the plot indicate the spray current produced by 10 μm and 8 μm i.d. SilicaTip™ emitters respectively under the same conditions (applied potential is 1.2 kV).

One of the most popular applications for electrospray emitters is to couple a LC separation to a mass spectrometer for detection. Nearly all LC separations involve the use of a solvent gradient, which aids in the resolution, range, and throughput of a chromatographic separation. For this reason, the multi-nozzle MSF emitters were tested offline with imaging and spray current measurement during a change in solvent composition typical in LC/MS. The spray current measured during the solvent change is presented in Figure 4.11. Over two gradient cycles from 99:1 water:methanol (by volume, with 1% acetic acid) to 50:50 water:methanol and back, electrospray remained stable at

each individual nozzle. The spray current followed the change in solvent composition, without significant change in current each time the solvent composition returned to the same value. An interesting result of this experiment is that the inclusion of methanol up to 50% by volume did not affect the ability of the hydrophobic coating to maintain MESs at the tip face.

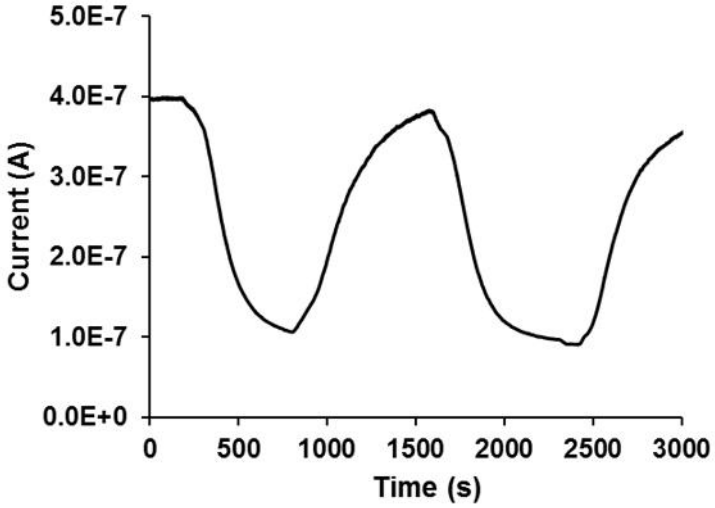

Figure 4.11 Spray current changes with solvent composition using a multi-nozzle MES emitter. Following a typical solvent gradient encountered during LC/MS analysis, the emitter experienced two gradient cycles from 99:1 water:methanol to 50:50 water:methanol and back. The first cycle has a 1 minute hold time at 50% methanol while the second has a 5 minutes hold time. Conditions: 2.8 kV applied potential and 300 nL/min flow rate.

4.3.4 Online electrospray testing with a mass spectrometer

The multi-nozzle MSF emitters were coupled with a Thermo Scientific Orbitrap mass spectrometer to test them for their practical application. The enhancement of electrospray current using MES emitter technology manifests in mass spectrometry as increased signal intensity for a given peak in the mass spectrum obtained for a given analyte. Being essentially due to the collective electrospray of lower flow rates generating smaller charged droplets, MES causes a much improved ionization efficiency without sacrificing

the benefits of a larger total flow rate. To test this, a continuous flow of 1 µM leucine enkephalin (LE) in 50% acetonitrile (v/v in water) was electrosprayed using a multi-nozzle emitter, and a commercial SilicaTip™ emitter with 10 µm tip diameter at a flow rate range from 100 to 500 nL/min. The extracted ion current (XIC) for the LE peak over a 10 minute period for each type of emitter is presented in Figure 4.12A. Online experiments showed excellent electrospray stability, as judged by the XIC intensity of the LE peak. The relative standard deviation (RSD) for the multi-nozzle emitter over 10 minutes of spraying was only 2.1%, comparable to the commercial emitter which was found to have a RSD in XIC intensity of 1.8% over the same time under similar conditions (flow rate: 500 nL/min). The voltage applied to the commercial emitter (1.5 kV) is only half of that applied to the multi-nozzle emitter (3.0 kV), which is ascribed to the electric shielding experienced by the nozzles in the vicinity of the fiber tip face. Furthermore, the XIC intensity for the multi-nozzle emitter and the commercial emitter was found to be $6.2 \pm 0.04 \times 10^6$ cps and $5.5 \pm 0.1 \times 10^6$ cps, respectively. The preliminary results indicate that the emitter is more effective at ionizing the analyte and shows a ~13% improvement over the commercial emitter in the XIC. The larger electrospray plume generated by the silica multi-nozzle emitter due to electrostatic repulsion of the high ion density and gradual hydrolysis of the hydrophobic coating on the tip face probably affect the ion transmission efficiency resulting in this lower sensitivity enhancements than expected as a large part of ions failed to go through the small MS orifice and thus not detected. The MS sensitivity would be further increased if the multi-nozzle emitters are optimized and used in conjunction with an electrodynamic ion funnel to capture more of the ions.[32]

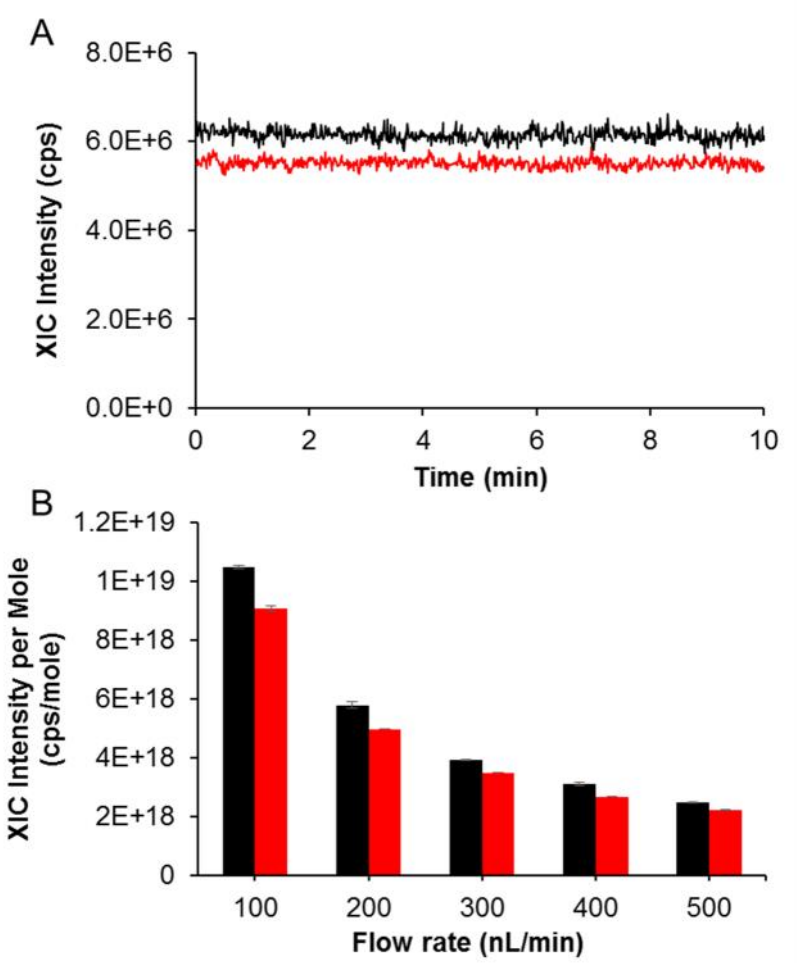

Figure 4.12 A) XIC intensity for the LE peak over 10 minutes showing comparable stability of a multi-nozzle emitter (top, black), and a 10 µm i.d. SilicaTip™ emitter (bottom, red) under conditions: 1 µM LE in 50% acetonitrile/water with 0.2% formic acid with 500 nL/min flow rate, 1.5 kV applied potential for the commercial emitter while 3.0 kV applied potential for the multi-nozzle emitter; B) XIC intensity relative to the number of moles of analyte as a function of flow rate, showing the increase in sample utilization efficiency as flow rate drops and comparing sample utilization efficiency of the multi-nozzle emitter (black) and a commercial 10 µm i.d. SilicaTip™ emitter (red) relative to the total flow rate applied.

If the signal is plotted relative to the number of moles of analyte delivered by the system, *e.g.* the XIC intensity for the LE peak divided by its molar concentration, as a function of flow rate, as in Figure 4.12B, the sensitivity rises as flow rate decreases, demonstrating the sample utilization efficiency of the system as one can use much less sample without greatly compromising sensitivity.[18] Consistent with nanoelectrospray

theory,[10] when the flow rate drops, the initial electrospray droplets get smaller and ionization efficiency increases. As seen in Figure 4.12B, the signal per mole is greater for the multi-nozzle emitter than it is for a commercial fused-silica emitter having an 10 μm tip diameter at any given total flow rate, this effect diminishing as flow rate increases.

4.4 Summary

A MSF with boron-doped regions was designed, fabricated and tested for MES ability. Nine equivalent channels were spaced evenly in a radial pattern to ensure each experienced the same electric field during electrospray experiments, and their distance from each other was set to avoid interference among channels. Most importantly, the glass surrounding the silica channels was doped with boron, allowing the accelerated etching of this material to reveal raised nozzles at each channel exit. Conditions were optimized for a 48 wt% HF solution to etch the MSF emitter tip to generate pointed nozzles ~61 μm from the flat tip face. This nozzle architecture, along with hydrophobic coating of the tip surface, allowed the individual channels to support independent electrosprays. The MES behaviour of the emitter was demonstrated offline by the square root dependence of the electrospray current on the number of working nozzles in the multi-nozzle MSF emitter. Using this approach, highly sensitive and robust MES emitters can be rapidly fabricated, showing theoretical MES current enhancement and an exceptionally wide range of operating voltages and flow rates. While drawing MSFs may be expensive, a single batch can generate extremely long fibers making the process cost effective and amenable to mass production.

Further studies can improve on the nature and application of the hydrophobic coating to increase the longevity of the emitter. Additionally, more online ESI-MS tests to

verify the potential sensitivity improvement indicated in the offline electrospray tests are necessary to completely characterize the emitter and to confirm the already observed increase in spray current. A realistic LC/MS separation using the multi-nozzle emitter compared to a commercial emitter would be also conducted in the future to demonstrate the applicability and robustness of the emitter which has dimensions compatible with conventional LC and MS systems without any special adaptations. The single-fiber MES emitters described in this chapter offer a drop-in replacement for commercial tapered emitters to greatly improve electrospray signal and flexibility in spray conditions with much-improved resistance to clogging, without a significant sacrifice in signal stability or physical robustness. These attributes make these emitters highly applicable to a wide variety of fields where ion signal is important, especially where sample is scarce, such as in proteomics.

4.5 References

[1] P. Russell, *Science* **2003**, *299*, 358-362.

[2] J. C. Knight, T. A. Birks, P. S. J. Russell, D. M. Atkin, *Optics Letters* **1996**, *21*, 1547-1549.

[3] J. Folkenberg, M. Nielsen, N. Mortensen, C. Jakobsen, H. Simonsen, *Optics express* **2004**, *12*, 956-960.

[4] J. Noda, K. Okamoto, Y. Sasaki, *Journal of Lightwave Technology* **1986**, *4*, 1071-1089.

[5] Y. Kunii, S. Nakayama, M. Maeda, *Journal of The Electrochemical Society* **1995**, *142*, 3510-3513.

[6] J. Buehler, F. P. Steiner, H. Baltes, *Journal of Micromechanics and Microengineering* **1997**, *7*, R1-R13.

[7] S. Pevec, E. Cibula, B. Lenardic, D. Donlagic, *Photonics Journal, IEEE* **2011**, *3*, 627-632.

[8] G. A. C. M. Spierings, *Journal of Materials Science* **1993**, *28*, 6261-6273.

[9] J. B. Fenn, M. Mann, C. K. Meng, S. F. Wong, C. M. Whitehouse, *Science* **1989**, *246*, 64-71.

[10] M. S. Wilm, M. Mann, *International Journal of Mass Spectrometry and Ion Processes* **1994**, *136*, 167-180.

[11] G. T. T. Gibson, S. M. Mugo, R. D. Oleschuk, *Mass Spectrometry Reviews* **2009**, *28*, 918-936.

[12] K. Tang, Y. Lin, D. W. Matson, T. Kim, R. D. Smith, *Analytical Chemistry* **2001**, *73*, 1658-1663.

[13] I. Marginean, R. T. Kelly, J. S. Page, K. Tang, R. D. Smith, *Analytical Chemistry* **2007**, *79*, 8030-8036.

[14] R. T. Kelly, J. S. Page, I. Marginean, K. Tang, R. D. Smith, *Analytical Chemistry* **2008**, *80*, 5660-5665.

[15] W. Deng, C. M. Waits, B. Morgan, A. Gomez, *Journal of Aerosol Science* **2009**, *40*, 907-918.

[16] R. Bocanegra, D. Galán, M. Márquez, I. Loscertales, A. Barrero, *Journal of Aerosol Science* **2005**, *36*, 1387-1399.

[17] P. Mao, R. Gomez-Sjoberg, D. Wang, *Analytical Chemistry* **2012**, *85*, 816-819.

[18] S. Su, G. T. T. Gibson, S. M. Mugo, D. M. Marecak, R. D. Oleschuk, *Analytical Chemistry* **2009**, *81*, 7281-7287.

[19] G. T. T. Gibson, R. D. Wright, R. D. Oleschuk, *Journal of Mass Spectrometry* **2012**, *47*, 271-276.

[20] R. T. Kelly, J. S. Page, Q. Luo, R. J. Moore, D. J. Orton, K. Tang, R. D. Smith, *Analytical Chemistry* **2006**, *78*, 7796-7801.

[21] X. Wu, R. D. Oleschuk, N. M. Cann, *Analyst* **2012**, *137*, 4150-4161.

[22] D. Ge, L. Yang, G. Wu, S. Yang, *Chemical Communications* **2014**, *50*, 2469-2472.

[23] I. W. Moran, D. F. Cheng, S. B. Jhaveri, K. R. Carter, *Soft Matter* **2008**, *4*, 168-176.

[24] L. Xu, R. G. Karunakaran, J. Guo, S. Yang, *ACS Applied Materials & Interfaces* **2012**, *4*, 1118-1125.

[25] S. B. Quang Tran, D. Byun, V. D. Nguyen, H. T. Yudistira, M. J. Yu, K. H. Lee, J. U. Kim, *Journal of Electrostatics* **2010**, *68*, 138-144.

[26] M. R. Emmett, R. M. Caprioli, *Journal of the American Society for Mass Spectrometry* **1994**, *5*, 605-613.

[27] H. Zhu, M. Holl, T. Ray, S. Bhushan, D. R. Meldrum, *Journal of Micromechanics and Microengineering* **2009**, *19*, 065013.

[28] A. Paul, T. Laurila, V. Vuorinen, S. V. Divinski, in *Thermodynamics, Diffusion and the Kirkendall Effect in Solids*, Springer, 2014, 115-139.

[29] L. Yuan-Hui, S. Gregory, *Geochimica et cosmochimica acta* **1974**, *38*, 703-714.

[30] P. Somasundaran, *Encyclopedia of surface and colloid science*, Vol. 8, CRC Press, 2006.

[31] I. Marginean, R. T. Kelly, D. C. Prior, B. L. LaMarche, K. Tang, R. D. Smith, *Analytical Chemistry* **2008**, *80*, 6573-6579.

[32] R. T. Kelly, A. V. Tolmachev, J. S. Page, K. Tang, R. D. Smith, *Mass Spectrometry Reviews* **2010**, *29*, 294-312.

Chapter 5 Polymer Microstructures with High Aspect Ratio and Low Polydispersity using Photonic Fibers as Templates

5.1 Overview

One dimensional micro- or nanostructures, *i.e.* tubes or fibers with diameters in the μm or nm (typically ≤100 nm) range, respectively, have been studied extensively for years. Shortly after the first organic microtubules were produced, a panel of experts brainstormed over 100 possible applications for such structures.[1] Since then, micro- and nanotubes and fibers have been proposed for a wide variety of applications including separation science, DNA transport, drug delivery, and optical, thermal or electronic sensing.[2-6]

Small 1D structures have been prepared using self-assembled templates including surfactants,[7] block copolymers[8] and even self-rolling thin films,[9, 10] whereby a polymer or metal is formed within a sacrificial channel. Such systems, however, are not widely amenable to possible materials and preparation conditions, and it is more difficult to control the length. The so-called "hard" template systems, whereby structures are formed within or around a preformed solid template and released following template removal, typically allow more dimensional control.[11] The most suitable substrates for this purpose are thin membranes with arrays of holes such as anodic aluminum oxide,[12] track-etched polymer[13] or nanochannel array glass.[14] After template removal, typically by wet etching, the remaining 1D structures can maintain a pre-arranged, axially aligned array, which is particularly useful for a wide range of applications including data storage and engineered surfaces for tailored wetting or sensing properties.[15, 16] As these templates are structurally rigid and relatively unreactive, they are compatible with preparation techniques

for a wide variety of materials, and depending on the template preparation can be more versatile in the morphology of the microstructure. These membrane templates, however, are thin by their nature and generally limit the length (and hence aspect ratio) of the 1D structures. Long fibers and tubes would be useful for applications such as wires (if electrically conductive),[17] fluidic conduits[2] or structural components for miniaturized devices. For longer polymer fibers, spinning/drawing or electrospinning of polymer melts or solutions are continuous processes that give essentially infinitely long 1D structures. These processes rely on drawing out thin streams of polymer using either mechanical[18] or electrostatic forces,[19] and conditions have been found to produce fibers with diameters from ~10 nm to ~10 μm. It is, however, difficult to spin fibers with monodisperse diameters[18] or align them,[20] and tube structures are complicated to fabricate.[21]

In this work we propose the use of a class of solid templates, namely photonic crystal fibers, that yield 1D microstructures in an array with both high aspect ratio and low dimensional polydispersity. These fibers, also known as microstructured fibers (MSFs), are silica-based waveguides developed for the telecommunications industry.[22] MSFs are designed to confine light to the core, which is usually solid (but may be hollow), by a periodic refractive index change induced by an array of parallel channels surrounding the core. Typically fabricated by stacking larger tubes and rods in a pre-determined pattern and drawing the bundle to a much smaller fiber,[23] the channel (hole) size and spacing are considerably uniform and consistent along the length.[24] These fibers have already been used for microfluidic applications including multichannel liquid chromatography,[24] capillary electrophoresis,[25, 26] and nanoelectrospray ionization MS.[27] Current availability of these template fibers is limited to those with useful optical properties, but as such there

is already a variety of channel shapes and sizes commercially available, including circular holes with diameters from 600 nm to >5 µm. In one example, 501 holes are arranged in a hexagonal array that is 37 µm wide (point to point) as shown in Figure 5.1. Smaller-scale templates can be drawn from these fibers or in the initial drawing process for the production of structures with nanoscale dimensions. Being fashioned from silica, the template is easily removed by wet chemical etching leaving an array of 1D structures. MSFs have previously been used as templates for the production of tubes and wires composed of semiconducting material (*e.g.* Si, Ge) by a microfluidic chemical deposition technique for optoelectronic devices.[28] In this chapter, we demonstrate the production of microtubes and microfibers, as well as sheathed and bare porous polymer monoliths, comprised of different organic polymers taking various cross-sectional shapes from MSF templates. As with other inorganic templates, however, ultimately any material capable of solidifying in the channels can be prepared in MSFs, including metals, pre-ceramic polymers,[29] fluoropolymers,[2] etc. This general procedure should prove useful for the production of any small 1D structures where alignment or size uniformity is a critical parameter.

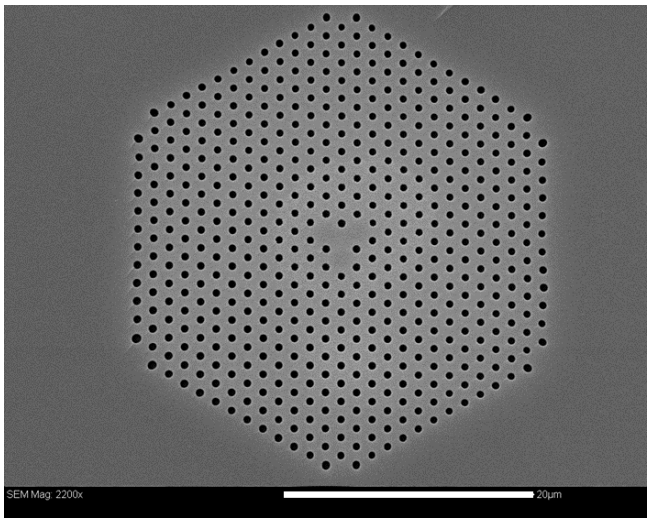

Figure 5.1 Scanning electron microscopy (SEM) image of a MSF template with 501 holes arranged in a hexagonal array, hole diameter is ~620 nm. Scale bar is 20 µm.

5.2 Experimental

5.2.1 Reagents and Materials

Glacial acetic acid, acetonitrile (HPLC grade) and deionized water (>18 MΩ•cm, Protocol) were purchased from Fisher Scientific (Ottawa, ON, Canada) and used without further purification. Butyl acrylate (BA, **1**), benzoin methyl ether (BME, **2**), 1,3-butanediol diacrylate (BDDA, **3**), 3-(trimethoxysilyl)propyl methacrylate (γ-MPS) (98%), divinylbenzene (technical grade, 80%, mixture of isomers), hydrofluoric acid (48 wt% in water, ≥99.99%), and 2,2'-azobisisobutyronitrile (AIBN) (≥98%) were purchased from Aldrich (Oakville, ON, Canada). Anhydrous and 95% ethanol were purchased from Commercial Alcohols Inc. (Brampton, ON, Canada).

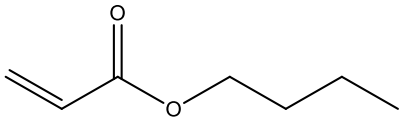

1

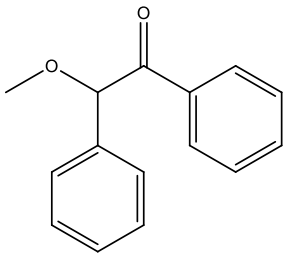

2

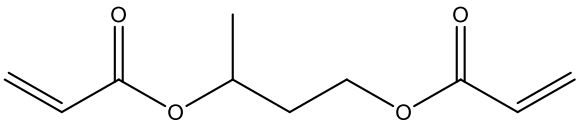

3

Commercial microstructured fiber templates were purchased from NKT Photonics (Birkerød, Denmark), with product numbers LMA-20 (126 holes), LMA-PM-15 (54 holes), NL-1550-POS-1 (501 holes), MM-HNA-5 (6 triangular holes), MM-37-01 (19 trapezoidal

holes). Additional MSF templates were designed in our lab and fabricated at INO (Quebec City, QC, Canada), each having 9 holes in a radial pattern.

5.2.2 Preparation of 1D structures

For a general idea of which procedures lead to which 1D structure morphology, see Figure 5.2.

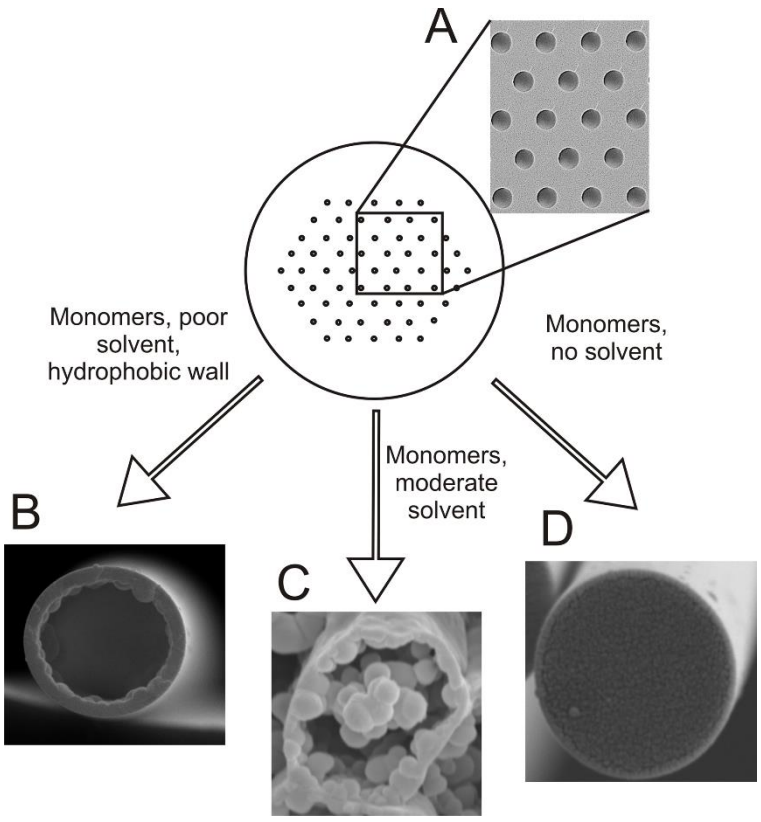

Figure 5.2 Schematic showing a typical MSF template with A) a representative SEM image of the zoomed region, along with the generalized conditions leading to the three distinct polymer morphologies in this work: B) hollow tube, C) porous monolith and D) solid fiber.

5.2.2.1 Template pretreatment

In line with typical silica functionalization work,[30] the MSFs were flushed with 0.1 M NaOH (aq.) for 1 hour with a syringe pump (Harvard Apparatus 11plus, Holliston, MA, USA) to expose surface siloxane groups for a more homogeneous surface and for

subsequent reaction with silanizing reagents. The residual alkaline solution in the MSFs was neutralized by flushing with 0.1 M HCl (aq.) for 1 hour and deionized water for 1 hour.

In most cases, the inner walls of the MSFs were then functionalized with vinyl groups using a pre-treatment procedure described previously.[31] Briefly, the MSFs were filled with a solution of γ-MPS (20% v/v), deionized water (50% v/v) and glacial acetic acid (30% v/v) using a syringe pump, then each end was immersed in the solution and it was left filled overnight to optimize surface coverage. Afterward, the MSFs were flushed with acetonitrile (95% in water) and could then be used directly or stored (filled with the flushing solution) until needed.

5.2.2.2 Formation of DVB tubes and solid rods

The procedure for the formation of polymer tubes in MSFs was adapted from studies on coated capillaries for open-tubular capillary liquid chromatography.[32] Briefly, a degassed solution containing 5 mg of AIBN, 300 µL of divinylbenzene (DVB) and 700 µL of anhydrous ethanol was pumped into the pretreated MSF using a syringe pump for sufficient time to ensure every channel is filled. Both ends of the MSF were sealed with gas chromatography injection septa, and the MSF was heated at 80 °C overnight (~16 hours) in an oven. The MSF, now containing polyDVB tubes, was then flushed with acetonitrile (95% in water) to remove any unreacted reagents.

Solid polymer rods were prepared in the same way as tubes, but the prepolymer solution contained no solvent, *i.e.* 5 mg AIBN and 1000 µL DVB.

5.2.2.3 Formation of porous polymer monoliths

The formulation for the porous polymer monolith is similar to that described in our previous papers.[33] The polymerization mixture is composed of 67% porogenic solvent (60% acetonitrile, 20% ethanol (95%), and 20% deionized water), 23% BA, 10% BDDA, and 5 mg BME (photoinitiator). Polymerization was initiated using 312 nm UV light (Spectroline ENF-280C hand-held UV lamp; Fisher Scientific) with 3 minutes irradiation time. The MSFs were then flushed with acetonitrile (95% in water) to remove any unreacted monomer and cross-linker.

5.2.2.4 Template removal

The MSF templates containing polymer were cut into ~4 cm-long pieces by a ceramic cleaving stone. The acrylate coating of the MSF segments was facilely removed after softening by immersion in acetonitrile for 2 minutes. For the custom-designed MSFs, the coating was much thicker and was thus removed by burning it off with a fiber-stripping tool (StripAll TWC-1, Teledyne Impulse, San Diego, CA, USA). To facilitate subsequent handling of the 1D structures, only one end of the cleaved fiber was inserted in 48% hydrofluoric acid (aq.) for 15 to 30 minutes to remove the silica template. The etched end of the fiber was inserted in deionized water for 30 minutes to remove the HF and any debris from the material.

5.2.3 Scanning electron microscopy (SEM)

The polymer tubes, rods and monoliths fabricated using MSFs as templates were mounted normal to the aluminum stub using tape to facilitate imaging of the cross-section.

SEM images were obtained using either a Jeol JSM-840 (Tokyo, Japan) or a Leo 1530 field emission (Oberkochen, Germany) scanning microscope.

5.3 Results and Discussion

5.3.1 MSF Template

As templates for small 1D structures, microstructured fibers (MSFs) have several features that distinguish themselves from other templates. As they are formed by drawing a stack of larger tubes down to a smaller fiber, the length scale of the template is essentially continuous, allowing infinitely high aspect ratios for the resulting materials not possible with membrane-type templates. Furthermore, the template channels are aligned perfectly parallel in any desired pattern or spacing. As an added convenience, the typical diameter of the circular template is such that the fiber can be easily coupled to a liquid delivery pump (such as that used for HPLC, or a syringe pump) using standard fluidic fittings, allowing a simple means of introducing prepolymer solutions or other reactants into the template.

The stack-and-draw technique for drawing MSFs, is improving constantly. With sufficiently pure preform tubes, even heating, and controlled force applied to the end of the fiber in the drawing process, the variation in the size, shape and spacing of the template channels in the final fiber mostly matches the same parameters in the preform, which are much easier to control on the macroscopic scale. This leads to exceptional uniformity in the resulting 1D structures, at least as good as those prepared by electrospinning. A detailed analysis of the hole diameters of several MSFs obtained for this study, as measured by SEM imaging, is presented in Table 5.1. The greatest variation in channel diameter was less than 4% relative standard deviation (RSD), even for custom-made fibers. A visual example of the hole uniformity in a MSF appears in Figure 5.2.

Table 5.1 Measurements from SEM images of various dimensions of selected MSF templates and polyDVB tubes prepared therein.

Fiber Type[1]	Average MSF Hole Diameter (μm)	Average Tube Outer Diameter[2] (μm)	Average Tube Wall Thickness[2] (μm)
206	17.74 ± 0.52	17.63 ± 0.28	1.02 ± 0.14
207	9.09 ± 0.35	9.15 ± 0.17	0.76 ± 0.12
126-hole	5.58 ± 0.07	5.88 ± 0.08	0.53 ± 0.05
54-hole	3.93 ± 0.03	4.29 ± 0.07	0.47 ± 0.03
501-hole	0.619 ± 0.015	0.748 ± 0.034	0.100 ± 0.015

[1] 206 and 207 are codes given to distinct draws of custom-made MSFs having 9 holes in a radial pattern. The other MSFs were obtained commercially for various optical applications, coincidentally having the number of holes indicated. [2] Values are known to be higher than actual due to gold coating for SEM, especially for the smaller tube diameters. Uncertainty is calculated by the standard deviation of measurements (n>3).

5.3.2 Microtubes

Polymeric tubular structures formed in membrane templates are common. This is typically accomplished by a kinetic wetting effect whereby a viscous polymer solution or melt is allowed to wet the high-energy pore surface of a template, which occurs quickly relative to complete pore filling.[2, 34] Such wetting occurs as the adhesive forces between the liquid and solid dominate interactions between the liquid and vapour, leaving a vapour-filled wetted vessel. If the polymer is solidified by evaporating the solvent (for solutions) or lowering the temperature (for melts) after the precursor film is formed but before pore filling, the result is a polymer tube. In-channel polymerization has also been used to form tubes in templates. This technique usually involves pore filling with a monomer solution, but polymerization is directed to the channel surface by immobilizing initiator there prior to introducing the reaction solution.[6, 35]

The approach taken in the current study is conceptually a combination of these ideas, utilizing in-channel polymerization but directing it to the surface by a partitioning phenomenon. Essentially, template channels completely filled with solutions can still lead

to tubes if the interactions between the solidifying components and the channel surface dominate those between the components and the solvent. This corresponds with the set of conditions in Figure 5.2B, where a relatively poor solvent is used to increase the interactions between polymerizable materials and the surface. In this work, the cross-linking monomer divinylbenzene (DVB) was dissolved in ethanol along with the free radical initiator AIBN. Ethanol is a relatively poor solvent for the forming DVB polymer, and because the channel surface is functionalized with the hydrophobic vinyl-containing reagent γ-MPS, the reaction components partition to the channel wall and polymer forms primarily there. After the solvent is flushed out, the polymer tube remains covalently attached to the channel surface via the γ-MPS. The choice of solvent for this purpose is typically determined experimentally, essentially requiring that it dissolves all the monomers and initiator but not the forming polymer. Indeed, many combinations of solvents have been used depending on the system. The polymer morphology that results from choice of solvent, wall coating, tube size, etc. was the topic of a recent review.[36]

When fabricated in a variety of MSF templates followed by wet etching in HF (aq), polyDVB tubes can be made with various diameters and in various array patterns (co-polymers comprising up to 50% styrene/ 50% DVB v/v were also prepared, showing similar behaviour). Examples of tubes from 4 different MSF templates are shown in Figure 5.3, demonstrating the excellent tube uniformity and alignment in each case as well as the range of tube diameters possible from currently available templates. If the outer diameter of the tubes is treated in a manner similar to polymer molecular weights, the polydispersity index for the diameter of tubes from any given MSF template was calculated to be <1.002. Measured tube diameters appear in Table 5.1, which also shows that the structures match

the diameter of the template holes, within error. Unfortunately, the outer diameter and tube thickness appear greater than they actually are due to the layer of gold deposited on the samples for SEM analysis. Using the chart provided with the sputtering instrument, the given protocol deposits a gold layer up to 300 nm thick, thickening the tube walls in the process. Taking this into account, even the smaller tubes for which the extra gold is most significant would match well with the diameter of the template channels.

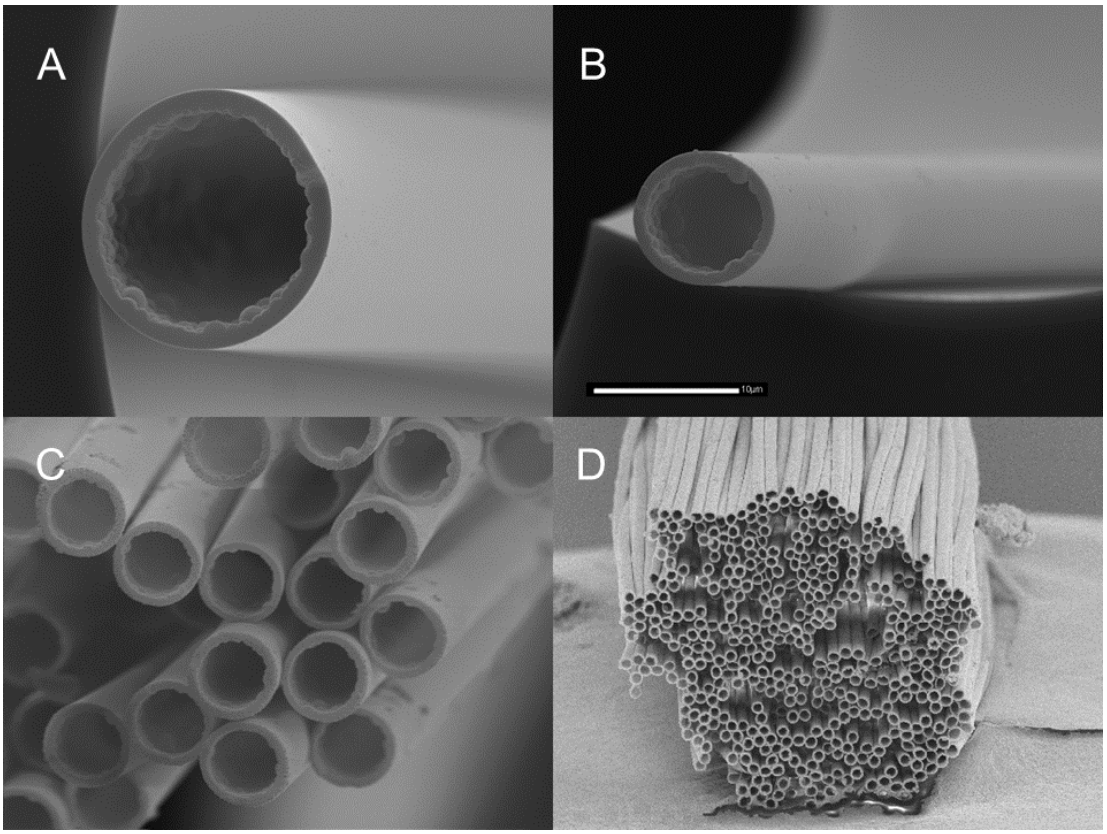

Figure 5.3 PolyDVB tubes fabricated in MSF templates having A) 9 holes (17.7 µm each), B) 9 holes (9.1 µm each), C) 126 holes (5.6 µm each) and D) 501 holes (620 nm each) showing tube monodispersity, tube wall thickness variation and the range of diameters possible from commercial MSFs. Scale bar is 10 µm and all four images are to scale.

Furthermore, as seen in Figure 5.3 and Table 5.1, the wall thickness of the tubes formed in different templates is dependent on the channel diameter. Tube wall thickness measurements are also presented in Table 5.1, and a plot of thickness as a function of tube

diameter is presented in Figure 5.4. In theory, if the polymerization is complete and the resulting polymer occupies the same space in the channel in each case, the tube wall thickness is expected to increase linearly with channel diameter. Assuming the volume fraction that the polymer tube occupies relative to the channel matches the volume fraction of polymerizable material in the initial solution (30%), the expected tube thickness was calculated and is displayed on the plot as a straight line. For the smaller tubes, the additional gold coating causes the tube thickness to appear greater than it actually is, and taking this into account the points fall very near the theoretical line. For the largest tubes, however, the actual tube thickness is lower than expected. This effect can be explained by the mechanism of tube formation described above, where partitioning of the polymerizing components to the channel surface causes polymer to form there primarily. This describes a confinement effect where the channel surface influences the nearby solution to a certain depth, in this case involving the attraction of reactant materials. As the channel diameter decreases, the surface-area-to-volume ratio increases and hence the fraction of solution volume that is influenced by the channel wall increases to the limit where the entirety of the reaction solution is dominated by surface effects. Similar observations were made in our recent work on porous polymer monolith formation in tubes with[33] and without[37] microspheres present, where the polymer morphology within the influence of surface effects was completely different than that in the bulk material. In that work it was also demonstrated that the extent of the surface's influence was increased when the interactions between the wall and polymer were enhanced (*e.g.* by making the surface more hydrophobic) or when the polymer-solvent interactions were weakened (*e.g.* by making the solvent more hydrophilic). In the case of the polymer tubes in the current study, the largest

channels have significant volume outside of the wall's influence, and hence some of the polymerizable material in the initial solution does not become associated with the channel surface, explaining why the volume fraction occupied by the largest tubes is lower than the expected 30%.

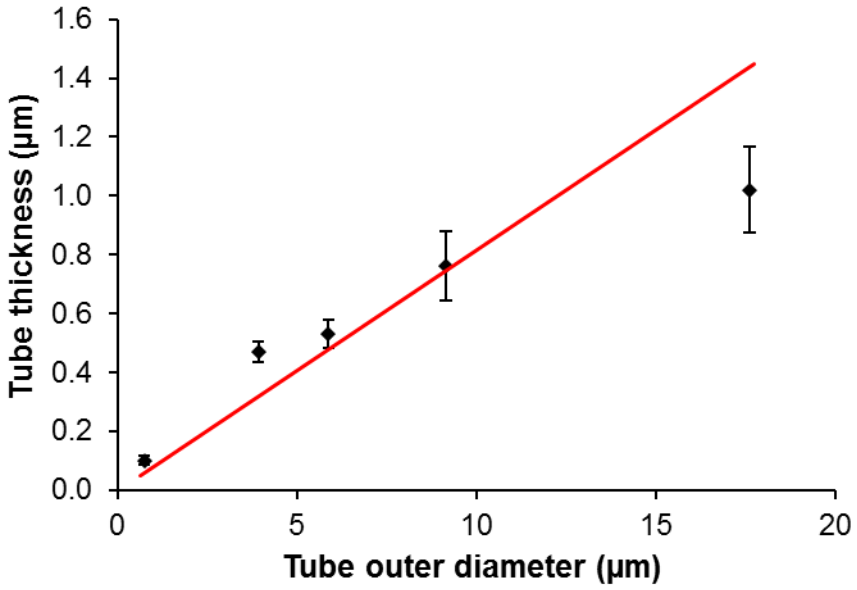

Figure 5.4 Plot showing the dependence of tube wall thickness on the tube diameter. The straight line represents the theoretical tube wall thickness assuming the volume of polymer present relative to the channel in each case matches that of the volume fraction of monomer in the polymerization solution (30%).

The length of the tubes matches that of the template, which can be prepared in continuous fashion and thus can be kilometres long. The ability to form polymer within the template is limited mostly by the ability to fill the channels with polymerization solution, which may require a more powerful pump. A simple calculation using Bernoulli's and Poiseuille's equations suggests that 5 m of the 126-hole MSF would have a pressure drop of about 200 bar (3000 psig) when flowing water at 1 µL/min (which would take ~20 minutes to fill the template), making the synthesis of structures having aspect ratios in excess of one million achievable. In our experience, lengths up to 1 m have been prepared

without difficulty (aspect ratio would be 178000). Limited by our current procedures for handling HF solutions, sections up to ~2 cm have been etched to yield bundles of tubes ~2 cm long, and an example of one from the 501-hole MSF template appears in Figure 5.5 as both optical and SEM images. For these smaller tubes, the aspect ratio of a tube this length is ~32000.

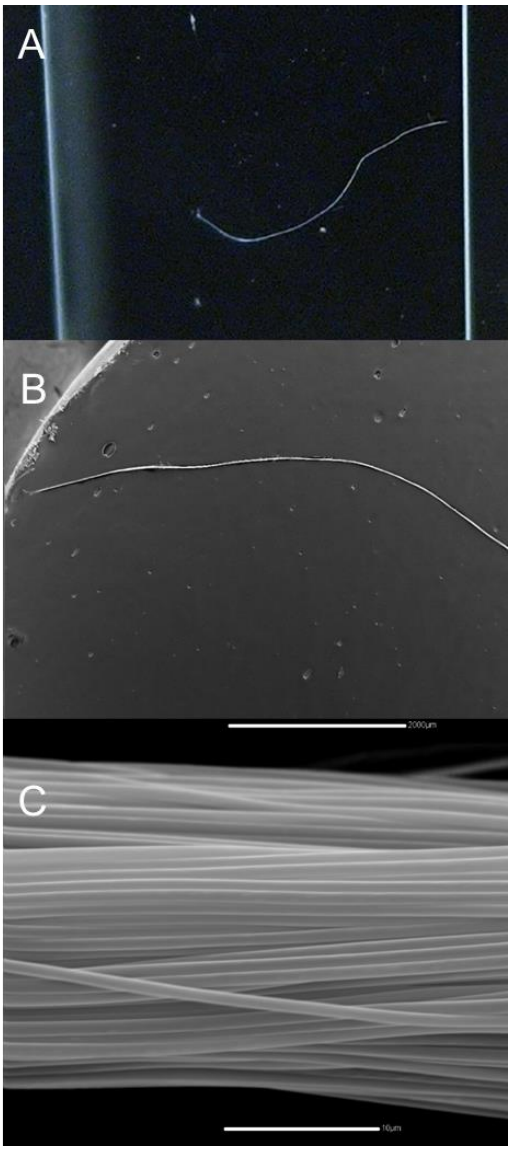

Figure 5.5 Images of a full bundle of polyDVB tubes prepared in a 501-hole MSF template. A) Optical image of a ~2 cm length of tube bundle on a glass slide with a magnification of 5x (visible mounting slide is 2.5 cm); B) SEM image of a ~4 mm length of tube bundle on copper tape with a magnification of 20x (scale bar is 2000 μm); C) SEM image of the side of a tube bundle with a magnification of 3500x (scale bar is 10 μm).

The polyDVB structures prepared in the manner described in this section are highly cross-linked, structurally rigid tubes, maintaining cylindrical shape even under SEM conditions. The shape of the tube, however, is dependent only on the shape of the template. A potential advantage of pulled MSFs as templates is the ability to design and control a variety of possible channel shapes. By varying the hole placement in the fiber and the distance between holes, or even by creating shapes in an MSF preform disc, circular holes can become significantly (but reproducibly) deformed into many possible shapes. Two examples were selected from commercially available MSFs and were used to generate polyDVB tubes that reproduced the template channels with high fidelity, one having a rounded trapezoidal shape and one having a rounded triangular (petaloid) shape (Figure 5.6).

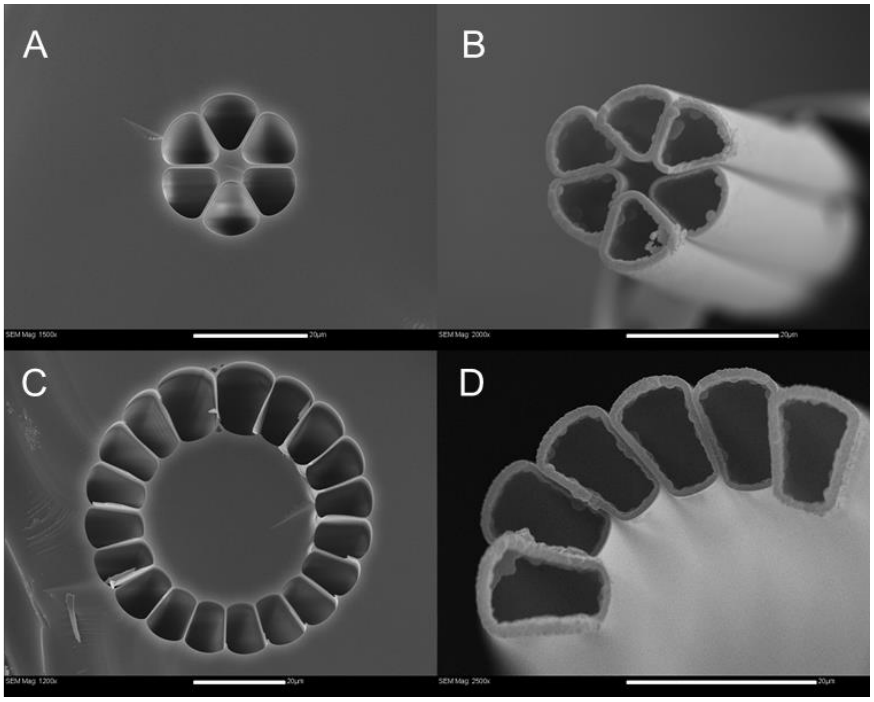

Figure 5.6 SEM images showing the MSF template with A) 6 rounded triangular (petaloid) holes and B) the polyDVB tubes prepared in it, as well as the template with C) 19 rounded trapezoidal holes and D) the polyDVB tubes prepared in it. Scale bars are all 20 µm.

5.3.3 Alternative 1D microstructures

Aside from polymer tubes, the variety of possible 1D structures that can be prepared using this very general template approach is extended to any material capable of resisting wet etching (other polymers, metals and etch-resistant inorganics), and any imaginable morphology that can be made on a small scale (tubes, solid fibers/rods/wires and a continuum of porous materials with various shapes and sizes). Examples of alternative 1D structures presented in this work include solid polymer fibers and porous polymer monoliths, by altering the conditions as shown generally in Figure 5.2.

5.3.3.1 Solid polymer fibers

Whereas a monomer solution will leave a void in the resulting polymer occupied by solvent, which leads to various polymer morphologies based on partitioning between the template surface and bulk solution, a liquid comprising only monomer and initiator will result in a solid 1D structure that occupies the entire channel. As an example, neat DVB containing AIBN initiator (also works with pure BDDA and BME initiator under a UV lamp) was polymerized in a MSF template to produce an aligned array of 126 homogeneous smooth microfibers, some of which are shown in the SEM image in Figure 5.7. Again, the fiber dimensions reproduced those of the template channel diameter very well.

An obvious extension of the solid fiber structure would be a solid fiber formed within a tube prepared by the method described in section 5.3.2. Sometimes known as a "cable" structure, it is essentially a fiber sheathed in polymer, especially useful when the fiber is electrically conductive and the sheath insulating.[38, 39]

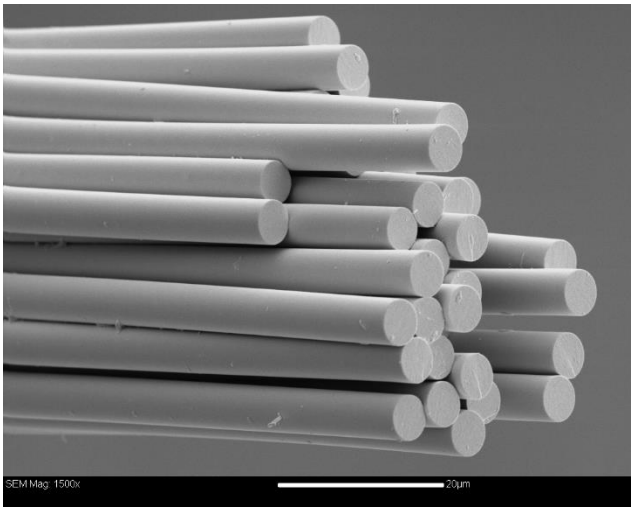

Figure 5.7 SEM image showing an aligned array of solid polyDVB fibers fabricated in the 126-hole MSF template. Scale bar is 20 µm.

5.3.3.2 Porous polymer monoliths (PPMs)

In the presence of solvent, polymerization of monomers occurs around the space occupied by the solvent, leaving a bicontinuous macroporous polymer structure that makes PPMs extremely useful for flow-through processes requiring high surface area.[36] The formation of the familiar interconnected globules that defines PPM morphology (see Figure 5.2) can be described using similar descriptive language as for the tubes. During polymerization, the forming polymer remains in solution until it phase separates, at which point further polymerization occurs primarily at the surface of the globules.[40] For example, when the solvent is poor and polymer phase separates early, there are typically fewer globules and larger macropores.[41, 42] When the PPM is formed in a confined space, it was found that the surface of the vessel influences the bulk PPM formation nearby, instead forming a non-porous outer wall or sheath when the polymer and surface are both hydrophobic.[37] Using a similar formulation in the current study, a cross-linked butyl acrylate PPM was formed in the channels of a MSF template and isolated following etching. Presented in Figure 5.8A is an array of PPMs featuring an outer sheath arising

from strong interactions between the polymerizing components and the hydrophobic wall of the γ-MPS-functionalized channel surface. Unlike the polyDVB tubes in Figure 5.2, however, the acrylate monoliths here contain much less cross-linking monomer and are thus less rigid and do not retain their cylindrical shape as well.

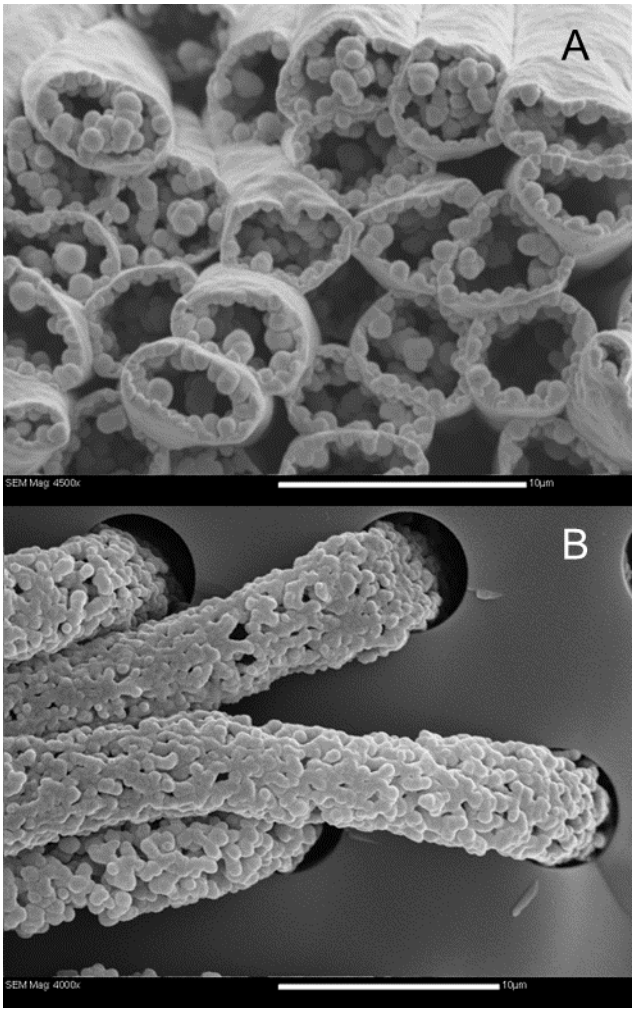

Figure 5.8 SEM images of poly(butyl acrylate-co-butanediol diacrylate) porous monoliths fabricated in the 126-hole MSF template. A) PPM with a dense polymer sheath from a MSF template functionalized with γ-MPS; B) PPM with no sheath extruded from an unfunctionalized MSF template. Scale bars are 10 μm.

In contrast, when the surface of the template channel is not functionalized with γ -MPS and is thus not hydrophobic, interaction between the reactant components and channel surface is poor and no dense sheath of polymer forms there. Instead, only bulk PPM

morphology, *i.e.* interconnected globules, forms within the channels. Having no significant attachment to the template surfaces, chemical or physical, the sheathless PPM string is easily extruded from the channels by flowing solvent through the MSF. Presented in Figure 5.8B is a SEM image showing several of these monoliths coming from the holes in the MSF template in which they were formed.

The ability to extrude the PPM fiber in this way increases production throughput because the etching step is not required, and more importantly, the template may be reused indefinitely. It is also possible to generate 1D structures in a continuous manner under flowing conditions if the polymer formation is rapid and photoinitiated, as was the case for the PPM in Figure 5.8B. However, when the polymer is attached to the channel walls, even by van der Waals forces, it is unrealistic to expect the structures to reliably extrude from such small diameter channels by force.[37]

With a sheath surrounding the PPM, the structures more closely resemble tubes that contain high-surface-area material. Liquids can be transported within the monolith much like it can on a larger scale, making them very useful for small-scale separations or flow-through solid-supported catalytic reactions. With no sheath present, liquids or gases can access the large surface area of the globules from the outside. This aspect may be useful for applications where high surface area is important in a bulk material, such as for solid-phase microextraction or solid-supported catalysis.

5.4 Conclusions

Microstructured fibers, developed by the photonics industry and available commercially, have been demonstrated to be excellent templates for the formation of small-scale 1D structures having highly monodisperse size and shape and any desired length. While a wide variety of materials or structure types can be prepared using these templates, we have prepared 3 different polymer morphologies (tubes, fibers and porous monoliths) from 2 different polymer systems (DVB and cross-linked butyl acrylate). In principle, appropriate choice of solvent and channel wall coating can result in any of these morphologies from nearly any polymer system, and indeed methacrylate-based tubes[43, 44] and DVB-based PPMs[45, 46] have been previously prepared in capillaries. The process has the added convenience of being able to be filled with reaction solution by coupling with a syringe pump using standard commercial fittings. The resulting 1D structures fabricated in this study matched well with the size and shape of the template, showing extremely low variation in these parameters, and were axially aligned as they were in the template. Taking the length of the template as well, these structures could be made to have aspect ratios in excess of one million, limited mostly by the ability of the liquid pump to fill the template channels, where tubes having >30000 aspect ratio were demonstrated in this work. The channel size, shape and number (scalability) are currently limited to the MSF designs useful as photonic waveguides, but modification of the stack-and-draw MSF fabrication process can yield a variety of channel shapes with a wide range of sizes (10's of nm to 10's of μm), and a density of 1000's of channels per MSF.

Small 1D structures with ultrahigh aspect ratio are extremely interesting due to their myriad applications in nano/microscience, including structural or electronic components in

microdevices, and fluidic conduits for separations, catalysis or transporting liquids or gases. The MSFs presented here represent a versatile template for the production of a large number of possible 1D materials for all these applications, offering exceptional structure reproducibility in long, aligned structures. This approach, therefore, should find wide applicability across many disciplines as devices and their components become ever smaller.

5.5 References

[1] C. R. Martin, *Advanced Materials* **1991**, *3*, 457-459.

[2] M. Steinhart, J. H. Wendorff, R. B. Wehrspohn, *Chemphyschem* **2003**, *4*, 1171-1176.

[3] J. Jang, S. Ko, Y. Kim, *Advanced Functional Materials* **2006**, *16*, 754-759.

[4] M. R. Abidian, D.-H. Kim, D. C. Martin, *Advanced Materials* **2006**, *18*, 405-409.

[5] J. L. Perry, C. R. Martin, J. D. Stewart, *Chemistry - A European Journal* **2011**, *17*, 6296-6302.

[6] Y. Cui, C. Tao, Y. Tian, Q. He, J. Li, *Langmuir* **2006**, *22*, 8205-8208.

[7] T. Shimizu, M. Masuda, H. Minamikawa, *Chemical Reviews* **2005**, *105*, 1401-1443.

[8] G. Liu, *Advanced Materials* **1997**, *9*, 437-439.

[9] K. Kumar, B. Nandan, V. Luchnikov, E. B. Gowd, M. Stamm, *Langmuir* **2009**, *25*, 7667-7674.

[10] M. T. Todaro, L. Blasi, C. Giordano, A. Rizzo, R. Cingolani, G. Gigli, A. Passaseo, M. de Vittorio, *Nanotechnology* **2010**, *21*, 245305/245301-245305/245305.

[11] J. C. Hulteen, C. R. Martin, *Journal of Materials Chemistry* **1997**, *7*, 1075-1087.

[12] R. O. Al-Kaysi, T. H. Ghaddar, G. Guirado, *Journal of Nanomaterials* **2009**, DOI: 10.1155/2009/436375.

[13] C. R. Martin, *Science* **1994**, *266*, 1961-1966.

[14] R. J. Tonucci, B. L. Justus, A. J. Campillo, C. E. Ford, *Science* **1992**, *258*, 783-785.

[15] G. Chen, S. A. Soper, R. L. McCarley, *Langmuir* **2007**, *23*, 11777-11781.

[16] S. Grimm, K. Schwirn, P. Goering, H. Knoll, P. T. Miclea, A. Greiner, J. H. Wendorff, R. B. Wehrspohn, U. Goesele, M. Steinhart, *Small* **2007**, *3*, 993-1000.

[17] Y. Zhou, M. Freitag, J. Hone, C. Staii, A. T. Johnson, Jr., N. J. Pinto, A. G. MacDiarmid, *Applied Physics Letters* **2003**, *83*, 3800-3802.

[18] A. S. Nain, J. C. Wong, C. Amon, M. Sitti, *Applied Physics Letters* **2006**, *89*, 183105/183101-183105/183103.

[19] D. Li, Y. Xia, *Advanced Materials* **2004**, *16*, 1151-1170.

[20] E. Zussman, A. Theron, A. L. Yarin, *Applied Physics Letters* **2003**, *82*, 973-975.

[21] I. G. Loscertales, A. Barrero, M. Marquez, R. Spretz, R. Velarde-Ortiz, G. Larsen, *Journal of the American Chemical Society* **2004**, *126*, 5376-5377.

[22] P. Russell, *Science* **2003**, *299*, 358-362.

[23] A. S. Cerqueira, Jr., *Reports on Progress in Physics* **2010**, *73*, 024401-024421.

[24] A. B. Daley, R. D. Wright, R. D. Oleschuk, *Analytica Chimica Acta* **2011**, *690*, 253-262.

[25] Y. Sun, N.-T. Nguyen, Y. C. Kwok, *Analytical and Bioanalytical Chemistry* **2009**, *394*, 1707-1710.

[26] B. Rogers, G. T. T. Gibson, R. D. Oleschuk, *Electrophoresis* **2011**, *32*, 223-229.

[27] S. Su, G. T. T. Gibson, S. M. Mugo, D. M. Marecak, R. D. Oleschuk, *Analytical Chemistry* **2009**, *81*, 7281-7287.

[28] P. J. A. Sazio, A. Amezcua-Correa, C. E. Finlayson, J. R. Hayes, T. J. Scheidemantel, N. F. Baril, B. R. Jackson, D.-J. Won, F. Zhang, E. R. Margine, V. Gopalan, V. H. Crespi, J. V. Badding, *Science* **2006**, *311*, 1583-1586.

[29] C. Vakifahmetoglu, *Advances in Applied Ceramics* **2011**, *110*, 188-204.

[30] J. Courtois, M. Szumski, E. Bystroem, A. Iwasiewicz, A. Shchukarev, K. Irgum, *Journal of Separation Science* **2006**, *29*, 14-24.

[31] S. M. Ngola, Y. Fintschenko, W.-Y. Choi, T. J. Shepodd, *Analytical Chemistry* **2001**, *73*, 849-856.

[32] Q. Luo, G. Yue, G. A. Valaskovic, Y. Gu, S.-L. Wu, B. L. Karger, *Analytical Chemistry* **2007**, *79*, 6174-6181.

[33] G. T. T. Gibson, T. B. Koerner, R. Xie, K. Shah, N. de Korompay, R. D. Oleschuk, *Journal of Colloid and Interface Science* **2008**, *320*, 82-90.

[34] X. Feng, Z. Jin, *Macromolecules* **2009**, *42*, 569-572.

[35] C. Zou, Z. Luo, D. H. Le, K. Dessources, A. Robles, G. Chen, *Journal of Materials Chemistry* **2011**, *21*, 14543-14548.

[36] I. Nischang, O. Brueggemann, F. Svec, *Analytical and Bioanalytical Chemistry* **2010**, *397*, 953-960.

[37] G. T. T. Gibson, S. M. Mugo, R. D. Oleschuk, *Polymer* **2008**, *49*, 3084-3090.

[38] V. M. Cepak, C. R. Martin, *Chemistry of Materials* **1999**, *11*, 1363-1367.

[39] A. Zahoor, Q. Teng, H. Wang, M. A. Choudhry, X. Li, *Metals and Materials International* **2011**, *17*, 417-423.

[40] I. Nischang, I. Teasdale, O. Brueggemann, *Analytical and Bioanalytical Chemistry* **2011**, *400*, 2289-2304.

[41] S. Eeltink, F. Svec, *Electrophoresis* **2007**, *28*, 137-147.

[42] E. C. Peters, F. Svec, J. M. J. Frechet, *Advanced Materials* **1999**, *11*, 1169-1181.

[43] Z. J. Tan, V. T. Remcho, *Analytical Chemistry* **1997**, *69*, 581-586.

[44] J.-L. Chen, Y.-C. Lin, *Journal of Chromatography, A* **2010**, *1217*, 4328-4336.

[45] D. Sykora, E. C. Peters, F. Svec, J. M. J. Frechet, *Macromolecular Materials and Engineering* **2000**, *275*, 42-47.

[46] C. Viklund, F. Svec, J. M. J. Frechet, K. Irgum, *Chemistry of Materials* **1996**, *8*, 744-750.

Chapter 6 Conclusions and Outlook

6.1 Conclusions

In this Ph.D. thesis, two individual but related subprojects have been extensively studied. In the first subproject (Chapter 2 to Chapter 4), a series of multi-nozzle emitters made from microstructured fibers (MSFs) for electrospray ionization mass spectrometry (ESI-MS) were developed and evaluated to improve the MS sensitivity and stability compared with standard tapered nanoelectrospray emitters. In the second subproject (Chapter 5), small-scale, one-dimensional polymer microstructures were fabricated using MSFs as templates to generate various morphologies with high aspect ratio and low polydispersity. MSFs were chosen to be investigated because they have many consistent micron-sized channels built into the same fiber, and possess dimensional similarity with conventional capillary tubing. Furthermore, they can be fabricated with a wide variety of channel numbers, patterns, and shapes, offering a convenient, highly customizable template material.

The morphology and performance of all the multi-nozzle emitters developed and investigated in the thesis study are presented and summarized in Figure 6.1 and Table 6.1. A commercially available MSF, which has 126 air channels arranged in a hexagonal pattern with a small pitch (~12.3 μm) was first investigated to develop multi-nozzle ESI emitters (Figure 6.1A). The commercial MSFs are designed for optics applications, thus the densely packed channel array for this type of MSF were not able to directly support the multiple electrosprays (MESs). MES emitters have been found to significantly improve MS sensitivity results from the much greater ionization efficiency associated with lower (nano)

flow rates without sacrificing the benefits of a larger total flow rate, as well as to elongate the emitter lifetime by reducing clogging tendencies due to the multiple fluidic paths. In order to isolate the channels, prevent tip surface wetting and promote individual electrosprays, polymer nozzles were formed at the exit by *in-situ* polymerization within the channels of a MSF, and then raised above the MSF tip face after the surrounding silica channels are partially removed by wet chemical etching. Conditions of polymerization and etching process were optimized to promote homogeneity between nozzles, in terms of both tubular shape and nozzle protrusion length as well as to achieve the longest polymer nozzles without interference between adjacent nozzles. The etching process was also investigated to understand the resulting morphology. MSFs could be consistently fabricated with polydivinylbenzene nozzles having uniform shape and length in every channel based on the optimized polymerization conditions, which were later employed to fabricate polymer nozzles in the custom-designed MSFs. The resulting multi-nozzle MSF emitters were demonstrated as efficient nanoelectrospray emitters, both offline and coupled to a triple quadrupole mass spectrometer for the detection of a peptide, showing good electrospray stability over a wide range of conditions. However, as the nozzles were too close together and their protrusion length was limited, MESs from individual nozzles were not observed but a single electrospray appeared under any of the conditions tested, thus no sensitivity enhancement was achieved.

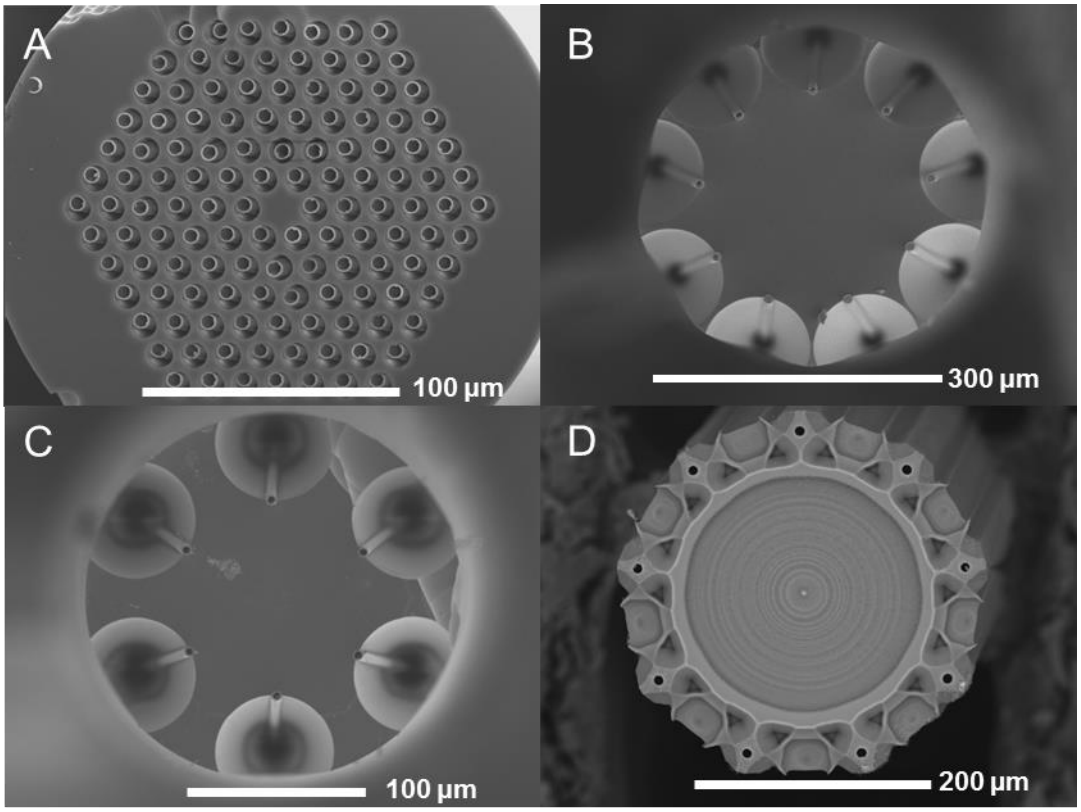

Figure 6.1 SEM images of all the multi-nozzle emitters for nano-ESI-MS produced by commercial and custom-designed MSFs in the thesis. A) 126-nozzle emitter; B) 9-nozzle emitter; C) 6-nozzle emitter and D) 9-silica-nozzle emitter. Scale bars are labelled on the images.

Because of the limitations of the commercial MSFs, custom silica MSFs with a larger pitch and fewer channels (nine or six channels) arranged in a radial pattern were designed and fabricated for the first time to achieve MES and to minimize inter-channel electric field inhomogeneities (Figure 6.1B and 6.1C). Polymer nozzles produced by the optimized polymerization/etching procedure were still required to prevent the sprays from coalescing and minimize the interference. Nine or six individual electrosprays operating in the cone-jet mode were successfully generated from a single emitter with the micro-nozzles. Offline electrospray experiments showed the expected square root relationship between the electrospray current and the number of nozzles, confirming MES behaviour. When coupled online with a LTQ Orbitrap mass spectrometer, the extracted ion current intensity for the

9-nozzle emitter was found to be 2.5 times greater than that for the 1-nozzle emitter. The signal enhancement is close to the expected factor of 3, which corresponds to the square root of the number of emitters. Furthermore, LC/MS data from a protein digest obtained at an independent laboratory demonstrates the applicability and robustness of the emitter for real scientific challenges using modern LC/MS equipment. However, these emitters have some issues associated with the polymer nozzles, including fragility of the polymer tubes and potential incompatibility with certain analytes. Therefore, MSF with built-in silica nozzles would have great advantages.

To this end, a novel MSF was designed and fabricated, which has a structure inspired by polarization-maintaining photonic crystal fibers with channels made of pure silica which have slower etch rate surrounded by doped regions which have faster etch rate in hydrofluoric acid to facilitate nozzle formation at each channel exit (Figure 6.1D). Furthermore, effective multiple silica nozzles were only produced when the inner channels of the MSF were protected by flowing water to prevent the etchant from entering the channels and widening the openings. Conditions were optimized to generate long and pointed nozzles from the flat MSF tip face. Nevertheless, the nozzles themselves made by wet chemical etching were not able to support MESs because the surface of the etched emitter tip has very small water contact angle and was rapidly wetted resulting in sprays coalescing. To counteract this, the emitters were functionalized with a fluoroalkyl chlorosilane to render the tip surface hydrophobic, allowing the nozzles to support independent electrosprays. The MES behaviour of the emitter was demonstrated offline by the square root dependence of the electrospray current on the number of working nozzles in the multi-nozzle emitter. Using this approach, highly sensitive and robust MES emitters

can be rapidly fabricated, showing theoretical MES current enhancement and an exceptionally wide range of operating voltages and flow rates. Although MSFs may be difficult and expensive to fabricate at beginning, fibers of hundreds of meters can be generated in a single batch when the parameters are well defined. The long fiber is able to make thousands of emitters which are several centimeters long, offering a cost effective material. The multi-nozzle MES emitters described in this thesis present high commercialization potential for ESI-MS due to greatly improve electrospray signal, flexibility in spray conditions and enhanced resistance to clogging, which could supplant the standard single-aperture tapered emitters in future. These benefits of the MES emitters render them highly applicable to various fields where ion signal is important, especially where analyte is scarce.

Table 6.1 Summary of multi-nozzle emitters developed during the thesis study

Characterizations	**126-nozzle emitter**	**9-nozzle emitter**	**6-nozzle emitter**	**9-silica-nozzle emitter**
Morphology				
MSF outer diameter, µm	230	460	280	360
Channel pitch, µm	12.3	115	90	96
Nozzle inner diameter, µm	4.7	7.5	3.8	8.2
Nozzle protrusion length, µm	5	51	26	61
ESI performance				
Multiple electrospray behaviour	No	Yes	Yes	Yes
Flow rate range, nL/min	100-1000	300-3000	100-1000	100-3000
Applied potential range, kV	2.2-3.5	1.5-4.0	2.4-5.9	2.2-3.4
Various solvent composition	ND	Excellent	ND	Good
Stability	Good	Excellent	Good	Excellent
Sensitivity	Moderate	Excellent	Good	Excellent
Robustness	Good	Good	Good	Excellent

ND: not detected

In the second subproject, MSFs were demonstrated to be excellent hard templates to generate small-scale tubes, wires and porous monoliths from poly(divinylbenzene) or poly(butyl acrylate-co-butanediol diacrylate). In the current study, the fabrication approach utilized in-channel polymerization and directed it to the channel inner surface by a partitioning behaviour. In theory, nearly any polymer compositions forming any of the morphologies can be obtained by the appropriate choice of solvent and channel wall coating. Due to the compatible dimensions of the MSFs, reaction solutions were able to fill the template channels conveniently using standard commercial fittings. The fabricated polymer 1D structures matched well with the dimension of the template channel, showing extremely low variation and high aspect ratio, and were axially aligned as they were in the template. A wide variety of materials including metals, polymers and semiconductors or structure types can be prepared using these templates which possess assorted channel shapes with a wide range of sizes (10's of nm to 10's of μm). The resulting materials are applicable in diverse fields such as medicine, catalysis, microelectronics and chemical analysis.

6.2 Outlook

As to outlook of the emitter project, several aspects are suggested as a follow up. Firstly, for the custom-designed MSF with doped regions, more studies can be conducted to investigate and improve the nature and application of the hydrophobic coating to increase the longevity of the multi-nozzle emitter. Additionally, to completely characterize the emitter, more online ESI-MS tests are necessary to verify the potential sensitivity improvement indicated in the offline electrospray tests. A realistic LC/MS separation using the multi-nozzle emitter compared to a commercial emitter would be also conducted in the

future to demonstrate the applicability and robustness of the emitter. These multi-nozzle emitters can also be functionalized or packed with particles as integrated emitters for on-line sample preparation such as preconcentration, desalting, and separation before conducting a MS analysis with greatly reduced dead volume.[1, 2] Additionally, the emitters can be incorporated in microfluidic devices (microchips) for online analysis and MS detection, offering advantages of reduced sample and reagent consumption, fast and high-throughput analysis, and compact system with low cost. The coupling of microfluidic devices to mass spectrometer has been a particularly vibrant research area and various interfaces have been developed over the last two decades.[3, 4] The number of channels may be expanded to increase the nozzle density to further enhance spray current and promote sample throughput in future designs.

Furthermore, the development of multi-nozzle MSF emitters make it possible to study the mechanism of nanoelectrospray from multiple channels. The availability of various MSF emitter choices provides an opportunity for further study of the effects of emitter geometry on electrospray behaviour and performance. These patterns may also be used to generate computer models to simulate the nanoelectrospray from different geometries, which will help to explore novel emitter designs and elucidate ESI mechanism.[5] Additionally, these MES emitters can be utilized as electrospray devices in various application fields including microcombustion, nanoparticle synthesis, thin film deposition, colloidal and ion propulsion.[6-8]

What is the future for MSFs as template? Firstly, fabricating structures with significantly small dimensions can be used to further explore the size effect on the properties of the materials for fundamental study. Secondly, new chemistries will be

developed to produce an even larger variety of materials with unique structures, morphologies and properties. Furthermore, new applications will be explored for the template-synthesized materials ranged from fundamental optical studies to ultra-trace molecule detection to high surface area catalysis.[9-11] Some of the ideas have already been put into practice in our group, for example using MSFs as templates to fabricated functional 1D materials such as conducting polymer: polypyrrole and fluorescent polymer: acrylates and methacrylates with Rhodamine moieties, showing application potential as chemical, optical and bio-sensors, polymer light-emitting diodes, field-emission and electrochromic displays, fuel and photovoltaic cells and drug-delivery devices.

6.3 References

[1] C. L. Gatlin, G. R. Kleemann, L. G. Hays, A. J. Link, J. R. Yates, III, *Analytical Biochemistry* **1998**, *263*, 93-101.

[2] Q. Luo, J. S. Page, K. Tang, R. D. Smith, *Analytical Chemistry* **2007**, *79*, 540-545.

[3] R. D. Oleschuk, D. J. Harrison, *Trends in Analytical Chemistry* **2000**, *19*, 379-388.

[4] S. Koster, E. Verpoorte, *Lab on a Chip* **2007**, *7*, 1394-1412.

[5] X. Wu, R. D. Oleschuk, N. M. Cann, *Analyst* **2012**, *137*, 4150-4161.

[6] W. Deng, J. F. Klemic, X. Li, M. A. Reed, A. Gomez, *Proceedings of the Combustion Institute* **2007**, *31*, 2239-2246.

[7] B. Almeria, T. M. Fahmy, A. Gomez, *Journal of Controlled Release* **2011**, *154*, 203-210.

[8] G. Lenguito, A. Gomez, *Journal of Microelectromechanical Systems* **2014**, *23*, 689-698.

[9] Y. Liu, J. Goebl, Y. Yin, *Chemical Society Reviews* **2013**, *42*, 2610-2653.

[10] J. R. Sparks, P. J. A. Sazio, V. Gopalan, J. V. Badding, *Annual Review of Materials Research* **2013**, *43*, 527-557.

[11] X. Lu, W. Zhang, C. Wang, T.-C. Wen, Y. Wei, *Progress in Polymer Science* **2011**, *36*, 671-712.